**Carolina Amaral Duarte de Barros**

Bachelor in Sciences of Physics Engineering

# Towards a Copper Metallic Printer based on Solid Electrolytes - Proof of Concept

Dissertation submitted in partial fulfillment
of the requirements for the degree of

Master of Science in
**Physics Engineering**

Co-advisers: Nenad Bundaleski, Doctor,
Faculty of Sciences and Technology, NOVA University of Lisbon

Orlando Manuel Neves Duarte Teodoro, Professor,
Faculty of Sciences and Technology, NOVA University of Lisbon

FACULDADE DE
CIÊNCIAS E TECNOLOGIA
UNIVERSIDADE NOVA DE LISBOA

**September, 2017**

**Towards a Copper Metallic Printer based on Solid Electrolytes - Proof of Concept**



This document was created using the (pdf)LaTeX processor, based in the "novathesis" template[1], developed at the Dep. Informática of FCT-NOVA [2].
[1] https://github.com/joaomlourenco/novathesis [2] http://www.di.fct.unl.pt

# Acknowledgements

I want to thank Faculty of Sciences and Technology, NOVA University of Lisbon for giving me the opportunity to develop this work.

I want to thank my advisers, Dr. Nenad Bundaleski and Professor Orlando Teodoro, for the constant support and motivation as well as for the good advices and ideas.

I want to thank Ana Fonseca, Afonso Moutinho and João Santos for the company, help and for the constant good mood.

Also, I want to thank Faustino and Eduardo for providing me their workshop and for helping with the construction of some parts of the assemblies. I also thank Mr. Mesquita for his company during my time on the optical microscope.

I want to thank Professora Fátima Raposo for helping me with some of the conductivity measurements and Professora Susana Sério for providing me with one of the furnaces from her laboratories.

I want to thank Nuno Costa, from the Analysis Laboratory, for making the XRD analysis and for always being available to answer my questions. I also thank Professor Rui Igreja e Professora Rita Branquinho, from CENIMAT, for helping with the EIS measurements and for their availability to clarify some doubts about the technique.

To Andreia Lopes and Professora Regina Monteiro I want to thank for allowing me to use their laboratory to produce the electrolyte pellets.

To Professor Terence Warner, from University of Southern Denmark, for his availability to respond to all of my questions, either concerning his articles and his book or concerning other aspects of this work.

I want to thank Mauro Costa for always supporting me, in his own way, as well as for pushing me to my limits and for always making me think things through, even when I did not want to.

I want to thank my mother for always giving me her support, for believing in me and for pushing me up when I was unmotivated or doubting myself. I want to thank her for her interest in my work, even if most of the time she had no idea of what I was talking about, and I want to thank her for being the reason why I was able to take this course during the past five years.

Lastly I want to thank my father for always watching over me and for being the person that made me fall in love with physics since I was a little girl.

*If you can't explain it simply, you don't understand it well enough.*
*-Albert Einstein*

# Abstract

Nowadays the techniques used to fabricate electronic devices have their deposition resolution limited. The production of an ion source that could allow the deposition of copper onto substrates with high-resolution, in order to write those pathways, is extremely important.

The main objective of this MSc thesis was to prove that it is possible to emit copper ions from a copper tip that is covered with a copper-based solid electrolyte. This goal encompasses several important and complex tasks like the synthesis of the appropriate electrolyte, the production of sufficiently sharp copper tips, the transfer of the electrolyte onto the copper tip, while preserving its original geometry, performing field ion emission experiments and the detection of deposited copper. The solid electrolyte used in this work was the $Rb_4Cu_{16}I_7Cl_{13}$, which has the highest ionic conductivity reported until today.

During this work, we tried different options in synthesizing the electrolyte and ended up with an optimized approach to do so. The synthesized materials were characterized by X-ray Photoelectron Spectroscopy, Powder X-ray Diffraction and Electrochemical Impedance Spectroscopy, in order for us to confirm that the materials were in the desired phase. We tried different approaches to deposit the electrolyte onto the tips - the pressing of the powder electrolyte onto the tips, with and without heating, dipping the tips in an acetone suspension made with the electrolyte powder and physical vapour deposition, using an evaporator built for this purpose. None of these methods gave satisfactory results, but we were able to deposit some electrolyte onto the tip using the acetone suspension method. Even though the deposition of the electrolyte onto the tips was not as good as we desired, we still managed to get some ion current from the acetone prepared sample. Although the current was not very stable, Secondary Ion Mass Spectroscopy analysis of the graphite substrate showed that we were able to mostly emit copper ions, with a small contribution of rubidium ions.

**Keywords:** Copper ion, solid electrolyte, $Rb_4Cu_{16}I_7Cl_{13}$, conduction pathway

# Resumo

Hoje em dia, as técnicas usadas para fabricar dispositivos electrónicos têm a sua resolução de deposição limitada. A criação de uma fonte de iões que pudesse permitir a deposição de cobre em substratos, com elevada resolução lateral, de forma a poder escrever pistas condutoras, torna-se extremamente importante.

O principal objectivo desta tese de mestrado era provar que é possível emitir iões de cobre a partir de uma ponta de cobre coberta com um electrólito sólido à base de cobre. Para atingir este objectivo, foi necessário completar diversas tarefas, como a síntese do electrólito apropriado, a produção de pontas de cobre suficientemente afiadas, a transferência do electrólito para as pontas de cobre, mantendo a geometria destas, a realização dos testes de emissão de campo dos iões e a detecção dos iões de cobre depositados. O electrólito sólido usado neste trabalho foi o $Rb_4Cu_{16}I_7Cl_{13}$, que tem a condutividade iónica mais elevada, das até hoje registadas.

Ao longo deste trabalho, tentámos sintetizar o electrólito de diferentes maneiras, tendo acabado por usar um procedimento melhorado. Os materiais sintetizados foram analisados por espectroscopia de fotoelectrões de raio-X, difracção de raio-X de pós e espectroscopia de impedância, de forma a que pudéssemos confirmar que os materiais se encontravam na fase desejada. Tentámos diferentes abordagens para depositar o electrólito nas pontas de cobre - pressionar o pó nas pontas, com e sem aquecimento, mergulhar as pontas numa suspensão de acetona, feita com o pó do electrólito, e usar o evaporador que construímos para fazer evaporação térmica. Nenhum destes métodos nos deu resultados satisfatórios, mas conseguimos depositar algum electrólito em pontas de cobre, usando o método da suspensão de acetona. Embora esta deposição não fosse tão boa como desejávamos, conseguimos medir alguma corrente iónica a partir de uma ponta de cobre obtida por este método. Esta corrente não era muito estável, mas a análise feita ao substracto de grafite, por espectroscopia de massa de iões secundários, revelou que fomos bem sucedidos em emitir iões de cobre, com uma pequena contribuição de iões de rubídio.

**Palavras-chave:** Ião de cobre, electrólito sólido, $Rb_4Cu_{16}I_7Cl_{13}$, pista condutora

# Contents

# List of Figures

# List of Tables

Chapter 1

# Introduction

Ions have been used in science for many years, in different areas. From technological applications to natural sciences, the applications of these particles are diverse.

By studying ions, among other particles, fundamental science allowed us to learn about quantum mechanics and atomic physics. Ions can be used in different analytical techniques that allow to diagnose materials and they can be used as processing tools by using effects such as ion sputtering and implantation.

Nanotechnology uses ions as a particularly important tool, since ions with $keV$ energies have ranges below 10 $nm$ and can be used in Focused Ion Beams (FIB) to build microelectromechanical systems and nanoelectromechanical systems.

Being the result of an atom or molecule that lost or captured electrons, ions can be positively or negatively charged and their masses and available potential energy widely vary. For these reasons, there are interesting applications for these particles that could not be achieved using only electrons or atoms in general. When ions interact with material, their kinetic energy is transferred to atoms (unless they are of $MeV$ energies, in which case the kinetic energy is also mostly transferred to electrons), while their potential energy is transferred to electrons. By preparing different ions, it is possible to choose whether the energy is transferred to ones or the others.

The use of the electrolysis process, which is based on ions migrating from one electrode to another, has an application in the industry, as a process to obtain the pure form of different materials, such as ores or metals and it is also applied in the production of oxygen for submarines or spacecrafts, as well as in the production of hydrogen to use as source of electrical energy. Electroplating is another technique that uses ions for the production of metallic coatings, like for nickel or chromium plating.

In medicine, ions are used as diagnostic tools and in different types of treatments, like in nuclear medicine and radiation therapy, medical imaging and radiation biology [1, 2].

In electrochemistry, the production of batteries usually includes an electrolyte that allows the movement of ions, in order to complete the chemical reactions and deliver the energy to the external circuit.

In the area of astrophysics, ions are sometimes used in spacecraft propulsion, as rocket engines. Even though ion engines still have low propulsion, with respect to the standard propulsion engines, they can still be used just for small corrections of trajectories of stallites, typically micro-sattelites. A review on this topic was made by Tolstoguzov [3]. In this article, it is demonstrated how is it possible to use liquid electrolytes in aerospacial applications, nanotechnology and microprobe analysis.

In applied physics, ions are used in different equipment to analyse surfaces or modify them. They can be used, for example, in ion guns or plasmas to sputter surfaces and to clean them. The sputtering is done by focusing an ion beam over the surface and it allows to either clean the surface, as has been referred, or to perform material depth profiling in combination with different surface sensitive techniques. These ion beams usually have energies of the order of 10 $keV$. Ions can also be used to modify materials. For that is used ion implantation and the ions typically have energies of the order of 100 $keV$.

Even though ions are used in many and varied areas, the ones that matter the most for this work's purpose are microelectronics and nanotechnology. In these areas, ions with energies of typically 200 $keV$ can be implanted on different materials, below the surface. They can also be applied as diagnostic tools, like in Secondary Ion Mass Spectroscopy (SIMS), which allows to to identify concentrations of parts per million ($ppm$) of dopants in silicon, like phosphor and boron. Microelectronics and nanotechnology use ions as the key to the manufacturing of electronic chips and other electronic components.

In 1975, Gordon Moore predicted that the number of transistors in a chip would double every eighteen months. This concept became known as Moore's law and the development of electronics seems to still be following it.

The constant development of electronic devices results in the need to increase their functioning speed. For that it is critical to reduce the size of the constituting electronic components. To make this possible, it is necessary to obtain a higher lateral resolution when depositing materials on the substrates, allowing to build on them smaller conducting pathways. The physical limit for this resolution in the writing of conductive pathways should be about 1 $nm$, which is equivalent to the widths of three atoms side by side.

Nowadays, the techniques used to fabricate electronic devices have their deposition resolution limited.

One of those techniques is lithography, which has different variations and is the technique with the best resolution in the field of fabrication of semiconductors and integrated circuits. One of the main types of lithography is photolithography, or UV lithography. This process of deposition allows to print a pattern on the material that is going to be modelled into the component. Photolithograpy consists in the application of a photoresist onto the material and then the printing of the pattern cut into a mask of metal.

This printing is done by putting the mask above the substrate covered with the photo-resist and then irradiating an UV light over it. The exposed parts are then removed or stay in the substrate, depending on the type of photo-resist used. Like the process just described, there is another one that instead of UV light uses x-rays to print the mask on the substrate [4].

Another lithography process is called electron beam lithography and is used to make the smallest components on substrates as well as to create patterns on them, just like photolithography and X-ray lithography. However, instead of using photo-resist, the electron beam is used to etch the resist directly. It is possible to control by a computer the pattern that the beam is supposed to draw on the substrate [4].

The lithography process has its resolution limited by the wavelength of the radiation used, by the diameter of the electron beam and by the precision of its control, which depends on the sensitivity, precision and linearity of the power supplies used to deflect the beams and on how good the electron optics is. However, the most recent lithography technique that does not use masks, that is, electron beam lithography, has a width of deposition of about 20 $nm$. If a mask is still used to draw the pattern, the extreme UV lithography is able to reach a resolution of 13 $nm$ [5].

A particularly interesting and competitive technique is the Focused Electron Beam Induced Deposition, or FEBID. In this technique a gas is introduced inside a chamber, which becomes adsorbed onto a substrate. A focused electron beam interacts with the adsorbate and dissociates it in its volatile and non-volatile parts. The non-volatile part stays on the substrate, forming a deposit of the material with the same resolution as the electron beam. This is a one-step technique and since it does not use masks or photo-resists, there is some freedom to choose any geometry or material. The structures obtained with this technique can be scaled from hundreds of micrometers to only one nanometer. However, the deposits have a low purity level and the throughput is low [6].

The production of copper pathways with high lateral resolution is extremely important. The reason to choose copper is that it is one of the most used materials to make the contacts between different components, for example, integrated circuits, and it is also cheaper than most of those materials. Also the ability to draw on the material or deposit the desired species onto a substrate without the need of a photo-resist should increase of the resolution of the process. Consequently, it is of high technological interest to produce a source of copper able to deposit atoms in a controllable way with very high resolution. Although such atomic source is not currently available for any element, an interesting possibility appears in the area of field emission ion sources.

In 1897, Wood discovered the basic mechanism of field emission. He verified that if a voltage is applied between a sharp cathode and a flat anode, a current flows. Some years later, Hibi stated that a when a point of tungsten was heated, instead of a tungsten wire, its brightness was higher [7]. Thus, a smaller source would result in higher brightness.

Field emission sources can be of two types: cold or thermal. The cold field emission occurs when operating in ultra-high vacuum, at room temperature, while the thermal field emission occurs at a higher pressure and temperature, since there is a source of thermal energy that assists the field emission. Field emission sources have some advantages, like the low operating temperature, long lifetime, small energy spread and small size of the source. However, these type of sources usually need to operate under ultra-high vacuum and the current emission is not as stable as in other types of sources, like the thermionic emission source [7].

Nowadays, some of the ion sources that exist consist of liquid metals covering a tip. This tip is heated, in order for the metal to melt. When an electric field is applied, the balance between the electrostatic forces and the surface tension results in the formation of a cone made of the metal on the tip's apex. The atoms from the cone's apex are ionized and then emitted. The ions that are lost from the cone are replaced by the ones in the metal reservoir. This technique allows to focus ion beams to diameters of 5 $nm$ [8].

The electric field necessary to provoke ion emission on a tip's apex is of the order of $10^9 - 10^{10} V/m$. This magnitude is enough to cause field emission of most metals and other materials. To calculate the electric field on the apex of a tip, equation 1.1 can be used [9].

$$E = \frac{V}{\beta r} \tag{1.1}$$

In equation 1.1, $V$ is the voltage applied to the tip, $\beta$ is a coefficient that takes into account the tip's apex shape and $r$ is the tip's radius. From that equation, it is possible to conclude that the smaller the radius of the tip, the higher the field on the apex.

For the ion to leave the tip, it is necessary that a voltage is applied to the system, so the ion is able to overcome the potential well in which it is. The electrical field modifies the potential energy curve and reduces the potential barrier so that ions are able to escape from the tip. Figure 1.1 shows the potential curves for an atom, an ion and for an ion in the presence of a field [10].

Usually, there is some confusion when speaking about field emission and field evaporation. The main difference between these two processes is the type of particle that leaves the surface. In field evaporation, the ions are the particles that leave the surface of the material. Ions are evaporated without ionization, since they are already ionized. In field emission of ions, there are two processes involved - first, the atoms from the surface are emitted and then they ionize, as they move away from the surface [9, 11].

Since electrolytes are ionic conductors, the ions exist in that state in the material. Moreover, if there were atoms and not ions on the material, the application of a voltage to the tip would not make them move through the electrolyte, away from the applied

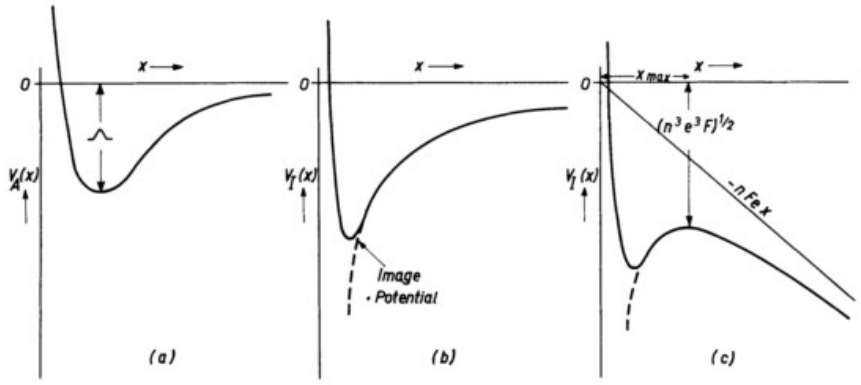


Figure 1.1: Potential curves for (a) an atom; (b) an ion and (c) an ion in the presence of a field. This image was taken from the book [10].

voltage or towards it. For this reason, the process that should occur on our assembly should be field evaporation and not field emission.

There have been some developments on the ion emission field that proved that it is possible to use ionic conductors on the solid state to emit ions from tips. Escher *et al.* have proposed an alternative source for focused ion beams that is based on solid electrolytes [8]. They used a silver ion based electrolyte and were able to develop an ion source that provided a stable current in the microampere regime. The findings of Escher and his team, that is, the possibility of emitting ions from a solid electrolyte covering a tip, have advantages compared with the liquid metal ion sources. This new ion source should have a smaller spreading of energy, a higher mechanical stability and, consequentially, an ion optical performance that is better than in other technological solutions [8].

In the work described in this thesis, instead of a liquid metal, a solid electrolyte is used to cover a tip. The principle used in this work is very similar to the one described by Escher in his already mentioned article [8].

If a solid electrolyte has a good conductivity ($10^{-4} - 10^{-1} S/cm$), the mobile ions should be able to move as if they were in a liquid [12]. Being made of the same material as the ion that is going to be extracted from the electrolyte, the tip's ions should migrate from the tip to the electrolyte, compensating the loss of these ions from the ionic conductor.

By positioning the tip, with an apex radius as small as possible (in the order of the micrometers), at less than a millimetre from the substrate, it should be possible to use a voltage in the order of kilo-Volts to extract the ions from the electrolyte and to focus them on a small area, in the order of nanometres. This way, a low energy ion beam would be produced and could be used to deposit the ions on a substrate, without damaging the surface. This is the main difference between what is the objective of this thesis and the commonly used ion beams.

The vast majority of the solid electrolytes with the highest ionic conductivities reported until today have copper ions as the mobile species. Since copper is one of the main metals used to interconnect different electronic components, like integrated circuits, and is also cheaper than most of those, our work uses a copper-based solid electrolyte to reach its goal.

The main objective of this MSc thesis was to demonstrate that it is possible to emit copper ions from a tip covered with a copper-based solid electrolyte. For that it was necessary to synthesize the ionic conductor and test its properties, which lead to the necessity to explore different characterization techniques and play with different parameters. Then, it was necessary to find the best way to transfer the electrolyte onto the copper tip, whilst preserving the tip's geometry. Once the electrolyte was covering the tip, we tried to perform field ion evaporation. The high fields necessary to successfully perform these type of evaporations are strongly dependent on the size of evaporation area - the smaller this area, the higher the field. The use of the copper tips comes from this relation. The tip's geometry, if the copper is well sharpened, should allow to obtain high fields needed to have field ion evaporation.

From the concept proven in this work, it should be possible to develop a copper metallic printer based on solid electrolytes that allows to achieve high lateral resolutions, when depositing copper onto substrates. This high-resolution should be achieved by controlling the current in the ion source. Another characteristic that this technique should achieve is the possibility for this ion source to be self-sustained. That would be accomplished if the copper ions from the tip could migrate into the electrolyte, thus compensating the loss of ions emitted from the apex.

Figure 1.2 shows a schematic of what is proposed to be achieved with this work. The image represents a copper tip with the apex covered with the $Rb_4Cu_{16}I_7Cl_{13}$ electrolyte. The tip is at a small distance from the substrate. In the schematic is also possible to see how the voltage is going to be applied. For this work, the applied voltage should be positive, so the copper ions are repelled and move towards the apex of the tip. The small dimensions of the apex and, consequentially, the presence of a high field should allow for the evaporation to occur. Initially, some copper ions should be emitted, which results in a concentration gradient that in turn provokes the migration of copper atoms from the bulk of the tip to the apex surface. The copper ions diffuse through the electrolyte, due to that concentration gradient, whilst all of the potential drop is between the apex of the tip and the substrate's surface. Once copper ions are deficient in the electrolyte, we expect to get copper migration from copper metal into the electrolyte.

This MSc thesis has six chapters.

The second chapter gives an insight on ionic solids - their history, classification and conduction mechanisms. After that, one of the main techniques used to measure the ionic

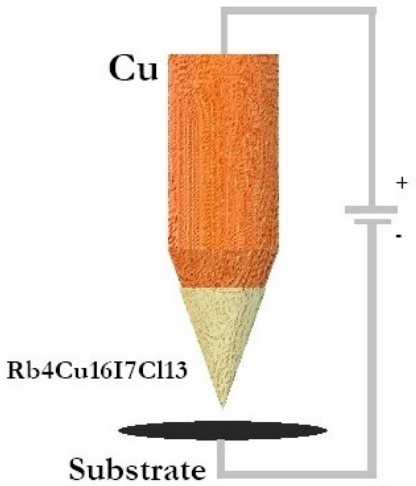


Figure 1.2: Schematic of the final assembly that is proposed in this work.

conductivity is briefly explained. At last, a more detailed insight on the electrolyte chosen to this thesis is given.

The third chapter describes the experimental steps taken during the development of this work.

The fourth chapter shows the results and discusses the different syntheses, analyses and tests made in this work.

The fifth chapter resumes the main conclusions of this MSc thesis and the sixth describes some of the future tasks that might be done to continue this work.

Chapter 2

# Ionic Conductors

This chapter covers the theory behind the ionic conductors, more specifically, the ones in the solid state. The first section introduces solid state ionics. The second section explains one of the techniques that exist to measure the ionic conductivity, the Electrochemical Impedance Spectroscopy, or EIS. The third and last section of this chapter covers the electrolyte used in this work, the Rubidium Copper Iodide Chloride, or $Rb_4Cu_{16}I_7Cl_{13}$.

## 2.1 Solid Electrolytes

### 2.1.1 Background

Before 1960, the vast majority of the devices that existed used materials based on electron conduction and until the late 1960s only a few materials based on ionic conduction were known. Most of these ionic conducting devices were liquid-aqueous electrolyte-based, such as batteries. These batteries had some disadvantages, e.g., short temperature range of operation, device failure due to electrode corrosion and large dimensions. These disadvantages led to the need to obtain a replacement for liquid electrolytes. The first attempt to replace the old devices was to use the solid ion conductors that were already discovered, like silver halides. However, materials like these had a poor conductivity so they were not a good replacement for the old liquid-state batteries [13].

Hence, scientists started a search for new solid materials with high ionic conductivity, making the solid state ionics a very active field of science in the last third of XX century [14].

Even though it was just in the 1960s that the first reports of solid systems with extremely high ionic conductivity, like $MAg_4I_5$ (with M=$NH_4$, Na, Rb) and Na-$\beta$-alumina began to show, there were reports of conductivity in solid electrolytes since 1834. In that year, Faraday reported the transport of silver ions through silver sulfide. However,

the decade of 1960 was the one in which the solid state ionics field was born. This field studies the high ionic conduction in solids, in all of its aspects - chemical, physical and technological [13].

Since the appearance of this field, the interest in solid state electrolytes grew worldwide. The main advantage of these materials over the liquid-aqueous electrolytes is the wide range of temperature in which they can be used. Unlike the liquid electrolytes, solid state devices can work in temperatures below 0°C and above 100°C. This fact can lead to miniaturization of batteries and allow the application of this type of materials in different areas. There are reports of pacemakers made using batteries with solid electrolytes, timers and memory cells that use silver-ion based electrolytes, supercapacitors and even sensors that use oxide conductors since 1972 [14].

The interest in solid state ion conduction led to the report of many new materials with high ionic conductivity. Amongst them are electrolytes whose mobile ions are $Ag^+$ and $Cu^+$. In fact, until the discovery of the electrolyte used in this work, the majority of the electrolytes that were reported as having the highest ionic conductivity (around $10^{-1}\ Scm^{-1}$) had $Ag^+$ as the mobile ion. The $RbAg_4I_5$ (used in the works of Dália Martins and Fábio Fernandes, in Faculty of Sciences and Technology, NOVA University of Lisbon - [9, 15]) was discovered in 1965 and had an ionic conductivity of 0.26 $Scm^{-1}$ at 25°C. In addition to these crystalline electrolytes, based on silver and copper ions, many more types of materials have been found. The list goes from glassy materials to amorphous ones, conducting glasses, polymers, conductive thin films and even conductive gel. The majority of them are based on the lithium ion [14].

There were various conferences and meetings over the years whose theme was the solid state ionics. Many different materials and batteries were presented during these conferences and it was in one of these meetings that the electrolyte used in this work was presented. In the year of 1978, Takehito Takahashi reported his team's discovery of the most conductive solid electrolyte, at room temperature - the Rubidium Copper Iodide Chloride, or $Rb_4Cu_{16}I_7Cl_{13}$ [14]. This electrolyte is, until today, the one with the highest ionic conductivity - 0.34 $Scm^{-1}$.

Before the discovery of this electrolyte, there were many attempts to synthesize the compound $RbCu_4I_5$, which is the copper analogue to the already referred silver ion conductor $RbAg_4I_5$. These attempts proved that this compound does not exist, so the next step taken was to replace some iodide ions with chloride ones, within the compound desired (the hypothetical $RbCu_4I_5$). This lead to the simultaneous discovery of $Rb_4Cu_{16}I_7Cl_{13}$, as already referred, and $\alpha$-$RbCu_4Cl_3I_2$, by Geller *et al.* After the discovery of these two compounds, a solid-solution series appeared and both of them were proven to be part of it. This solid-solution series was the $Rb_4Cu_{16}I_{7+x}Cl_{13-x}$ [16].

Figure 2.1 shows two tables with the chronology of some important points in the solid state ionics area. The tables are from an article by Owens [14].

| Time | Event | |
|---|---|---|
| 1833 | Faraday's Law | |
| 1897 | $ZrO_2$Glower (Nernst) | |
| 1920 | High Ionic Conduction in a-AgI | |
| 1934 | Ion Transport Mechanism for a-AgI | |
| 1943 | Ionic Conduction Theory for $ZrO_2$ | |
| 1950–1960 | Solid State batteries: | Cell Voltage: |
| | $Ag/AgI/V_2O_5$ | 0.46 |
| | $Ag/AgBr/CuBr_2$ | 0.74 |
| | $Ag/AgBr–Te/CuBr_2$ | 0.80 |
| | $Ag/AgCl/KICl_4$ | 1.04 |
| | $Ni–Cr/SnSO_4/PbO_2$ | 1.2–1.5 |
| 1957 | Applied Use of $ZrO_2$ (Wagner) | |
| 1962 | High Temperature Fuel Cell Using $ZrO_2$ | |
| 1967 | β-alumina; Rb $Ag_4I_5$ | |
| 1969 | Electro-chromism in $WO_3$ | |
| 1972 | Solid State Li Battery Memoriode | |
| 1976 | NASICON Automotive Sensor Using $ZrO_2$; Secondary Battery Using $TiS_2$ Intercalation | |
| 1979 | High $Cu^+$ Conductor Organic Polymer Solid-electrolyte | |
| 1981 | Plastic Battery | |
| 1983 | Commercial ECD | |

| Date | Electrolyte | Log s, $W^{-1}$ $cm^{-1}$ | Typical cell system |
|---|---|---|---|
| 1950–1960[a] | AgI | −5 | $Ag/V_2O_5$ |
| 1960–1965[a] | $Ag_3SI$ | −2 | $Ag/I_2$ |
| 1965–1972[a] | $RbAg_4I_5$ | −0.55 | $Ag/Me_4NI_5$ |
| 1965–1975[a] | Na β-alumina | −1.5 | Na–Hg/$I_2$,PC |
| 1970–1975[a] | $LiI(Al_2O_3)$ | −5 | $Li/PbI_2$ |
| 1970–1980[a] | LiI | −7 | $Li/I_2(P_2VP)$ |
| 1978–1999[a] | LiX–PEO | −7 | $Li/V_6O_{13}$ |
| 1979–1995[b] | $Rb_4Cu_{16}I_7Cl_{13}$ | −0.47 | $Cu_2Mo_6S_{7,8}/Cu_2Mo_6S_{7,8}$ |
| 1980–1986[a] | $Li_{0.36}I_{0.14}O_{0.007}P_{0.11}S_{0.38}$ | −3.3 | $Li/TiS_2$ |
| 1983–1987[a] | MEEP | −4 | $Li/TiS_2$ |
| 1994–1999[c] | $Li_{1.26}Si_{0.365}O_{0.04}P_{0.01}S_{1.36}$ | −2.8 | $InLi_x/Li_{1-x}CoO_2$ |
| 1985–1992[a] | Plasticized (Gel) SPE | −3 | $Li/V_6O_{13}$ |
| 1985–1992[a] | $Li_{0.35}I_{0.12}O_{0.31}P_{0.12}S_{0.098}$ | −4.7 | $Li/TiS_2$ |
| 1990–1992[a] | $Li_{0.39}N_{0.020}O_{0.47}P_{0.12}$ | −5.6 | Li/a-$V_2O_5$ |
| 1990–1999[d] | Polymer Gel | −3 | $C/LiCoO_2$ |
| 1995–1999[e] | Lipon | −5.6 | $Li/LiMn_2O_4$ |

[a] Owens et al. [32].
[b] Kanno et al. [38], Sotomura et al. [39].
[c] Takada et al. [40].
[d] Osaka, [33].
[e] Bates et al. [41].

Figure 2.1: Chronology of solid state ionics [14].

### 2.1.2 Classification

The concept on which this work is based is the movement of ions from one place to another inside a material in an electric field, that is the ionic conductivity. This conductivity is specific to each material and is determined by the amount of charge carriers (in the case of ionic conductivity the carriers are ions), the amount of charge that each one of them carries and their velocity [17].

A material that has ions as the major charge carriers is called an electrolyte and the ones in the solid state are called solid electrolytes. This type of materials should have a high ionic conductivity, between $10^{-4}$ $Scm^{-1}$ and $10^{-1}$ $Scm^{-1}$, and usually have a low electronic conductivity ($< 10^{-6}$ $Scm^{-1}$). This results from the fact that the type of bonds in ionic crystals determines the non-existence of free electrons in these materials. According to Agrawal, these properties result both from structural and non-structural aspects. Some of these aspects are the crystal structure, the lattice disorder, the free volume of the cell,

the amount of ions present in that cell and its size, among others [13].

Ideally, the ions from a perfect ionic crystal should be in their original positions, causing the material to behave like an insulator. However if enough energy is given to the ions, they tend to move. This energy is usually given by thermal vibrations. When the ion gets enough energy to leave its original position, it can segregate at the surface of the crystal or for the interstitial site. These are called point defects and are classified as Schottky or Frenkel defects, respectively. Frenkel defects are also called Frenkel pairs, since for each vacancy there is an occupied interstitial site. Figure 2.2 shows a schematic of these two types of defects. The movement of the ions through these deffects results in ion conduction [13].

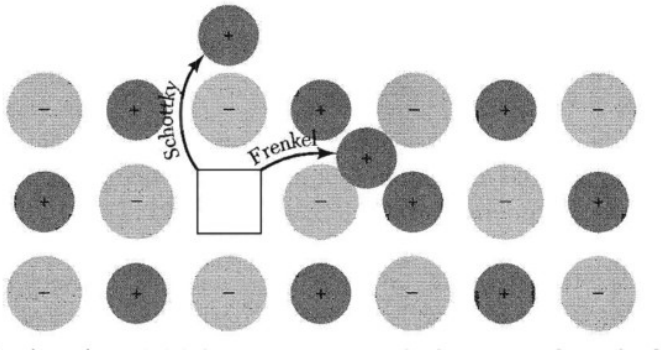


Figure 2.2: Schematic of Schottky and Frenkel deffects in an ionic crystal. This figure was obtained from the text *Introduction to Solid State Physics* [18].

The density of defects present in a crystal depends on various aspects, e.g., the temperature, the presence of impurities and the structure of the ionic crystal. From the type of defects present in a crystal, we can classify the ionic solid. One possible classification, made by Rice and Roth and explained by Padma Kumar, separates the crystalline ionic solids in three types, based on the concentration of defects and on the type of migration of the mobile ions - interstitial or vacancy [19].

Another classification of superionic solids divides them in four groups, depending on the phase they are in. The four groups are:

1. framework crystalline materials
2. amorphous-glassy electrolytes
3. polymer electrolytes
4. composite electrolytes

The different phases of these types of ionic solids result from the different microstructures and physical properties they have and these phases can be either ordered or disordered. The framework crystalline materials are the only type that has an ordered phase.

The other three types have disordered phases, the second and third type being disordered in the microscopical scale and the fourth type, the composite electrolytes, being disordered in the macroscopical scale [13].

The electrolyte used in this work fits in the first type of the list above, the framework crystalline materials. These materials have a crystalline skeleton made from the non-mobile ions of the material and its mobile ions are relatively free. Inside this type of ionic solids, we can divide them in two categories - soft-framework crystals and hard-framework crystals [13].

The soft-framework crystals usually have heavy species as the mobile ions. These ions are generally polarizable, the bonding type is, most of the time, ionic, the Debye temperature is low and there is a noticeable phase transition between the low and high conducting phase. These materials are usually solid solutions of double salts [13]. Having a low Debye temperature means that the lattice is not rigid and it is possible to make defects. This temperature usually follows the melting point, so the bonds are generally weak. This is the reason for these ionic solids being called soft-framework crystals.

On the other hand, the hard-framework crystals have covalent bonds, instead of ionic, a high Debye temperature, their mobile ions have a low polarizibility and the phase transition between the two conducting phases is not as noticeable, sometimes being non-existing. These materials are usually oxides and generally have the same compositions and structures [13].

From these two categories, our electrolyte can be classified as a soft-framework crystal. The reason for this classification will be explained in section 2.3.

### 2.1.3 Conduction Mechanisms

As stated before, for the ions in an ionic crystal to leave their original position it is necessary that they receive some energy. This energy is what allows them to jump from one site no another. To make this jump, the ions need to surpass an energy barrier. This quantity of energy is usually denominated activation energy. This energy is the parameter that influences the most the ionic conduction of a material [20]. Its value can be deduced using an Arrhenius-type equation 2.1.

$$\sigma = \sigma_0 e^{\frac{-E_A}{kT}} \tag{2.1}$$

In equation 2.1, $\sigma$ is the ionic conductivity, $E_A$ is the activation energy, $k$ is the Boltzmann's constant, $T$ is the temperature in Kelvin and $\sigma_0$ is the pre-exponential factor. This factor is obtained by a different expression depending wether the crystal's defects are Frenkel or Schottky ones. This pre-exponential factor contains all of the factors that influence the conductivity, aside from the activation energy [20].

Both pre-exponential factor and the activation energy, the later being particularly relevant, are affected by the presence of defects.

The presence of Frenkel pairs means that the ions are allowed to jump to interstitial sites, which should be present in a large scale. The activation energy necessary to jump between these sites should be lower than the activation energy needed to jump between the vacancies. This means that the activation energy for ion migration is higher if Schottky defects are exclusively present, than in the case when Frenkel pairs also exist.

The Nernst-Einstein equation allows to understand the ionic conduction from a different perspective. It relates the diffusion coefficient to the ionic conductivity - equation2.2 [13].

$$\sigma = D\frac{nq^2}{k_B T} \tag{2.2}$$

In equation2.2, $D$ is the self-diffusion coefficient of the ions, $n$ is the ion concentration and $q$ is the charge of each ion.

This diffusion coefficient comes from the first Fick's law, which relates the ion flux, J, to the concentration gradient, $\frac{dN}{dx}$, as shown in equation 2.3.

$$J = -D\frac{dN}{dx} \tag{2.3}$$

There are two factors that influence the diffusivity of ions. One of them is the ion radius. Since the cations usually have a smaller radii, it's plausible to believe that if the ion is smaller, the diffusion is faster. For this reason there are many more solid state materials with cations as the current carrying ions than anions. The other factor that influences the diffusivity is the amount of charge that the ion carries. The Coulombian attraction from the neighbouring ions is more likely to be higher if the charge that the mobile ions carry is larger. This confines the mobile ion to its site with a stronger force, making it harder for it to diffuse. The charge that an ion carries influences the energy barrier that the ion has to overcome to jump between sites. If the charge is larger, this barrier will be larger, making it harder for the ion to leave its site. This is the main reason why almost all of the ions used as mobile ions in solid state ionics have a monovalent charge ($Ag^+$, $Cu^+$, $Li^+$, ...). The only common ion also used that is not monovalent is $O^{2-}$, but the ionic solids that have it as mobile ion are only superionic at high temperatures [20].

There are many models that theoretically describe the ionic conduction in superionic solids, but there is still not an unified theory that explains all the common features of the different types of systems. Agrawal describes seven of these models in one of his articles [13].

## 2.2 Electrochemical Impedance Spectroscopy

Due to its extremely high sensibility and versatility from one side, and simplicity of the needed setup from the other, Electrochemical Impedance Spectroscopy (EIS) has a huge grow in popularity. The range of applications of this technique is wide. It is applied in electrochemistry, biomedical sciences, material sciences, etc. It goes from evaluating electrical properties of materials and interfaces to estimate dielectric properties. It can be used to inspect meat or to test the quality of leather. For this thesis, EIS is important because it allows to analyse ionic conductors in the solid or liquid state, as well as fuel cells, batteries and corrosion [21].

The Electrochemical Impedance Spectroscopy is a technique that measures the response of a system to a current or voltage, at different frequencies. This response is obtained by applying a sinusoidal perturbation to the system. It can be a current or a potential difference, depending if the perturbation is a voltage or a current, respectively. From the current or potential difference measured, using an expression analogous to Ohm's law, it is possible to obtain the complex impedance. The EIS technique also allows to obtain the admittance values of a system, since this physical quantity is the arithmetical inverse of the complex impedance. If these measurements are obtained in a wide range of frequencies, it is possible to study the different processes that occur in a system and classify it, by analysing the resulting plots.

Ohm's law is applied to linear systems that are not time dependent. In systems like the ones used in EIS, where voltage and current have a waveform, thus are time dependent, this impedance is complex.

Instead of the typical relation $R = U/I$, the impedance is related to the current and voltage through the relation in equation 2.4

$$Z_t = \frac{U_t}{I_t} \tag{2.4}$$

In equation 2.4, $U_t$ and $I_t$ are sinusoidal functions given by $U_t = U_0 \sin(\omega t)$ and $I_t = I_0 \sin(\omega t + \phi)$, respectively. In these equations $\omega$ is the angular frequency and $\phi$ is the phase shift. Another expression to the impedance, as a complex value, is $Z = R + jX$, where $X$ is the imaginary part of the impedance and $R$ is the resistance.

Since the admittance is the arithmetical inverse of impedance, if one wants to measure this physical quantity, equation 2.4 becomes equation 2.5.

$$Y_t = \frac{I_t}{U_t} \tag{2.5}$$

The real part of the admittance is called the conductance and the imaginary part is called the susceptance, what makes this physical quantity's general equation be $Y = G + jB$, where $G$ is the conductance and $B$ is the susceptance.

Table 2.1 shows the relations between the different physical quantities relevant for this chapter.

Table 2.1: Important relations between physical quantities

| **Impedance** | **Admittance** |
|---|---|
| $Z = R + jX$ | $Y = G + jB$ |
| **Resistance** | |
| $R = \rho\frac{L}{A}$ | |
| **Resistivity** | **Conductivity** |
| $\rho$ | $\sigma = \frac{1}{\rho}$ |

From here, the rest of this section will describe EIS only as if all the measurements were made for the impedance.

One of the first methods used to measure impedance, before the more modern instrumentation that we have nowadays, used an oscilloscope. In the screen of the oscilloscope one could see the plot of $U_t$ *vs* $I_t$, which is an oval figure, known as Lissajous figure. A schematic of the formation of this figure from the plotting of $U_t$ *vs* $I_t$ can be seen in figure 2.3.

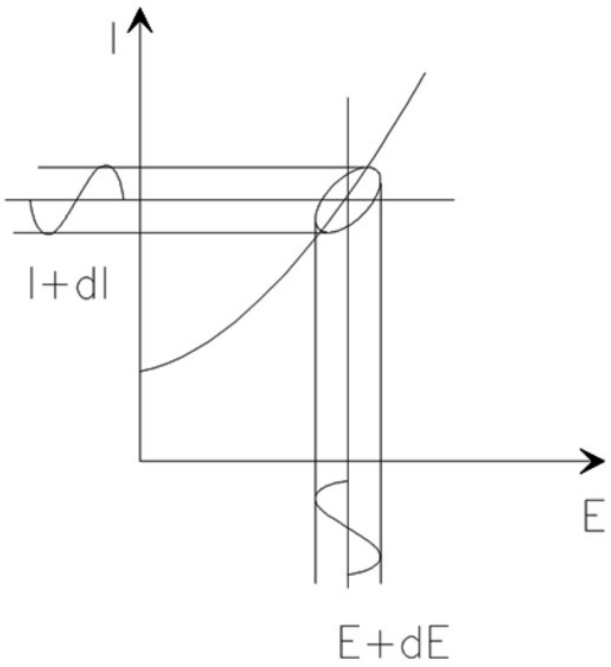


Figure 2.3: Schematic of how the Lissajous figure is formed, resulting from the plot of $U_t$ *vs* $I_t$ . In this figure, $E$ is the symbol for the potential difference, that we have been reffering to as $U$. This figure was obtained from the website *Basics of Electrochemical Impedance Spectroscopy* [22].

From equation 2.4 and using the $U_t$ and $I_t$ functions it is possible to obtain an expression for the complex impedance obtained from both the potential difference and the current in the system.

$$Z = Z_0 \frac{\sin(\omega t)}{\sin(\omega t + \phi)} \tag{2.6}$$

Equation 2.6 can be simplified, using Euler's relationship - equation 2.7.

$$e^{i\phi} = \cos(\phi) + j\sin(\phi) \tag{2.7}$$

Using the relationship in equation 2.7, the potential difference becomes $U_t = U_0 e^{j\omega t}$ and the current becomes $I_t = I_0 e^{j\omega t - \phi}$. Thus, equation 2.6 can be simplified and we obtain equation 2.8.

$$Z(\omega) = Z_0(\cos(\phi) + j\sin(\phi)) \tag{2.8}$$

With the simplification made to obtain equation 2.8, $Z(\omega)$ now has a real and an imaginary part. [22]

If we take the real part and plot it versus the imaginary part, we obtain a Nyquist plot. In this type of plots, the imaginary part usually becomes negative. This results from the fact that we are dealing with capacitances and not with inductivities. In each point of the plot, the value of the impedance is measured at one frequency. The common aspect of a Nyquist plot can be seen in figure 2.4.

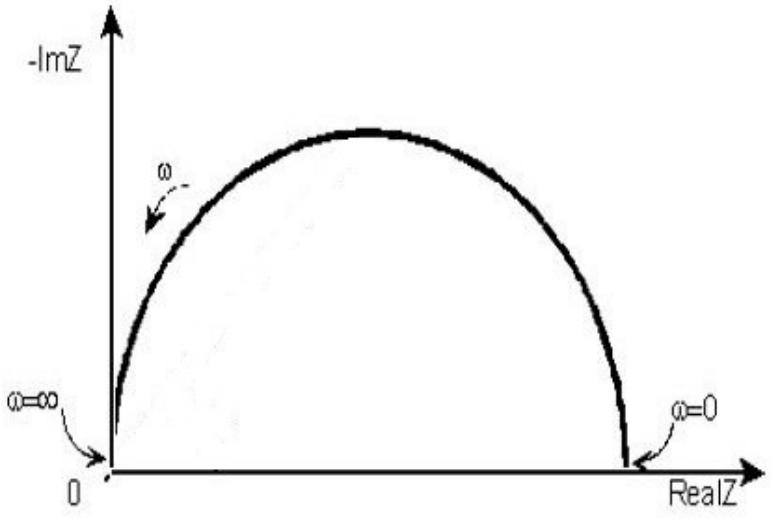


Figure 2.4: Typical Nyquist plot for a system with one time constant. This images was adapted from [23].

Aside from the complex quantity that can be determined from the plot, it is also possible to display the impedance as a vector, known as phasor, using the same Nyquist plot. This vector is defined by the phase angle and the impedance magnitude. The

vector representation of the impedance and the corresponding complex quantity are mathematically equivalent. Both of them can be seen in figure 2.5 [24].

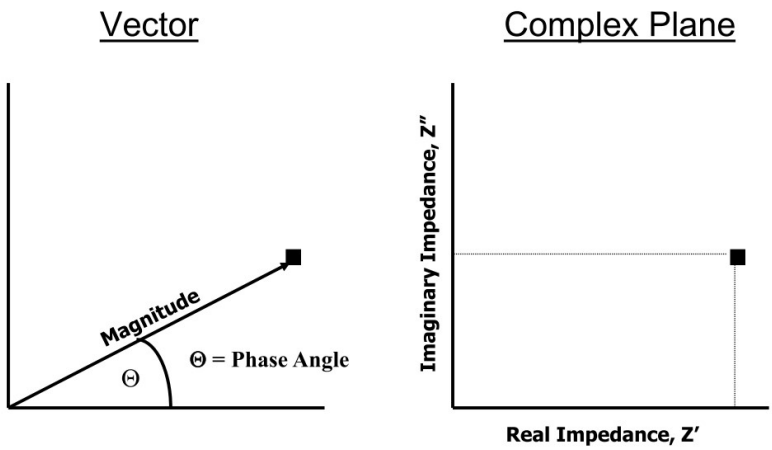


Figure 2.5: Display of the impedance vector and the complex quantity, both mathematically equivalent and determined from Nyquist plots. This figure was obtained from Gamry's presentation about EIS [24].

One of the main disadvantages of the Nyquist plots is the fact that when looking at it one cannot tell at which frequency one specific point was recorded. What is known from the beginning is that the higher frequencies are represented on the left and the lower ones are represented on the right side of the Nyquist plot.

Another way to present EIS results is through a Bode plot. It is obtained by plotting the absolute value of the impedance, or magnitude ($Z_0$), and the phase angle *versus* logarithm of the frequency. This type of plot gives direct information about the frequency in each point. Figure 2.6 shows the typical Bode plot obtained from the same equivalent circuit that results in the plot from figure 2.4.

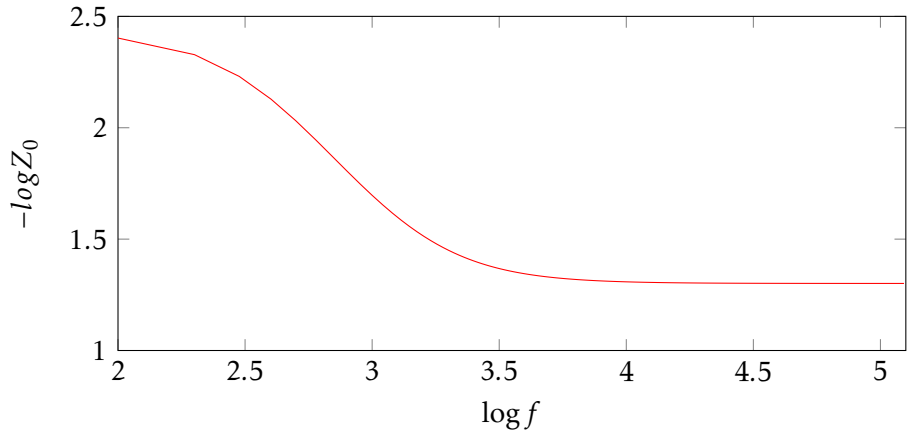


Figure 2.6: Typical Bode plot for a system with one time constant. The phase angle was not plotted.

The semicircle shape of figure 2.4 is characteristic to the circuits with only one time

constant. These circuits are generally represented as an RC circuit.

These equivalent circuits are used to simulate the actual system being studied in EIS. When measuring the impedance of a sample, specially if it is in the solid state, it is necessary to make an electrochemical cell. For that, one needs to attach two electrodes to the system. These electrodes in contact with the system add some resistance to it. Hence, the electrochemical cells that are analysed can be simulated as an electrical circuit. These equivalent circuits are called networks and its EIS response can be calculated and compared with the actual EIS response of the cell. [24]

The three circuit elements used to create the networks are resistors, capacitors and inductors. The impedance of each one is represented by a known expression. These expressions can be seen in table 2.2.

Table 2.2: Expressions for the impedance of the three basic circuit elements that form the networks.

| **Resistor** | **Capacitor** | **Inductor** |
|---|---|---|
| $Z = R\ (\Omega)$ | $Z = -\frac{j}{\omega C}\ (F)$ | $Z = j\omega L\ (H)$ |

Each of these elements has a different phase shift, so the EIS response of each one is different. While a real response is in phase with the applied signal (that is, the resistor's response), the imaginary response will be ±90° out of phase (that is, the capacitor's response or the inductor's response, respectively).

Figure 2.7 shows an example of a network applied to a real system. The sample being analysed is an electrolyte, more specifically a liquid one, and it is represented by the green circles. The sets of green circles surrounding the red ones are the so-called ionic complexes, which are approaching the electrolyte-electrode interface. The electrode is represented in grey, on the left, and its ions are represented in blue. The double layer formed in the interface is only a few *nm* thick and is where all the field is concentrated. The capacitance at the interface is extremely high, due to the small thickness of the double layer. Since the field is concentrated in the interface, it does not penetrate the electrolyte, so that the field inside it is almost zero. This system has only one contact, because the electrolyte is a liquid. Also in figure 2.7, on the right side, is represented the equivalent circuit that simulates the system on the left. These type of networks are called Randles circuits and consist of an active resistor in series with a RC circuit.

The active resistor represents the solution's resistance, while the capacitor of the RC circuit is in parallel with the resistor that represents the polarization resistance (or charge-transfer resistance) between the electrolyte and the electrode. [22]

The Randles circuit is one of the most useful and simple models used in EIS. It can be used on its own or be the starting point to build more complex networks.

The Nyquist plot for this type of circuit is similar to the one shown in figure 2.4, that is, a semicircle. The value of the solution's resistance is read on the high frequency

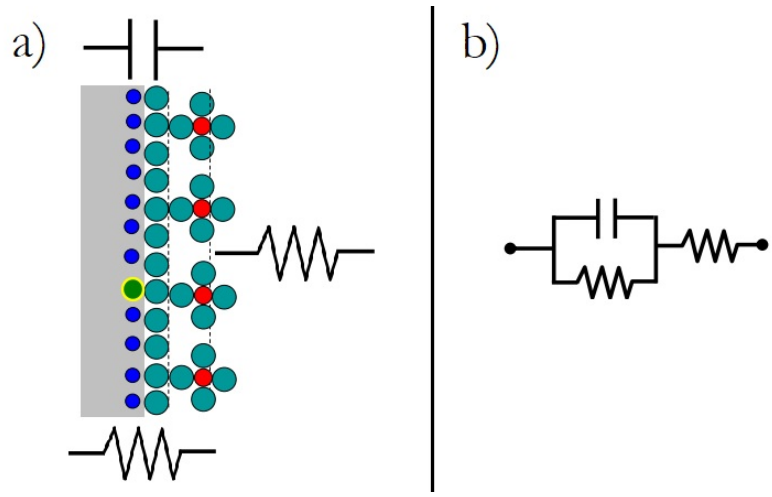


Figure 2.7: a) Network applied to a real system. The sample being analysed is a liquid electrolyte. b) Randles equivalent circuit for the system in a). These figures were adapted from Gamry's presentation about EIS [24].

domain, on the left, where the curve intercepts the X-axis. The value read on that axis is the solution's resistance, hence a real value. The diameter of the semicircle gives the value of the polarization resistance. [22] Figure 2.8 shows a Nyquist plot for the Randles circuit and where to read the value of each resistance. It also shows the Randles circuit, again, but with the identification of the circuit elements.

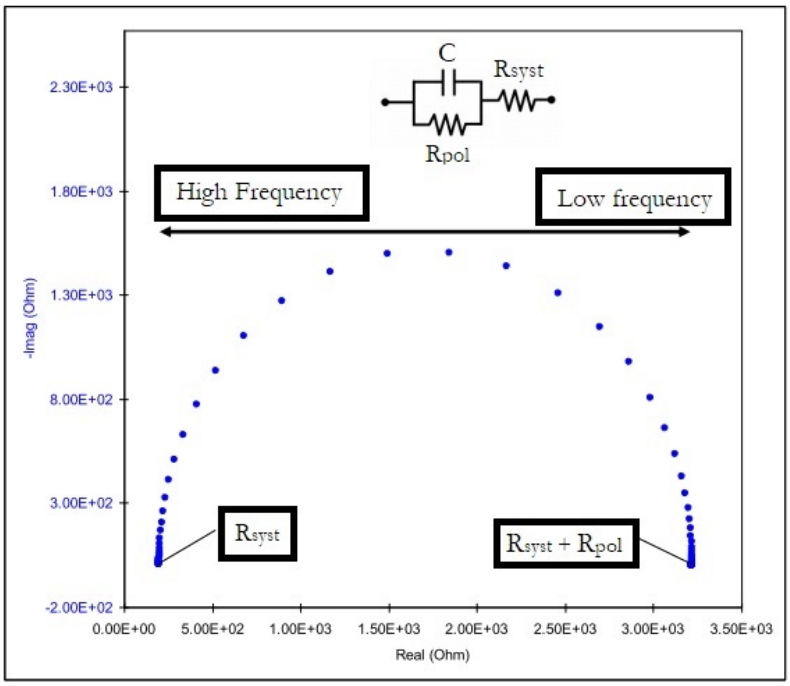


Figure 2.8: Nyquist plot for a typical Randles circuit. It is shown where the solution's resistance value and the polarization's resistance value can be read. This figure was adapted from Gamry's presentation about EIS [24].

From the values of the resistance, read from the Nyquist plot, it is possible to calculate the conductivity values for each part of the system - see table 2.1.

When creating a new network model, each of the circuit elements added should have a correspondence to a specific activity in the cell being studied. However, it is not necessary to build networks that are too complex. The one being used should be the simplest model that fits the data received [24].

One of the most commonly used components that simulates de process of diffusion is the Warburg impedance. This impedance is usually used with the RC circuit and has a 45° phase shift. The Warburg component has a characteristic response in the Nyquist plot, when the mobile species are mainly ions, i.e, the material is an ionic conductor. This response appears on the plot as a tail on the right side of the semicircle that results from the Randles circuit. This tail should make a 45° angle with the x-axis. Being on the right side, this means that the ionic conductivity should be present in the low frequency domain while the electronic conductivity should be seen at high frequencies. If we consider that electrons are smaller and lighter than all ions, it makes sense that their movement is faster, so it can be seen in higher frequencies, while the ions are heavier and bigger, therefore less mobile, so to see their movement it is necessary that the frequency is lower.

The Warburg impedance can be derived from equation 2.9 [25].

$$Z(\omega) = R_{syst} + R_{pol}(1 + \frac{\lambda}{\sqrt{2\omega}}) - R_{pol}^2\lambda^2 C_d - j\frac{R_{pol}\lambda}{\sqrt{2\omega}} \tag{2.9}$$

In equation 2.9, $\lambda = k_f/\sqrt{D_O} + k_b/\sqrt{D_R}$ , and $k_f$ and $k_b$ are the forward and backward electron-transfer rate constants, respectively, and $D_R$ and $D_O$ are the diffusion coefficients for the reductant $R$ and the oxidant $O$, respectively [25]. The frequency-dependent terms $\lambda/\sqrt{2\omega}$ from equation 2.9 are called Warburg impedance and appear both in the real and the imaginary parts of this equation [25]. When the imaginary part is plotted against the real part, with the Warburg impedance component included, the plot of this component is a straight line with a slope of 1. The interception of this line with the real axis is at $R_{syst} + R_{pol} - R_{pol}^2\lambda^2 C_d$. From this interception it is possible to obtain $\lambda$ and if $k_f$ is known and $k_b$ is obtained from another equation (see Park's article [25]), it is possible to calculate the diffusion coefficient [25]. Having the diffusion coefficient value, all the electrochemical system is described.

The typical circuit with a Warburg impedance can be seen in figure 2.9. The typical Nyquist and Bode plots can be seen in figure 2.10.

There are many more models that can be used in EIS. Every contact and process that occurs in a cell can be represented by a circuit element and many different circuits can be built, giving origin to different models. Bauerle shows some models applied to a zirconia-yttria solid electrolyte and explains their meaning in one of his articles [26].

The instrumentation used in EIS consists of a potentiostat and a frequency response analyser. Both of these components are connected to the cell and an external circuitry

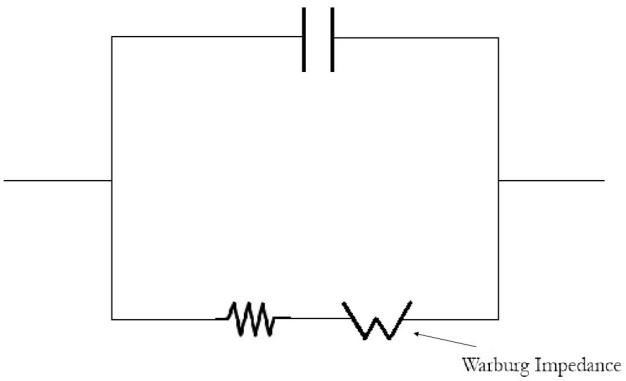


Figure 2.9: Typical Randles circuit including a Warburg impedance.

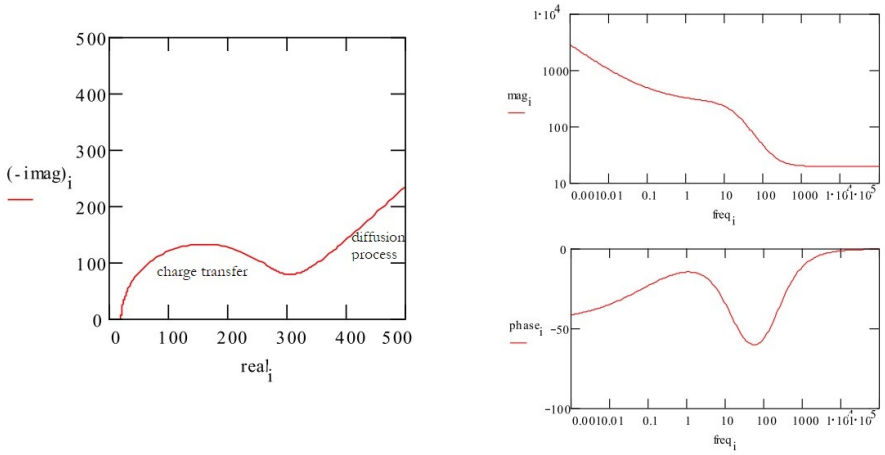


Figure 2.10: Typical Nyquist and Bode plots obtained for a Randles circuit with a Warburg impedance. This image was taken from Gamry's presentation about EIS [24].

is used to apply some DC voltage or DC current that might be needed to measure the properties of some cells. The control of the instrumentation is made by a computer, as well as the storage of data and the display of the results, either graphical or detailed [27].

The potentiostat is the main component of EIS and is preferred over other signal generators since it has many other different elements that are needed for the analysis assembled together. The potentiostat has a power amplifier, which supplies or takes power from the cell, it has at least one high input impedance potential difference measurement reference, a current measurement input, a control loop, which maintains the required potential difference (or current) across the cell, and the potentiostat can be connected to a frequency response analyser, which allows the analysis of the impedance of the cell [27].

The EIS technique has many advantages. Among them is the fact that it has a large frequency range, from $\mu Hz$ to $GHz$, the fact that usually there are analytical models available that can be applied to the system being studied, it is a non-destructive technique,

it provides a lot of information content, it is easy to run and the modeling analysis is pretty useful to adapt the results to the system being analysed [24].

## 2.3 Rubidium Copper Iodide Chloride - $Rb_4Cu_{16}I_7Cl_{13}$

The electrolyte chosen to be used in this work was the Rubidium Copper Iodide Chloride, or $Rb_4Cu_{16}I_7Cl_{13}$.

This electrolyte is a fast ion conductor that has copper(I) ions as the mobile species. Its conductivity is reported to be the highest ionic conductivity at room temperature, of all known solids. This ionic solid was first reported by Takahashi *et al.* in 1979.

It is a highly disordered complex salt and has an anomalous behaviour in the heat capacity and ionic conductivity, which is correlated to the progressive change in the occupancy of the copper sites. The decomposition potential of this electrolyte is low, having a value of $0.69V$ at room temperature. For this reason, this ionic conductor has limitations on its use within solid-state batteries [16]. Besides the low value of the decomposition potential, this material is chemically unstable under atmospheric conditions and has a low melting point. Thus, the applications of this material are limited [16]. However, even though copper is a relatively large atom (aproximatelly 157 *pm* of radii), when it ionizes, the copper ion becomes small, having a radii of aproximatelly 73 *pm* [28]. This fact contributes to the high mobility of these ions in electrolytes like the $Rb_4Cu_{16}I_7Cl_{13}$.

Like Agrawal describes in some of the models referred in his article [13], the crystalline materials that are superionic solids tend to have a rigid framework structure, with an ionic substructure. This substructure is only partially occupied and has a high concentration of vacancies that are meant to be for the mobile ions. The fact that these mobile ions are randomly distributed through the crystallographic sites makes it so that there is a high disorder degree. The fact that these vacancies are energetically similar and are close to each other allows for the ions to jump from site to site in an easy way, making its way through the channels opened in the framework structure [13, 16]. Another model described by Agrawal referred that the ions would be in a "molten" substructure. This would be due to the high concentration of charge carriers and the high ionic conductivity. These factors would make the ionic structure look like it was "molten", many degrees below the melting point of the material. Even though these two models might explain the ionic movement in crystalinne materials, like $Rb_4Cu_{16}I_7Cl_{13}$, the most accepted model is the one that says that the ions jump from site to site and not the one that states that the ions can move through the crystal as if they were in a liquid-like material [16].

There are many reports of analyses made with ionic solids with composition within the $Rb_4Cu_{16}I_{7+x}Cl_{13-x}$ solution in order to determine their structures. The first substance to have its structure determined was the most unstable composition from this family of

solutions - the $\alpha$-$RbCu_4Cl_3I_2$, by Geller *et al.*, in 1979 [29]. This substance belongs to the cubic crystal system and is enantiomorph, that meaning the crystal is mirrored.

In 1993, Kanno *et al.* used neutron diffraction to study the structure of the $Rb_4Cu_{16}I_{7.2}Cl_{12.8}$ [30]. In this study, Kanno *et al.* had interest in determining the *site-occupation factors for the copper ions as a function of temperature* [16]. The data obtained by Kanno's team confirmed the structure previously proposed by Geller's. Warner used the results from Kanno's work to draw the crystal structure for the $Rb_4Cu_{16}I_{7.2}Cl_{12.8}$ phase, at room temperature. The resulting crystal structure can be seen in figure 2.11. The unit cell seen in this figure has a cube edge of $a = 10.0134$ Å. This phase and the one used in this work can be considered the same. The only small difference is that the one shown in figure 2.11 has a slightly higher quantity of CuI, which should slightly increase the ionic conductivity.

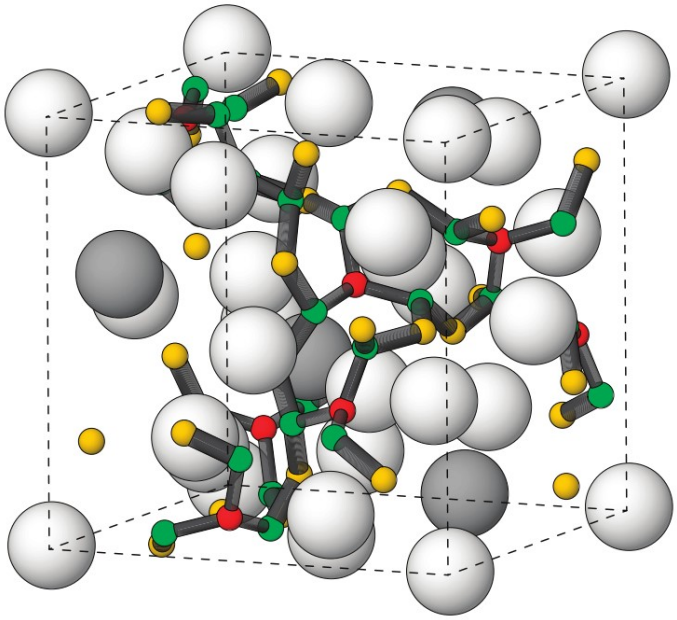

Figure 2.11: Schematic of the crystalline structure of $Rb_4Cu_{16}I_{7.2}Cl_{12.8}$, at room temperature. The grey spheres represent the rubidium ions, the white spheres represent the negative ions, iodide and chloride, and the various types of copper sites are in green, yellow and red (respectively, Cu(1), Cu(2) and Cu(3)). The thick sticks represent the fast conducting pathway Cu(1)-Cu(2)-Cu(1). This figure was obtained from the book *Synthesis, Properties and Mineralogy of Important Inorganic Materials* [16].

There are three sets of copper sites on the structure of the crystal of figure 2.11 - Cu(1), Cu(2) and Cu(3). The Cu(3) sites are arranged in an 8-fold set and the Cu(1) and Cu(2) sites are arranged in two 24-fold sets. Thus, in total, there are 56 sites for the copper ions to be, when there are only 16 copper ions per unit cell. This makes it so that approximately 71% of the sites are vacant. The variation of temperature makes the site occupation factors gradually vary. From this results that sometimes some Cu(3) sets turn into Cu(2) ones, when the temperature increases [16].

The Cu(1) and Cu(2) sites are the ones that form tunnels parallel to the unit cell axis. The Cu(3) sites interconnect the tunnels formed by the other two types of sites. Kanno *et al.* were the first to suggest that the conduction pathway was along the Cu(1)-Cu(2)-Cu(1) sites. They also suggested that the pathways that involved Cu(3) did not give a significant contribution to the total conduction pathways [30].

In figure 2.11 the grey spheres represent the rubidium ions, the white spheres represent the negative ions, iodide and chloride, and the various types of copper sites are in green, yellow and red (respectively, Cu(1), Cu(2) and Cu(3)). The thick sticks represent the fast conducting pathway Cu(1)-Cu(2)-Cu(1) [16].

Using electrolysis, which is considered as one of the best experimental methods that gives direct evidence of the migration of a specific ion in a solid, Warner *et al.* were able to transport copper ions through a $Rb_4Cu_{16}I_7Cl_{13}$ pellet compressed between two copper foils, meant to serve as electrodes. For a duration of $3040s$, at 200 °C, a current density of 37.7 $mA/cm^2$ was passed through the cell. After this time, the group was able to transport 100 $g$ of copper [31]. The fact that the deposit of copper was so extensive was a notorious evidence to the fact that $Rb_4Cu_{16}I_7Cl_{13}$ is truly a copper ionic conductor. The article by Warner also shows that copper migrates from the metal into the electrolyte, as well as from the electrolyte into the metal. This is particularly interesting for at least one of the long-term objectives of this project, since the ion source that is going to be the central part of this project should be self-sustained.

The low value of the decomposition potential of this electrolyte is due to the high mobility (i.e, low electro-positivity) of the copper ion and due to the fact that the iodide ion can be easily oxidised. However, these aspects do not make difficult incorporating $Rb_4Cu_{16}I_7Cl_{13}$ in rechargeable solid-state cells. There are some reports of batteries that use this electrolyte as the ionic conductor and that produce fairly good electromotive forces [32, 33].

Aside from batteries, there is another application of this electrolyte in microelectronics. There are reports of this material being patented as solid electrolyte for use in double-layer capacitors [16]. The fact that these devices have a low leakage current and a high capacity makes them a good candidate to the developing of RAM devices. Also, this electrolyte has already been used to make memory devices in the solid-state. These last devices are similar to the ones made with silver ions, as has been referred in section 2.1.1.

The method through which this ionic solid is synthezied is through a solid-state reaction between three components - rubidium chloride (RbCl), copper iodide (CuI) and copper chloride (CuCl). This type of reaction consist of the diffusion of cations and anions between the different phases of the reactant. The reaction rate depends on the mobility of the ions in the different phases. Since the copper ions are extremely mobile in the resultant phase and have a considerable mobility within the compounds CuCl and CuI,

the solid-state reactions are ideal to synthesize the policrystalline material $Rb_4Cu_{16}I_7Cl_{13}$ [16].

There are different reports on how to synthesise the $Rb_4Cu_{16}I_7Cl_{13}$ solid electrolyte. The first one was reported by Takahashi *et al*. [34] The main problem with synthesizing this ionic solid was the preparation of two of the components needed to make it. The CuCl and the CuI needed to be recrystallized and purified, before being mixed together with the RbCl. This set-back became overrun when these two components began to be commercialized ready to be used. Since then, the experimental procedure to synthesize $Rb_4Cu_{16}I_7Cl_{13}$ became relatively straightforward. The only thing that needs to be kept in mind is the fact that this electrolyte has an incongruent melting point at 234 $\pm$ 5°C. The existence of this melting point at that temperature leads to the necessity to make sure that, when heating the compounds to make the electrolyte sample, the temperature does not reach these values.

The original steps used by Takahashi and his team, if we do not need to previously prepare CuCl and CuI, are listed below:

1. Grind together the three initial components - RbCl, CuI, CuCl - in the appropriate quantities
2. To remove the water, heat the mixture in vacuum or in a nitrogen flow for 12 hours, at 130°C -140°C
3. Press the mixture into a pellet under 300 $MPa$
4. Heat the pellet to 200°C in an evacuated Pyrex tube and then anneal at 130°C

This procedure is the one that can be consulted in Takahashi's article [34], from 1981. However, there are some key points, for example the amount of time that the pellet should be heated, that are not explicit. Thus, there is an article by Warner [31], from 1992, that follows approximately the same procedure but uses a different pressure to obtain the pellets and uses different temperatures for the heating process. Instead of 300 $MPa$, Warner and his team use 220 $MPa$. To bake the pellet, they first heat it up to 230°C for 1 hour and then anneal it at 150°C for 24 hours. Even though this procedure is more explicit than the one reported by Takahashi, it goes to a temperature that is very close to the incongruent melting point of the electrolyte. This fact might become a problem if the furnace used for the heating does not have a precise temperature controller.

The most recent method to synthesize the $Rb_4Cu_{16}I_7Cl_{13}$ electrolyte is also described by Warner in his book *Synthesis, Properties and Mineralogy of Important Inorganic Materials* [16]. The steps to the synthesis described by Warner in his book are listed below:

1. Grind together the correct amounts of the compounds RbCl, CuI, CuCl with an agate mortar
2. Compress the powder mixture into a pellet, under a load of approximately 5 tonnes

3. Place the compressed pellet on a furnace, inside an alumina crucible
4. Place an oxygen getter between the gas inlet and the crucible, to scavenge oxygen as much as possible
5. Flush the air out of the furnace's tube by passing trough it an argon flow for about 30 minutes
6. Reduce the argon flow rate and leave it flowing during the heating cycles
7. Heat the pellet to 200°C at a rate of 1°C per minute
8. After 36 hours, cool the pellet to room temperature, again at 1°C per minute

This synthesis is simpler than the one first described by Takahashi and it is safer to follow than the first one described by Warner. Even though it takes longer to synthesise, the risk that the pellet reaches a temperature close to the incongruent melting point is much lower, since it is less likely that the furnace overshoots from 200°C to 230°C.

Chapter 3

# Experimental Steps

In this chapter, the procedures to the various steps of this work are described. Some of the key results are mentioned, but these results only are discussed in next chapters. The results that made us conclude that a procedure was not good enough might be mentioned and justified in this chapter if the reason for this conclusion does not need further explanation.

## 3.1 Electrolyte Synthesis

In order to obtain the desired electrolyte, three compounds have to be mixed together in the appropriate quantities (mol%): 20 % of rubidium chloride, RbCl, 35 % of copper iodide, CuI, and 45 % of copper chloride, CuCl. These components were ordered from Sigma-Aldrich ready to be used.

To obtain 3 $g$ of this mixture, one needs to weigh 0.53586 $g$ of RbCl, 1.47699 $g$ of CuI and 0.98713 $g$ of CuCl. After weighing all of the three components, it is necessary to grind them together. For the pellets synthesized in this work, an agate mortar was used for the grinding. After mixing the compounds, it is necessary to press the powder into pellets. This step of the synthesis is important so the solid state diffusion is promoted. Thus, the powder was pressed in pellets with 13 mm in diameter. The force applied to make these pellets was 2.2 tons. The 3 $g$ of powder allow the making of three pellets with a diameter of 13 $mm$, each one of them with approximately 1 $g$ and with a thickness of 2 $mm$. For the baking of the electrolyte, various procedures could be followed. Different approaches were used during the months of the work on this thesis. Some were exactly like the ones described in some articles and books, but some of them were adaptations, made to try to obtain the best results from the characterization methods.

- Pellet 1

The electrolyte synthesis was initially made following the procedure described in [31]. The pellet made by this procedure was put under vacuum. The aim was to heat it up to 230 °C for one hour and then let it anneal at 150 °C for twenty-four hours, as described in the article referred. However, the mixture of the compounds started to react with the aluminium from the support and at 186 °C it started to bubble on the edges. For this reason, even though the pellet was left baking at 100 °C for twenty hours, this first synthesis was not successful.

- Pellet 2

  Since the first procedure did not go well, we decided to move to another furnace and, instead of baking the pellet under vacuum, use an argon atmosphere. Also, we changed the support for the pellet from aluminium to an alumina boat. This second pellet had the same mass as the first one, 1.0126 $g$, and was supposed to bake in the same way as the first one, that being, heat it up to 230 °C for an hour and the anneal at 150 °C for twenty-four hours. This time, instead of just following the article previously cited - [31] - we also used some details we found on a book written by the same author that wrote the mentioned article [16].

  What we did was to use a controller to make sure that the temperature rise was made at 1 °C per minute and make sure that before heating the furnace we let an argon flow flush out all of the oxygen in the chamber. For the heating rate, an auto-tune of an Eurotherm controller was made and this controller was programmed so that the heating was made at the rate we desired. We also programmed the controller so that the pellet would stay at 230 °C for one hour and then anneal at 150 °C for twenty-four hours. Unfortunately, the furnace did overshoot and the pellet reached 246 °C. The consequences of this overshooting were the intense smell of iodine and the tube from which the argon was coming out turned brownish.

- Pellet 3

  Given that the synthesis of the previous two pellets did not go as expected, we decided to change the procedure we were using. The pellet used this time had 0.6105 $g$, meaning that it was thinner than the previous ones, since all of them had the same diameter. Even though we used the same furnace and the same controller, we were going to follow the procedure from the book written by Warner instead of the one described in the article written by him. This procedure consisted in heating the pellet only to 200 °C and leave it to bake for thirty-six hours. The heating rate should still be of 1 °C per minute and the argon flow should still be passing through the furnace. The chamber should also still be flushed of air in the beginning. Since we had some overshooting problems with the previous pellet, instead of heating the sample up to the 200 °C mentioned in the book, we decided to heat it up only to 195 °C. This change should not make a big difference in the diffusion process and this way we would be safer from overshooting. Even with all these changes, the

furnace heated up too fast and even though it did not overshoot this time, at least that we have noticed, the pellet still lost some iodine and the tube was brownish again.

- Pellet 4

  We decided that we should change the controller and the furnace and so we went back to the first furnace we used. However, this time we continued using the argon flow instead of vacuum and we still preferred to use the last heating temperature. The fourth pellet we synthesised had 0.9962 $g$ and was heated up to 185 °C. The heating control was made using an Omron PID controller. The pellet was left baking for twenty-three hours. Even though there was a constant argon flow during all the process, this pellet turned out to have a high quantity of oxygen. This did not change the fact that X-ray Photoelectron Spectroscopy (XPS) and X-Ray Powder Diffraction (Powder XRD) analyses revealed good results, concerning what we expected to have. The results of these two analyses will be discussed in the next chapter.

- Pellet 5

  The main problem we were facing was the fact that the pellets are supposed to look brownish and all the ones we had synthesised till then were black or really dark, with exception of the first one that reacted with the support and was not recoverable. For this reason, while we were waiting for the Powder XRD results of the fourth pellet, we synthesised another one. This time, we used a vacuum atmosphere again and decided to use lower temperatures. This pellet had 1.0026 $g$ and even though we left it baking for thirty-six hours at 130 °C, proper diffusion was not accomplished. We concluded this because the pellet was whitish instead of dark, like the previous ones, and when we put it in the XPS for analysis the pressure in the chamber kept going up. This means that some of the components were degassing, probably due to the fact that they did not have time to react with the others the way they should have.

- Pellet 6

  The sixth pellet we synthesised became the best we produced. This pellet had 1.502 $g$. This mass gain was made on purpose in order to enlarge the length/area ratio of the pellet. This ratio being large was important for the conductivity measurements, as will be described in one of the next sub-sections of this chapter. Like pellet four, this sixth pellet was made under an argon atmosphere. We flushed the air out of the tube for 15 minutes before start heating the sample and this time we used a higher argon flow during the whole procedure. We also used an oxygen scavenger (in the form of a bunch of thin copper wire) inside the furnace, on the gas inlet-side and before the pellet's support, in order to minimize oxygen content. We left the pellet baking at 180°C for thirty-six hours. The reason this pellet turned out to be

the best one was that it had much less oxygen and also both the XPS and Powder XRD results came back like we were expecting, once again. These results will be discussed in the next chapter.

- Pellet 7

  The seventh pellet was synthesised in the same way as the pellet six. Even though we did not analyse this pellet in XPS and Powder XRD, since the procedure was the same, the pellet should be as good as the sixth one. This was confirmed by its visual inspection, i.e. the colours of the pellets 6 and 7 were very similar. This pellet was synthesised to repeat some conductivity measurements. Its mass was $2.100g$ and the thickness was the greatest of all. The reason for this was to increase the length/area ratio of the pellet. This change should increase the resistance, even though the resistivity remained invariant. This should make the EIS measurements easier, since it allows more of the semicircle to be visible.

## 3.2 Tip Preparation

The tips were prepared from a block of copper. Each of them had 2 mm in diameter and 20 mm in length. The preparation of the tips was made so that they had an opening angle of 30°.

The first three tips were cut so the length was 15 mm instead of 20 mm. This shortening of the tips was made so that less of the body of the tip was out of the set screw contact used to support it, as can be seen in figure 3.1. The set screw contacts used are from Hositrad and their schematic can be seen in figure 3.2.

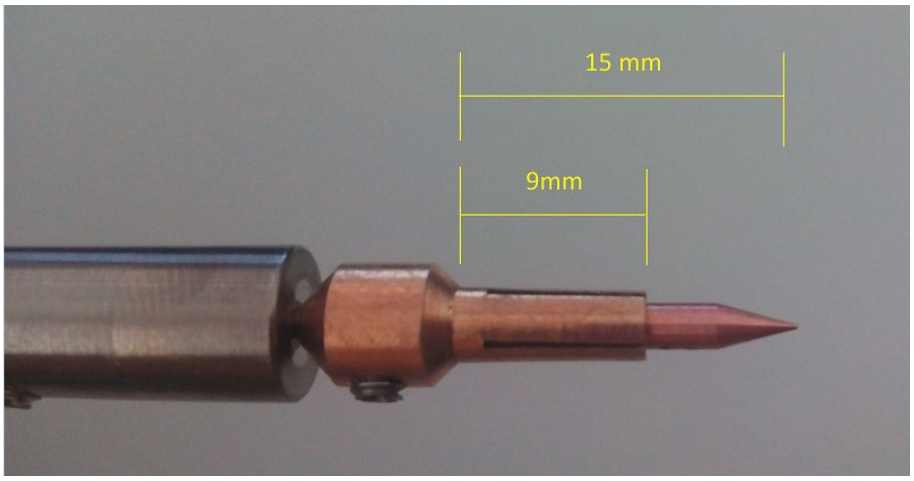


Figure 3.1: Copper tip in the set screw contact used to support it.

For the sharpening of the tips we put them on a rotary tool rotating at a high speed, then we approached them to sandpaper, first grit 800 and then grit 1000. The result of this sharpening can be seen in figure 3.3, taken by an optical microscope, where one of the six tips prepared is shown.

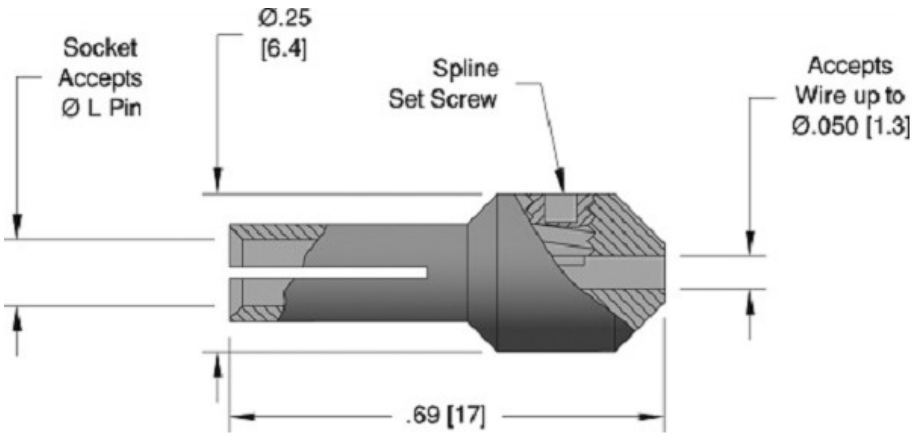


Figure 3.2: Set screw contact schematic from Hositrad [35]. The measures are in inches.

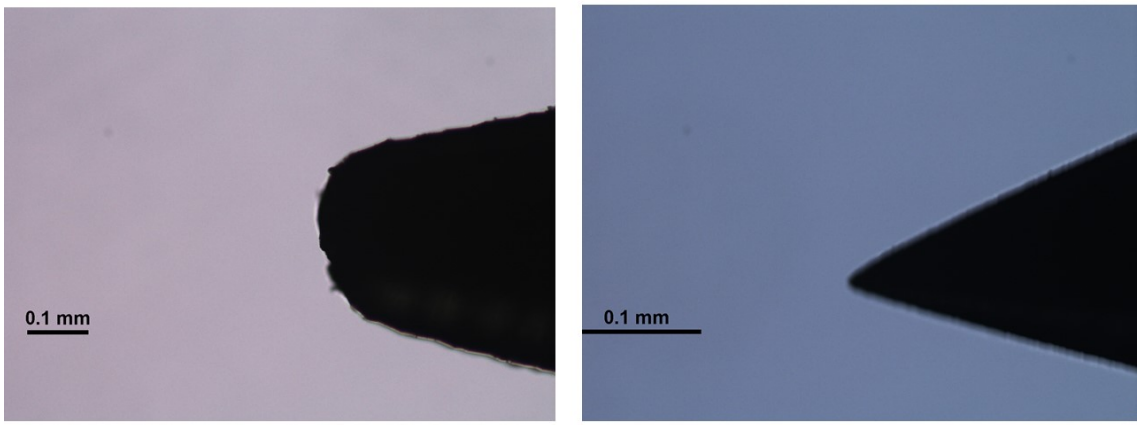


Figure 3.3: Optical microscopy of tip 2 before (left) and after (right) the sharpening.

## 3.3 Electrolyte Deposition

Different approaches were made to see which one delivered the best results, concerning the deposition of the electrolyte on the tip. In this section, the approaches will be described.

### 3.3.1 Synthesis and Posterior Deposition

The first method used to deposit the electrolyte on the tip consisted in having the powder already baked and then compressed around one of the copper tips. In order to promote the adhesion, the tip should be annealed after the compression. The setup used to do so can be seen in figure 3.4.

a) b)

Figure 3.4: Setup used to anneal the electrolyte around the tip. As shown before, the tip was supported by the set screw contact - figure 3.1.

This method proved to be inefficient since the powder did not adhere onto the tip after the annealing. For this reason, we tried to use another setup to anneal the powder around the tip. This new approach consisted in having the powder compressed in a ceramics and then dip the top of the tip in it. This setup can be seen in figure 3.5.

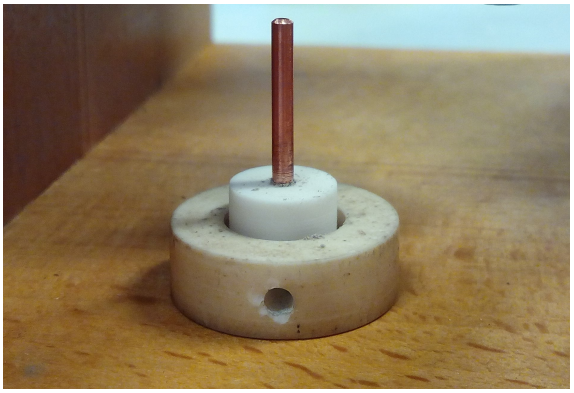

Figure 3.5: Second setup used to try to anneal the powder around the tip.

### 3.3.2 Simultaneous Synthesis and Deposition

This method is similar to the one described in the previous section, for the deposition of the electrolyte already synthesised. Only this time instead of using the baked powder, we used raw one. We compressed this powder around a copper tip and then baked it, in order to try and promote the adhesion while the diffusion occurred, for the electrolyte synthesis. The baking was made at 180 °C , in an argon atmosphere, for thirty-six hours,

the same procedure used to produce tip six. However, this method proved to be inefficient too, just like the one with the electrolyte already synthesised. The setups used were the same we had used for the deposition described in the previous sub-section - figures 3.4 and 3.5.

### 3.3.3 Acetone suspension

The acetone suspension method consisted in suspending raw powder of the electrolyte in analytic acetone. We dipped the two copper tips in this solution and then used a hot air blower to promote the acetone's evaporation. We then proceeded to bake these tips using the same procedure described before, the one used to produce pellet six. The results were not perfect, since the deposited electrolyte was not regularly distributed and there was too much electrolyte on the tip, but we did use one of the two tips covered in electrolyte that had resulted from this process to move forward with our copper ion emission tests.

### 3.3.4 Evaporator

Even though the acetone solution allowed us to move forward with this work, we decided to improve the deposition method. With that purpose and following the idea presented in Soga and Kuwabara's article [36], an assembly with an evaporator was built.

The material used for the part that supports the electrolyte (the evaporator itself, or crucible) was Macor ceramics, since the powder reacts with aluminium, as we could confirm with the first pellet we made. This part also has a thread around its body that serves to support the tungsten wire wrapped around it. This wire works as a resistance heater, when there is an electrical current through it. Figure 3.6 shows the final form of the evaporator. Although it is not visible in the photo, the ceramic has a hole for mounting the thermocouple used to control the temperature of the ceramics and another hole that allows fixing the evaporator to the rest of the assembly.

Figure 3.6: Evaporator made out of Macor ceramics. The image shows the cuts made on the part to put the Tungsten wire around the evaporator.

Along with the evaporator, we built the sample holder. This part is made of aluminium and includes two claws from the same material, that have the purpose of holding in place the glass plates onto which we desire the electrolyte to be deposited. It also has the capability of holding two tips, since our main purpose with this evaporator was to obtain the best method to deposit $Rb_4Cu_{16}I_7Cl_{13}$ onto the tips. This sample holder is heated by a resistance of approximately 200 Ω. Figure 3.7 shows a photo of the sample holder, with a glass plate into place. This picture was taken after one of the depositions we made using the evaporator.

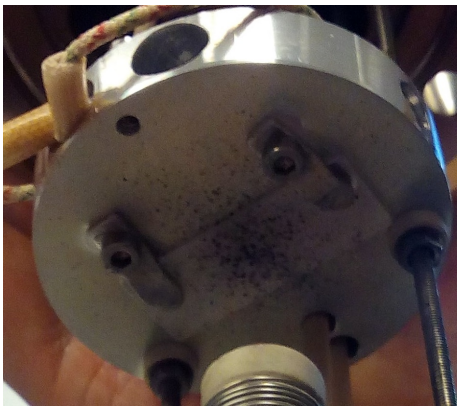

Figure 3.7: Sample holder made out of aluminium. The image shows a glass plate into place, held by the claws.

The whole assembly was put together using an ultra-high vacuum compatible flange as a support. This made the system compact and simple for mounting into the vacuum chamber in which the depositions were preformed.

The initial plan for the electrolyte deposition was to follow the procedure described in [36]. Previously synthesized powder is put in the evaporator and heated up to a temperature between 500 °C and 650 °C, under vacuum, so the electrolyte evaporates. On top of this, at a distance of 3 *cm*, is a glass substrate onto which the evaporated film is going to be deposited. When the electrolyte evaporates, it partially decomposes. For this reason, it is necessary that the glass slide with the deposited film is heated up again, this time to a lower temperature. Since we want the electrolyte to be fully functional and we know that it has a critical point at around 235 °C, as mentioned in chapter 2, we heated it up to a maximum of 200 °C.

Instead of heating up the evaporator to 650 °C, we decided to do different evaporations, using different temperatures. We started by going to a temperature of 590 °C to deposit a film onto a glass plate. Then we began to try to obtain thin films at lower temperatures. We evaporated our material onto two tips at 420 °C, having annealed the tips afterwards. We also tried to deposit a film onto a glass plate at 300 °C and at 200 °C. As expected, at 200 °C no film was obtained.

After these depositions, we decided to clean the system, by heating it up too 695 °C,

without electrolyte powder on the evaporator. When the cleaning was done, we repeated the deposition at 300 °C, to observe if there were any differences between the previously film obtained at 300 °C and this new one.

Figure 3.8 shows the whole assembly for the evaporation and a close-up for details of the evaporator part and the sample holder. The claws to hold the glass slide can be seen on the close-up, as well as the three holes made to hold three tips, in order to deposit electrolyte onto them. Only two of these holes became usable.

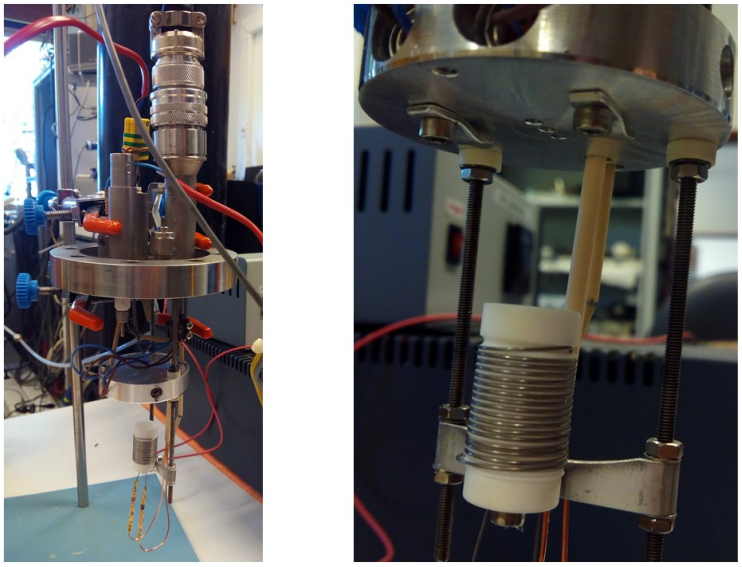

Figure 3.8: Evaporator assembly, on the left, and close-up on the evaporator and the sample holder, on the right.

## 3.4 Copper Emission

### 3.4.1 Ion Field Emission Setup

The main objective of this thesis was to prove that it is possible to have emission of copper ions from a copper tip covered by a copper-based solid electrolyte. To do so, the different parts needed to do the experiment had to be designed and manufactured. In this section, the different designs and the final assembly are described and shown. Also in this section will be described the simulations made in the software SIMION. These simulations were made to study the best positioning of the tip regarding the substrate, in order to have the highest electric field. The ion collector was made of graphite.

#### 3.4.1.1 Designs

The two main parts of the experimental assembly were the substrate's support and the tip's support.

One of the major features that we wanted to be able to get in the substrate's support was the possibility to move it forward and backwards during the experiment, i.e. while the whole assembly was under vacuum. For this reason, the body of this support was built around a linear motion feedthrough from MDC. Figure 3.9 shows a photo of the feedthrough with the M6 thread already made, to hold the body of the substrate's support.

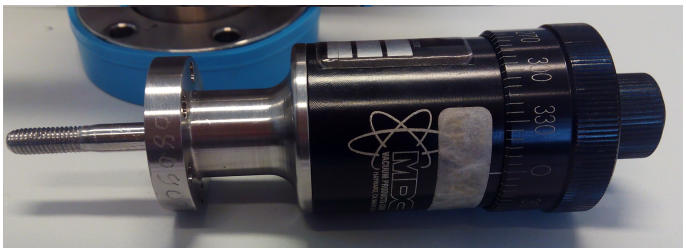

Figure 3.9: MDC's feedthrough with an M6 thread, used as to hold the body of the substrate's support

Another aspect that required some thinking was the fact that we needed the substrate to be isolated from the rest of the support. The reason for this was the fact that the current measured in the substrate was what was going to tell us if we had any emission from the tip. Also this substrate should be inside a Faraday cup, in order to properly measure the ion current. The isolation of the substrate from the rest of its support was made by using two ceramics.

The tip's support did not require the fabrication of any new parts, only the adaptation of a part used by Fábio Fernandes in his master thesis. [9] This small adaptation came from the fact that we wanted to use the set screw contacts that would support the tip in the opposite direction that Fábio did in his work. For that, the diameter of the top of the high-voltage contact was reduced. In figure 3.10 is shown the set screw contact used to hold the tip and it is possible to compare its orientation in this work and in Fábio's. On the right, it is also shown the high-voltage feeder used in both works.

#### 3.4.1.2 Assembly

The whole assembly was built using a double sided flange as the main body. The two main parts, the tip's support and the substrate's support, needed to be in front of each other, with the tip pointing in the direction of the substrate. In order to measure the current on the substrate, it was necessary to make a new opening on the side of the flange. In this opening, we put a BNC plug that was going to make the connection to the electrometer.

Figure 3.11 shows the final assembly used to perform a deposition test, with the tip and the graphite substrate in place.

#### 3.4.1.3 SIMION Simulations

As referred in chapter 1, for an ion to be emitted with high probability it usually needs an electric field of the order of $10^9$ volts per meter $[V/m]$. Our main objective with the

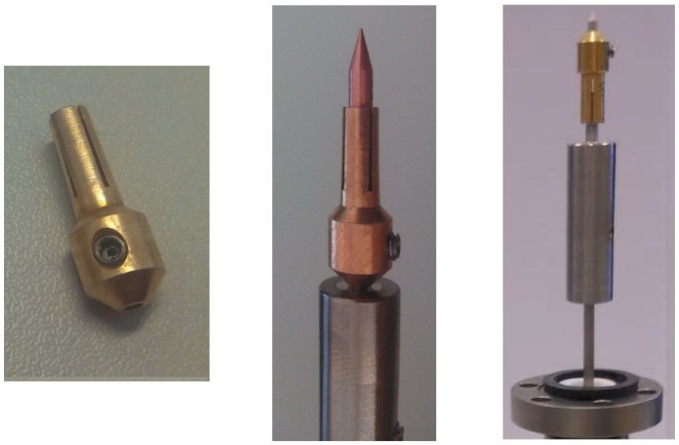


Figure 3.10: a) Set screw contact used to hold the tip. b) The set screw contact holding the tip. c) Fábio's tip holder and the high-voltage feeder used both in his work and in this one [9].

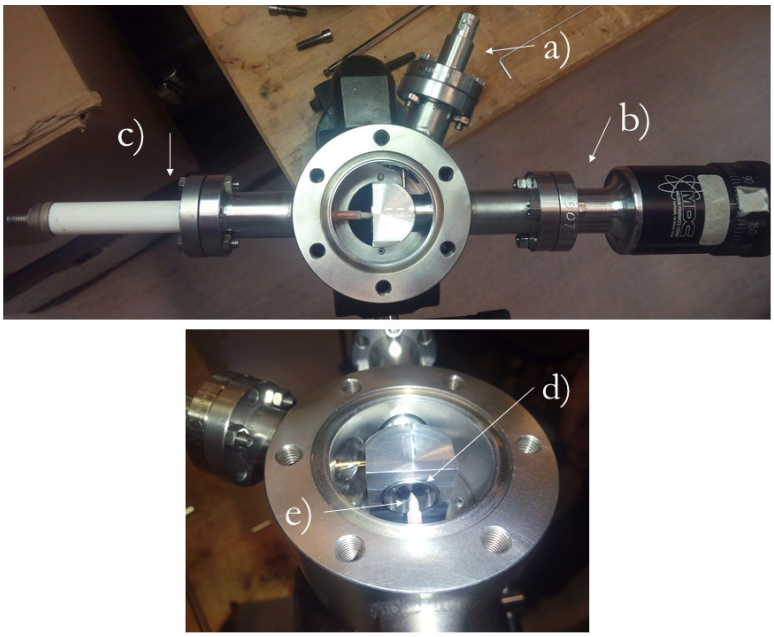


Figure 3.11: a) BNC plug b) Feedthrough holding the substrate and the Faraday cup c) High-voltage feeder connected to the set screw contact that holds the tip d) Graphite substrate e) Tip covered in the electrolyte

SIMION simulations was to see if we were going to have fields of that order. To do so, we did four simulations, each one differed from the others in at least one parameter. The parameters we took into account were the tip's apex diameter, its sharpness, i.e, the aperture angle on the apex, and distance to the substrate. We also applied different voltage values on the electrodes, these being the tip or the substrate. The final values of the fields presented below are the ones obtained when applying a voltage of 10000 V on the tip.

Figure 3.12 shows the four different setups we used to run the simulations.

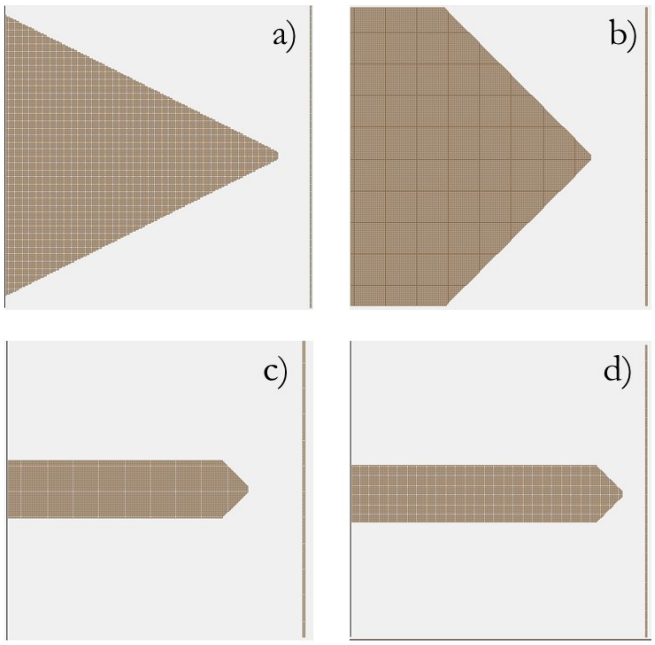


Figure 3.12: Four different setups for the simulations made in SIMION.

Tip a) had an apex diameter of 40 $\mu m$ and was positioned at 0.1 $mm$ from the substrate. Its shape was the second most sharpened, that is, it had the second smallest aperture angle on its apex. Tips b), c) and d) had and apex diameter of 17 $\mu m$. Both tips b) and c) were at 0.1 $mm$ from the substrate, like tip a). Tip d) was the one that was the closest. Its distance to the substrate was of only 0.04 $mm$. Tip's c) and d) shapes were similar and these were the sharpest ones. The fields we obtained were all of the order of $10^8$ $V/m$. The highest field was from tip d) and had the value of $7.265 \times 10^8$ $V/m$. Tips b) and c) had a similar field value - $4.538 \times 10^8$ $V/m$ and $4.883 \times 10^8$ $V/m$, respectively. Tip a) was the one with the lowest field. Its value was of $3.529 \times 10^8$ $V/m$.

- Tips' size

  From the simulations we could conclude that the tip's apex diameter has a high influence on the electric field. The bigger the tip's apex diameter, the lower the field. This can be confirmed from the fact that the field from tip a) was the lowest one.

- Tips' shape

It was also possible to conclude that if a tip is sharper it is more probable that its field is higher. However this increase is not as noticeable as the one we saw with the changing in the tips' apex diameter. For example, if we compare the field from tips a) and b), its values are much more distant than the field values from tips b) and c), that are almost the same.

- Tips' distance to substrate

  Comparing the fields from tip c) and d) and knowing that these tips were similar, we can conclude that the distance between the electrodes also contributes for the electric field. When we bring the tip closer to the substrate, the field gets almost twice as strong.

Even though these simulations allowed us to learn with which parameters we should play in order to increase the field, we did not obtain electric fields in the order of $10^9\ V/m$. The tip's radius should be the key point to obtaining high electric fields and this radius can be defined by the tip's apex diameter and its aperture angle. From this fact, we can conclude that our tips should have a smaller radius than the ones we simulated in SIMION.

### 3.4.2 Emission Test

After all the components of the experimental assembly were ready, the tip was covered with the electrolyte and the graphite substrate was in place, we were able to mount everything in the preparation chamber of the Time-of-Flight Secondary Ion Mass Spectroscopy (ToF-SIMS). The substrate approach to the tip was made carefully and we stopped the approaching when the distance between the two was less than 1 $mm$. The final position of the tip and the substrate can be seen in figure 3.13.

An electrometer was connected to the BNC plug and a high-voltage power supply was connected to the high-voltage feeder that was supporting the tip.

After all was plugged-in, we started to apply some voltage. When we hit a value that we saw that gave us some current and that its value was relatively constant, we started over so we could record the current values. By connecting a data acquisition system to the electrometer and to a computer, using the right software to work with this data logger we could save the data obtained. In order to be able to make an IV plot, we varied the applied voltage for a fixed amount every ten seconds. This way we could later take the values saved by the data acquisition system and then replace time with voltage, since we knew when we were increasing it.

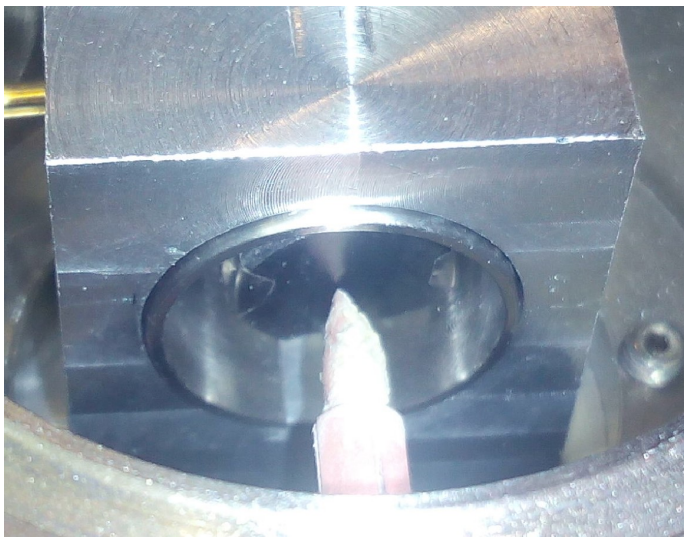

Figure 3.13: Final positions of the tip and the substrate.

Chapter 4

# Experimental Results and Analysis

In this chapter, the results from the different procedures used in this work are presented and analysed. The techniques used to analyse the electrolyte pellets, the glass plates and the graphite substrate are briefly explained, as well as the reasons to use them in these analyses.

## 4.1 Electrolyte Characterization

### 4.1.1 X-ray Photoelectron Spectroscopy

X-ray Photoelectron Spectroscopy, or XPS, is a technique that allows to identify and quantify the elements on a surface, as well as to determine chemical bonds. By directing an X-ray beam to the sample's surface, its atoms will emit photoelectrons. If we know the energy of the incident X-ray beam and the energy with which the photoelectron emitted reaches the detector, it is possible to infer the level from which it came from. Knowing this energy, one can identify the elements present on the surface. Since this technique has a high surface sensitivity, the obtained spectra correspond to surface atoms situated in the first few nanometres of the sample. This is both and advantage and a disadvantage of this technique: it is a great tool to analyse surface's compositions, but it will not give information on the composition of the bulk of the material.

One way of identifying chemical states with XPS is the Auger parameter technique. The Auger spectra have unique peak positions and shapes, which makes them useful to identify elements and chemical states, like oxidation. From the Auger and the photoelectron peak positions, it is possible to calculate the Auger parameter. This parameter is not affected by surface charging [37].

From what has been described above, it is easy to understand why this technique was

used on this work. We wanted to make sure we had synthesized the right electrolyte. To do so, we needed to see if we had the right elements on the pellet's surface and if their proportions were in accordance with the expectation. We also determined the Auger parameter, in order to reveal which oxidation states of copper were at the surfaces of three of our pellets - one before baking and two after baking. For this, we took the position of the copper $L3M4,5M4,5$ peak and the position of the copper $2p_{3/2}$ peak and calculated the modified Auger parameter as the sum of the binding energy of the photoelectron peak and the kinetic energy of the Auger peak. We then compared our value with the reference ones for different copper compounds.

The XPS spectra were obtained with Mg$K\alpha$ line, which corresponds to a photon energy of 1253.60 $eV$.

All of the produced pellets were analysed by XPS, except the first one, that reacted with the aluminium, and the seventh one, that was synthesised the same way as pellet six, so the results should be the same.

When analysing the XPS spectrum from a pellet that had not yet been baked, using modified Auger parameter technique, we concluded that the surface of that pellet had CuI on its surface. That means that we had Cu(I) oxidation state together with iodine. The obtained value for the modified Auger parameter was 1848.57 $eV$, while the reference value for the modified Auger parameter of this compound is 1848.55 $eV$ [38]. The proximity of these two values allowed us to conclude that we had the CuI compound on the surface of our pellet.

Pellet two was the first baked pellet we analysed. We could conclude that the iodine peak was not in the XPS spectrum of this pellet. This confirmed that while this sample was baking, the overshooting of the furnace to 246 °C did cause the iodine to evaporate, which we observed as the change of the exhaust tube colour, described in chapter 3.

Nonetheless, we wanted to confirm that we had Cu(I) oxidation state of copper in our electrolyte's surface, since Cu(II) oxidation state would reduce its conductivity value. For that, we calculated once again the Auger parameter. The obtained value was 1847.60 $eV$, which is really close to the reference Auger parameter value for the CuCl compound - 1847.40 $eV$ [39]. The fact that the reference Auger parameter value for $CuCl_2$ is 1850.40 $eV$ [40], which is not close to ours, allowed us to confirm that we indeed had $Cu^+$ ions on our electrolyte's surface instead of $Cu^{2+}$ ions.

Pellet three had all the components we expected to have - rubidium, copper, iodine and chlorine - but its quantities were not in the right proportions. Besides, presence of carbon and oxygen were also detected, which could be considered as standard surface contaminants. Since the colour of the pellet on the surface was different from the colour on the inside, we analysed this pellet before and after scratching its surface. The need to scratch the surface in order to analyse deeper layers of the material comes from the

already referred fact that XPS has a high surface sensibility, i.e it analyses the surface of the material without taking into account the contribution from bulk atoms.

The only difference between the two spectra was the intensity of the oxygen and the carbon peak - the scratched pellet showed less intense peaks for these two elements. Otherwise, all the elements were present and their relative quantities were approximately the same. The XPS spectra obtained from this pellet were very similar to the ones obtained from pellet four.

Pellet four was the one that apparently had the better XPS results. The proportions between elements were almost as expected. However, the pellet still had a fair amount of oxygen in its constitution. In figure 4.1, we can see the spectrum obtained from this pellet. Besides the four elements of the electrolyte, we can still observe an oxygen and carbon peaks. These two impurities constituted more than 50% of the pellet's surface content: it had about 13.7% of oxygen and about 49.3% of carbon. After renormalizing the element quantities, without the impurities, the obtained values were closer to the expected ones. The percentage of each element on the pellet's surface, after this renormalization, can be seen in table 4.1, as well as the expected values.

Table 4.1: Elemental percentages in pellet four, after renormalization to four elements.

| | **Rubidium** | **Copper** | **Iodine** | **Chlorine** |
|---|---|---|---|---|
| **Experimental** | 9.3 | 64.4 | 10.8 | 15.5 |
| **Expected** | 10 | 40 | 17.5 | 32.5 |

These values were not exactly what we expected, but we also knew that when analysing with XPS the quantities of each element, they come with an experimental error associated.

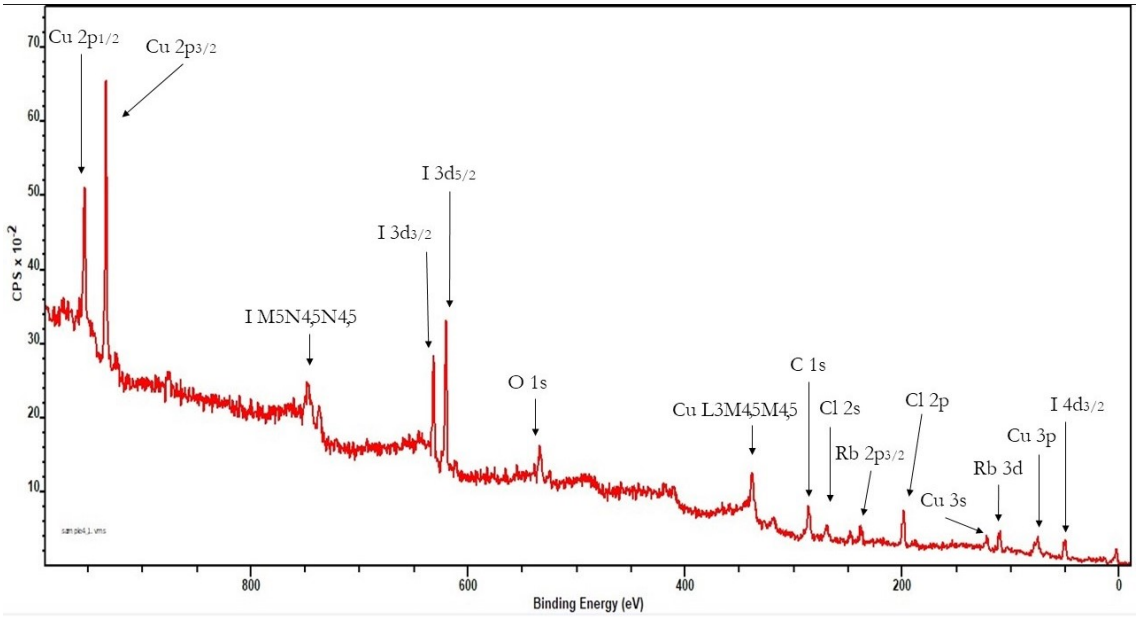


Figure 4.1: XPS spectrum obtained from pellet four. A peak of oxygen can be seen.

Pellet five did not allow us to conclude anything about its composition, since the diffusion reaction between the components of that pellet did not end. We could confirm this by seeing that the pressure of the analysis chamber was always going up, which meant that some of the components were being released from the surface.

Pellet six had all of the components almost in the right proportions. The spectra obtained for this pellet can be seen in figure 4.2.

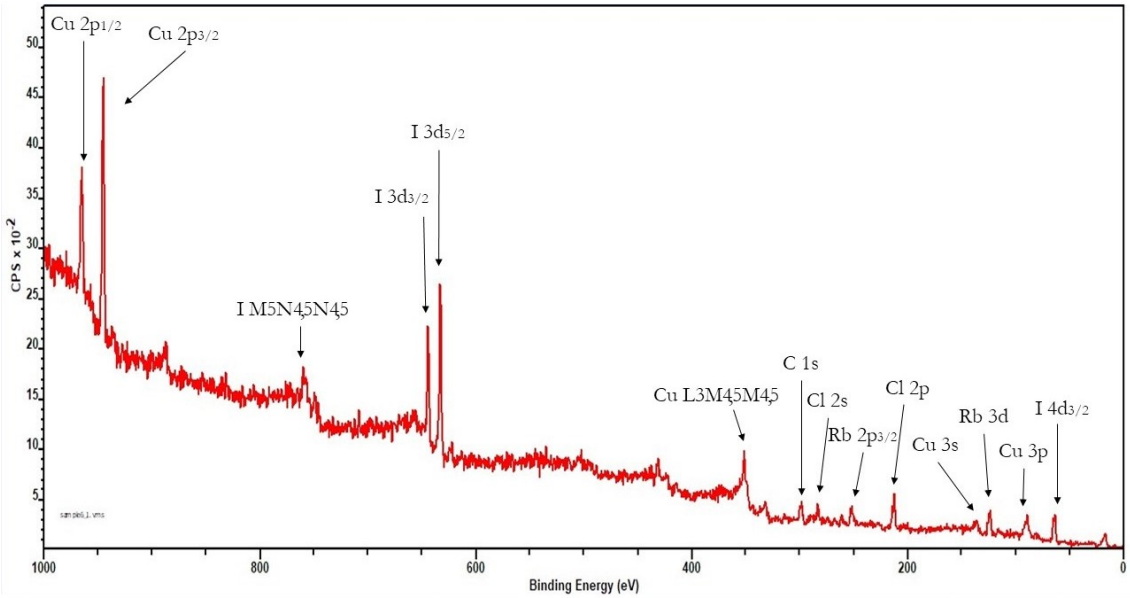


Figure 4.2: XPS spectrum obtained for pellet six. The oxygen peak is not visible.

The amount of oxygen was almost five times lower than in pellet four, as can be confirmed by the fact that the spectrum from this pellet has no visible oxygen peak, unlike the spectrum from pellet four - figures 4.2 and 4.1, respectively. The amount of carbon on this pellet's surface was about 21.1%. The percentages of each element present on the pellet's surface, after the renormalization to four elements, as well as the expected values can be seen in table 4.2.

Table 4.2: Elements percentages in pellet six.

| | **Rubidium** | **Copper** | **Iodine** | **Chlorine** |
|---|---|---|---|---|
| **Experimental** | 11.7 | 43.2 | 14.9 | 30.2 |
| **Expected** | 10 | 40 | 17.5 | 32.5 |

Since this pellet seemed to be the best one we produced, we also checked if we had CuCl on the electrolyte's surface, instead of $CuCl_2$. The reason for this was, once more, to make sure that we had $Cu^+$ ions and not $Cu^{2+}$ ions in the composition of our sample's surface. The obtained value for the modified Auger parameter was 1847.53 $eV$, which is again almost coincident with the reference value for CuCl - 1847.40 $eV$ [39]. Thus, we could confirm the presence of $Cu^+$ ions on our electrolyte's surface.

In conclusion, we can say that the peaks of the elements of the electrolyte can be identified in both spectra, but their percentages are different - tables 4.1 and 4.2. Pellet six had the values that were closer to the expected ones. We can see that the oxygen peak disappeared, from the spectrum of pellet four to the spectrum of pellet six - figures 4.1 and 4.2.

### 4.1.2 X-ray Powder Diffraction

X-ray Powder diffraction, or Powder XRD, is a technique used to identify the phase of a material and provide information on its crystalline lattice. The fundamental principle of XRD is the constructive interference between two X-ray beams scattered from two different atomic layers. The constructive interference of these scattered beams from two paralel planes of atoms results in the diffraction of the beams. If the path difference of the radiation from successive planes is an integer number, $n$, of wavelengths $\lambda$, the diffracted beam satisfies Bragg's Law - equation 4.1 [18].

$$n\lambda = 2d\theta \tag{4.1}$$

Knowing that $\lambda$ is the wavelength of the X-rays and $\theta$ is the diffraction angle, we can easily calculate the crystal plane separation of the analysed material, or lattice spacing, $d$ [41] .

By scanning the crystalline material in different angles, a different and unique diffraction pattern is obtained for each material. The diffraction pattern is obtained by plotting the intensity of the diffracted X-ray against the angle $2\theta$ (see figure 4.3). This pattern can then be compared with reference ones to identify the analysed material.

The configuration used for the analysis of our pellets was in $\theta - 2\theta$. Thus, when the incoming angle is changed by, for example, 1° the same goes for the outgoing angle (that is, the detector also moves). The peaks in the XRD patterns are evidence of crystal periodicity. When using the type of configuration used to analyse our pellets, we look for this periodicity in the direction normal to the sample's surface.

The advantage of Powder XRD in relation to conventional XRD is the fact that this technique allows to obtain a diffraction pattern for the whole sample instead of just a single crystal. It also allows to obtain the pattern of the bulk material, if the powder is from a crystalline solid [42].

The analysis of our different powders were made on the Chemical Analysis Laboratory, in the Chemistry Department of Faculty of Sciences and Technology, NOVA University of Lisbon. The equipment used was a RIGAKU MiniFlex II, with a K$\alpha$ X-ray tube. All of the analysis were made with a scanning rate of 1° per minute, with a 0.02° step, and with $2\theta$ varying from from 10° to 55°. Figure 4.3 shows a schematic of the experimental setup of Powder XRD technique.

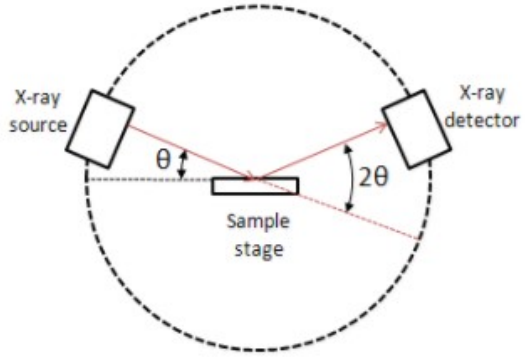


Figure 4.3: Schematic of the setup for the Powder XRD analysis. The scheme was obtained from [42].

Four different powders were sent to analysis. One of them was just the mixture of RbCl, CuI and CuCl and the other three were from pellets we had synthesised, more specifically, from pellet three, four and six. The reason for choosing pellets four and six was the fact that pellet four showed good results in XPS, despite the quantity of oxygen, and pellet six showed even better results in XPS, with much lower quantities of oxygen. Pellet three was sent to analysis after the results from pellet four were received. The reason to send this pellet afterwards was to compare it with pellet four, since they both seemed similar in XPS. Pellet three was the one we thought that had lost some iodine, thus we did not think it was good enough to send to Powder XRD analysis. Since the results of pellet four had returned like they should, we decided to send pellet three too, to compare both. It turned out that their diffractograms were also similar, like the XPS spectra.

Figure 4.4 shows the diffractogram obtained for the powder mixture of the compounds necessary for the electrolyte synthesis. We sent this powder to analysis in order to be able to identify the differences on the phase of the powder before and after the baking. In this diffractogram, we can clearly see the peaks of CuI and CuCl and we can also conclude that they did not react with each other. The reference diffraction pattern of RbCl could not be found in any literature, in order for us to see if its main peaks were visible in the spectra, but they should be present, just like the main peaks of the other two components.

Figures 4.5 and 4.6 show two digractograms for the synthesized powder of the desired electrolyte. Figure 4.5 was obtained from Terence Warner's book already mention in chapter 2 [16]. This image shows the diffractogram obtained by Warner for $Rb_4Cu_{16}I_7Cl_{13}$ overlapped with the reference diffractogram, which can be seen in the same image, marked by red lines.

Figure 4.6 shows the obtained diffractogram for the powder of the electrolyte we synthesised by the procedure described before (pellet six).

After analysing both figures 4.5 and 4.6, we were able to conclude that we had indeed produced the desired electrolyte, since all the peaks were present on the diffractograms,

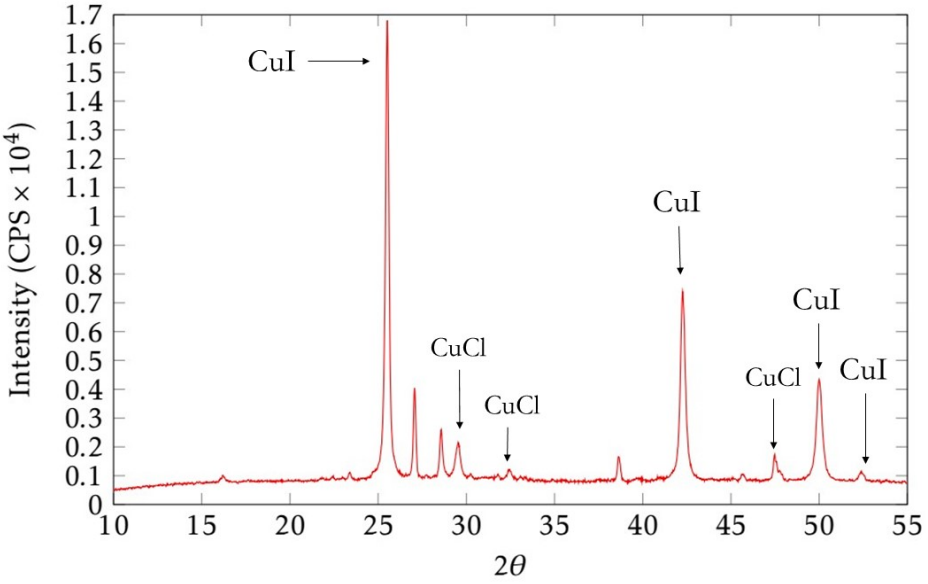


Figure 4.4: Difractogram obtained for the powder mixture of RbCl, CuI and CuCl.

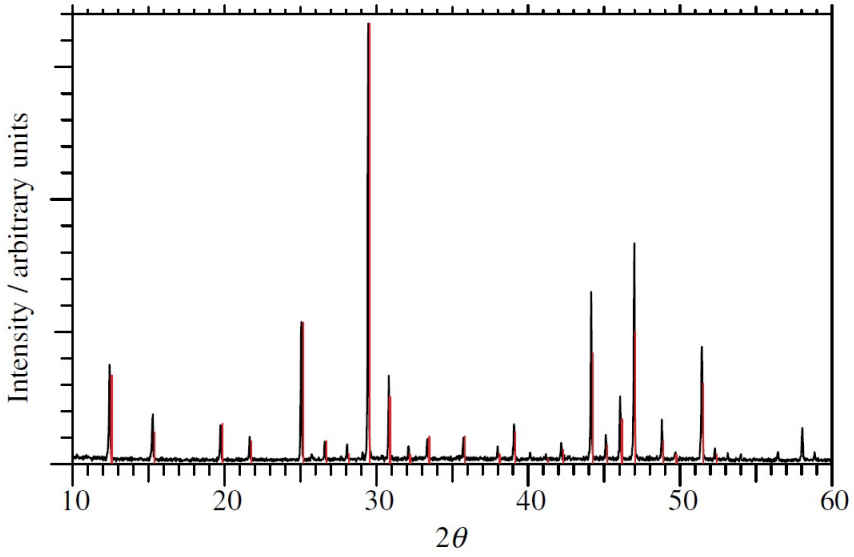


Figure 4.5: Digractogram obtained for a $Rb_4Cu_{16}I_7Cl_{13}$ sample overlapped with the reference diffractogram for the same electrolyte (in red). This diffractogram was obtained from Terence Warner's book [16].

when comparing ours with the reference one. Even though diffractograms from pellet four and six were practically identical, at first sight, their XPS spectra were clearly different. This could be due to the surface of pellet four being more oxidized than the surface of pellet six, while their bulk properties were the same. However, there are small differences in the diffractograms of these two pellets that lead to the belief that their bulks were different, even if just slightly. Pellet's six diffractogram has narrower peaks - the peaks of the diffractogram from pellet six have widths below 0.165 °, while the peaks of the

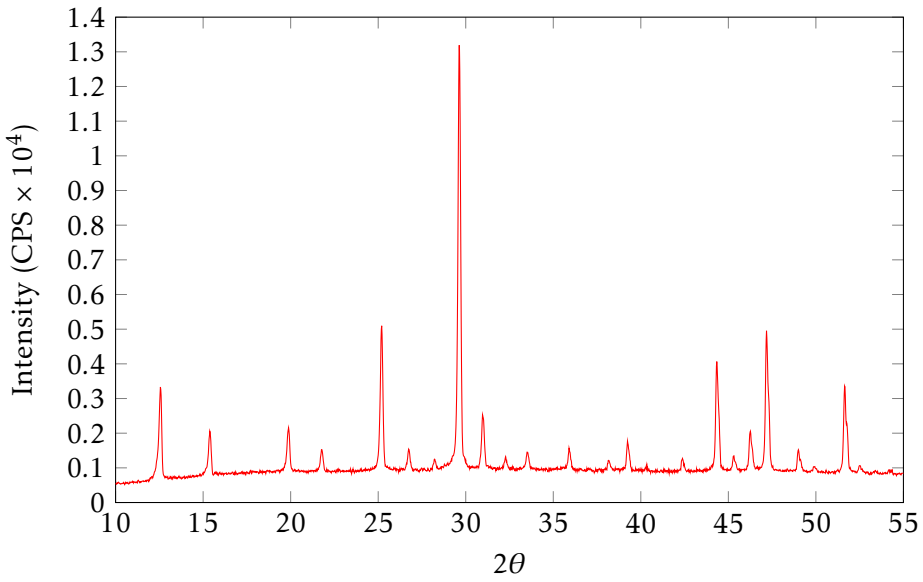


Figure 4.6: Diffractogram obtained for the $Rb_4Cu_{16}I_7Cl_{13}$ powder synthesised with the lowest quantity of oxygen (pellet six).

diffractogram from pellet four have widths above 0.271 °-, which corresponds to larger crystal sizes, and its peaks are also more intensive. From these differences, we can say that pellet six is with higher crystalinity and has less impurities than pellet four.

### 4.1.3 Ionic Conductivity Measurements

The technique used to make the conductivity measurements was Electrochemical Impedance Spectroscopy, or EIS. Like it was described in section 2.2, this technique has a wide range of applications.

The first EIS measurements were made in CENIMAT and the equipment used was a potentiometer from Gamry Instruments and a common sine wave generator. The sample was put in the support that was already in the laboratory. This support had already two electrodes, but for one of our analysed pellets we used our own electrodes along with theirs.

The pellets analysed with EIS in CENIMAT were pellet four and pellet six. These were the selected pellets, since these were the ones that came back with the better results, both in XPS and Powder XRD.

Unfortunately, even though pellet four had the best contact electrodes (indium foils), the high amount of oxygen in the sample did not allow us to obtain any good values or plots. The electrolyte behaved like a resistance of 45 kΩ and the IV curves were perfect lines, with 0 $V$ applied. When 1 $V$ was applied, the resistance value was reduced to 4 Ω. While applying voltage, the indium foils short-circuited, leaving one of the electrodes glued to the pellet and with an orange colour. What might have happened was that when we applied some voltage to the pellet, we opened new channels in the material that

allowed the ions to move from place to place, destroying the original structure of the electrolyte. This happens often with this type of materials and is one of the reasons why electrolytic capacitors cannot work with high voltages.

Initially, we thought that the electric field and voltage drops on the system were along the 2 *mm* thickness of the pellet. However, since our material is an electrolyte, the voltage drops happen on the interface, which is much thinner than the 2 *mm* of the pellet. This means that there is an extremely high local field, which deforms the potential barriers, as was explained in chapter 1. This resulted in the opening of the new channels on the material, as has been referred. Since all the field is on the interface, there is none on the bulk. This results in the fact that all the transport that occurs in bulk is mainly diffusive. Some extra ions are supplied on the interface, due to the field, and this generates a concentration gradient that allows for the conduction to begin. This justifies the employment of the Warburg impedance, when modelling systems with electrolytes, since there is no field in the bulk and all of the motion is diffusive.

After analysing one of the foils on XPS, the one not glued to the electrolyte, we concluded that it had all of the negative ions present in our sample. We suppose it may mean that the other foil would have the positive ions that are present on the pellet - copper and rubidium. This might mean that some conductive process was occurring before the short-circuit took place and it might justify the orange colour on the other foil.

Since pellet four became contaminated with indium, result of the short-circuit, we synthesised pellet six and analysed it in EIS, after confirming with XPS and Powder XRD that we had successfully prepared $Rb_4Cu_{16}I_7Cl_{13}$.

For this second sample, we used the electrodes used in standard measurements. This turned out to be a bad decision, since the results were not perfect, probably due to the bad contact between the electrolyte and the electrodes. However, this time the sample did not behave like the previous one. We did get a Nyquist plot with a curve closer to what was expected. Like referred in section 2.2, the Nyquist plot for an ionic conductor is expected to be a semicircle with a tail on the right, that makes a 45° angle with the x-axis. The obtained Nyquist plot for our pellet can be seen in figure 4.7.

Even though it cannot be easily seen, there is a tail starting to form on the left side of the semicircle. If we zoom in on that part of the plot, we obtain figure 4.8. The reason for this tail to be so small might be the fact that we needed to reach lower frequencies to obtain a more visible line.

While reading some literature, we found an article that had some Nyquist plots obtained for the same electrolyte [31]. In this article, they show different plots for different temperatures. At 291 $K$, room temperature, and a frequency range from 1 $kHz$ to 100 $kHz$, the plot they obtained is the one showed in figure 4.9.

In order to compare our results with theirs, we zoomed our Nyquist plot to the points with frequency between 1 $kHz$ and 100 $kHz$. The resulting plot can be seen in figure 4.10.

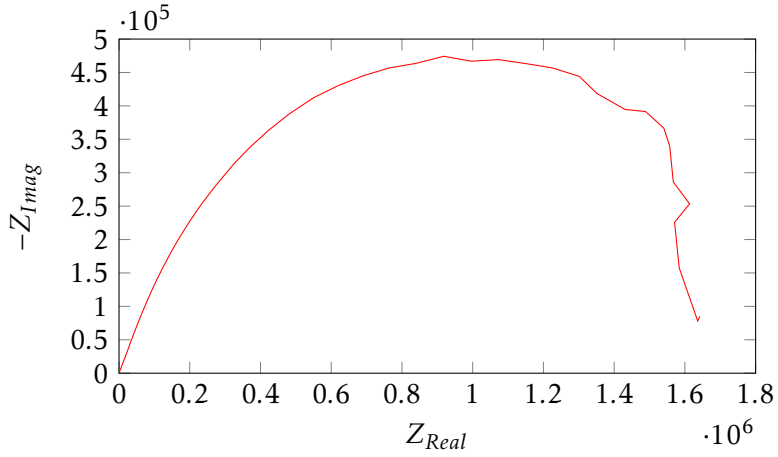


Figure 4.7: Nyquist plot obtained for pellet six.

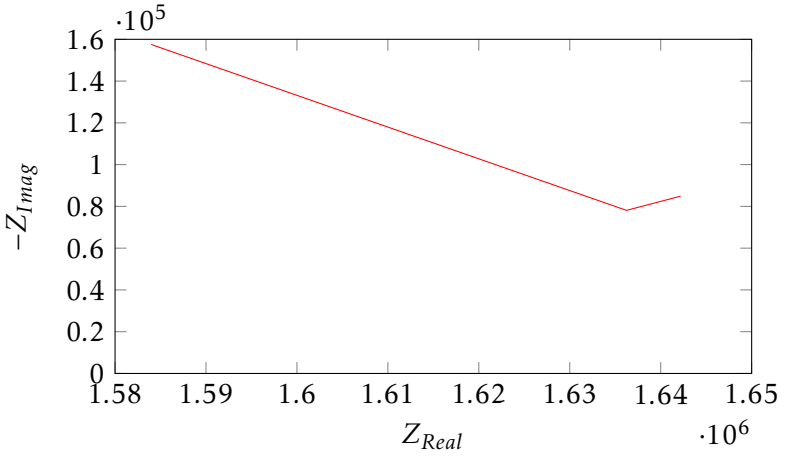


Figure 4.8: Plot resulting from zooming the tail on the right of the semicircle from figure 4.7.

Even though they have the same shape, the impedance values are much higher in our plot. Having higher resistance values means that the conductivity of the sample is lower. Thus, like it was already said, our measurements did not go as we expected. The fact that the contacts between the electrolyte and the electrodes were not done properly resulted in the fact that the resistivity of the system was too high and that we could not measure the conductivity value in a proper way.

In order to obtain more data about the conductivity of our electrolyte, we used pellet seven to repeat the impedance spectroscopy measurements. This time, we used the equipment from the Physics Department, instead of going to CENIMAT. The contacts used were made of aluminium, this time. Once again, this turned out to be a bad choice of material, since our electrolyte reacts with aluminium, as we could confirm from the synthesis of pellet one. However, it was possible to make a few measurements before the reaction between the ionic conductor and the contacts made it impossible for us to continue the experiment.

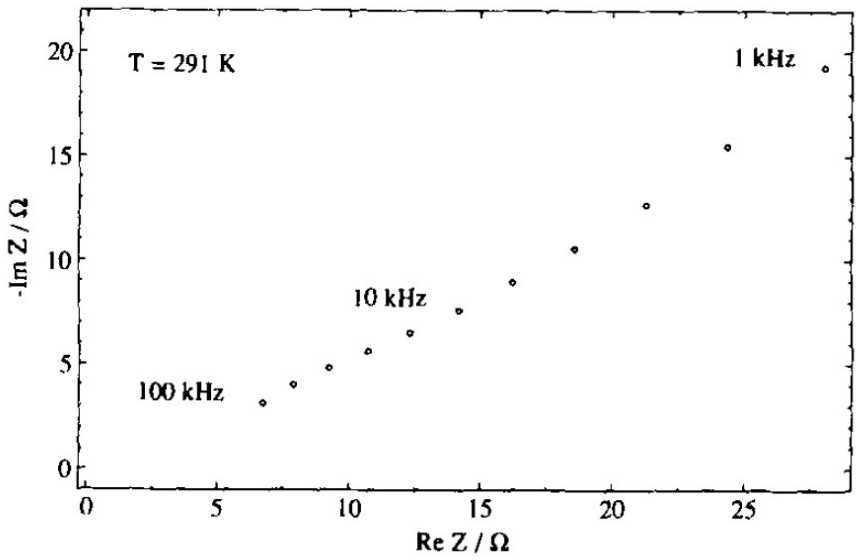


Figure 4.9: Nyquist plot obtained at room temperature, for a frequency range from 1 $kHz$ to 100 $kHz$. This figure was obtained from [31].

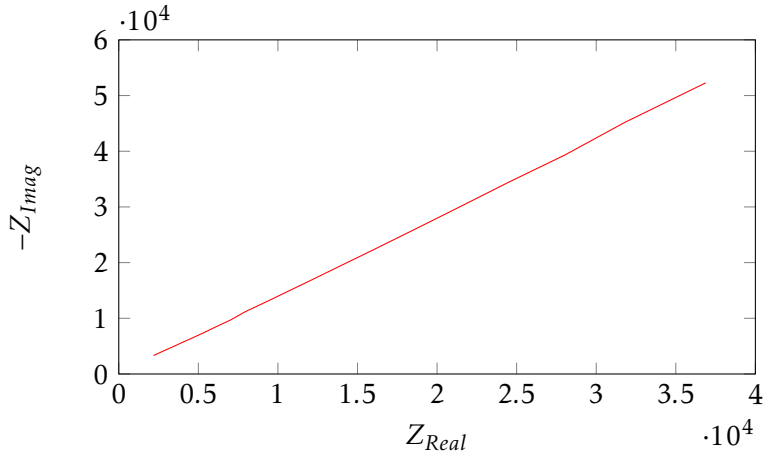


Figure 4.10: Plot resulting from zooming figure 4.7 to a frequency range from 1$kHz$ to 100$kHz$.

The new conductivity measurements were made with a frequency range that went from 100 $mHz$ to 32 $MHz$. Ideally, as can be read in Warner's article [31], the frequency range should reach the $GHz$ and even there, it might not be enough to correctly obtain the conductivity measurements for our electrolyte. However, we were able to obtain a Nyquist plot in which a semicircle is clearly seen. The obtained plot is represented in figure 4.11.

On the right side of the plot, it is possible to see the tail starting to form. This indicates that there is ionic movement in the pellet.

The value of the resistance of the electrolyte is read on the x-axis. By performing linear extrapolation of the tail attributed to ionic conductivity, the resistance can be determined

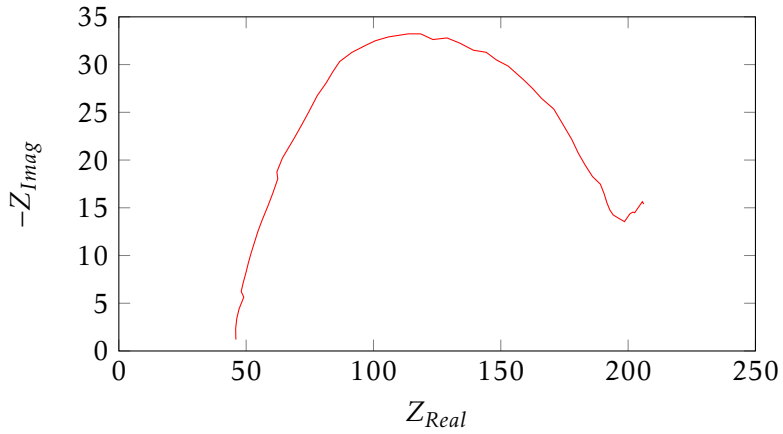


Figure 4.11: Nyquist plot obtained for pellet seven from the measurements made in Physics Department.

by its intersection with the x-axis. That being said, the resistance value obtained from the plot of figure 4.11 was 144.9 Ω.

The obtained value for the resistance of this pellet was lower than the one obtained for pellet six. This means that the conductivity of pellet seven should be higher.

Table 4.3 shows the resistance and conductivity values obtained for pellets six and seven. The conductivity values were obtained using the relations from table 2.1. The conductivity value obtained for pellet six is unreliable, given the small number of points available to do the extrapolation. The value of conductivity obtained for pellet seven still comes from an extrapolation made with few points (even though there were more points for this pellet than for the other one), but it shows better results than pellet six.

Table 4.3: Resistance and Conductivity values obtained for pellets six and seven.

| Pellet 6 | | Pellet 7 | |
|---|---|---|---|
| Resistance (Ω) | Conductivity ($S/cm$) | Resistance (Ω) | Conductivity ($S/cm$) |
| 1750853,5 | $1{,}3210 \times 10^{-7}$ | 144,9 | 0,0022 |

From table 4.3 it is possible to see that the conductivity values obtained for both pellets are very different from each other and that neither of them is close to the expected value of 0.34 $S/cm$.

It was mentioned above that in both experiments the contacts between the pellets and the electrodes were poorly made. Since we can interpret from Warner's article [31] that the contact should be one of the key points for a successful conductivity measurement, we can conclude that the reason for the bad conductivity results might come from the fact that the contacts were not made properly. However, the aluminium contacts used for pellet seven seem to have worked better than the ones used for pellet six, that were the ones already included in the EIS equipment.

As has been referred, the conductivity of $Rb_4Cu_{16}I_7Cl_{13}$ should be measured using

frequencies from the $mHz$ to $GHz$. This seems to go against what was said in section 2.2, about the ionic conductivity being measured on the low frequencies and the electronic conductivity being measured on the high frequencies. This inconsistency might result from the fact that our electrolyte does indeed have an extremely high conductivity and the copper (I) ions are extremely mobile. However, after observing the Nyquist plots obtained from the pellets analysed with EIS technique it is clear that we should also have tried to make the measurements at even lower frequencies, in order for the tail on the right side of the plot to be clearly seen.

## 4.2 Electrolyte Deposition

### 4.2.1 Electrolyte Deposition on Tip

After the deposition of the electrolyte on the tip using the method described in section 3.3.1, we took the tips to the optical microscope. The images obtained can be seen in figure 4.12. In this figure, we can compare the profiles of the tip before and after the deposition - images a) and b) - and we can see the images of the surface of the tip with some electrolyte on it.

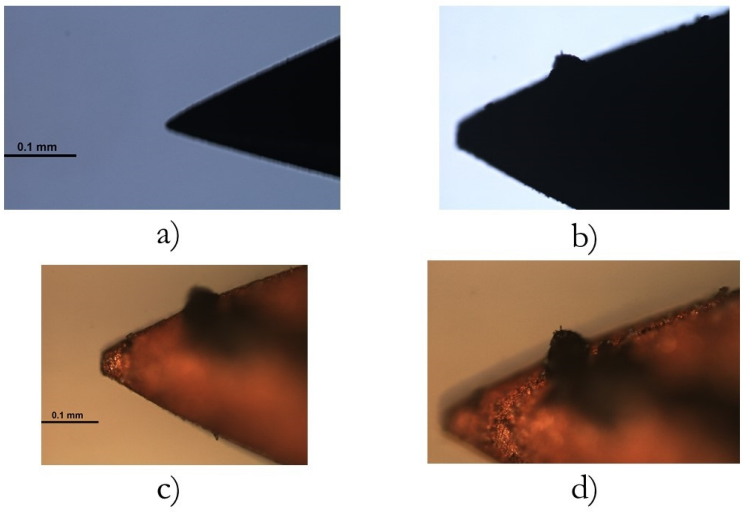


Figure 4.12: Images obtained in the optical microscope for the tip covered in electrolyte by depositing the powder already baked and then annealing: a) profile of the tip before the deposition; b) profile of the tip after the deposition; c) and d) show the tip with the electrolyte in some parts of its surface.

As described in section 3.3, once we concluded that the method we were using was not giving us the results we expected, we tried to deposit the electrolyte on the tip by making a solution of acetone and the electrolyte powder and then cover the tip with it and bake. We then took the tips to the optical microscope, once again. The images obtained can be seen in figure 4.13. In this figure, images a) and b) correspond to the same tip, while images c) and d) correspond to another tip.

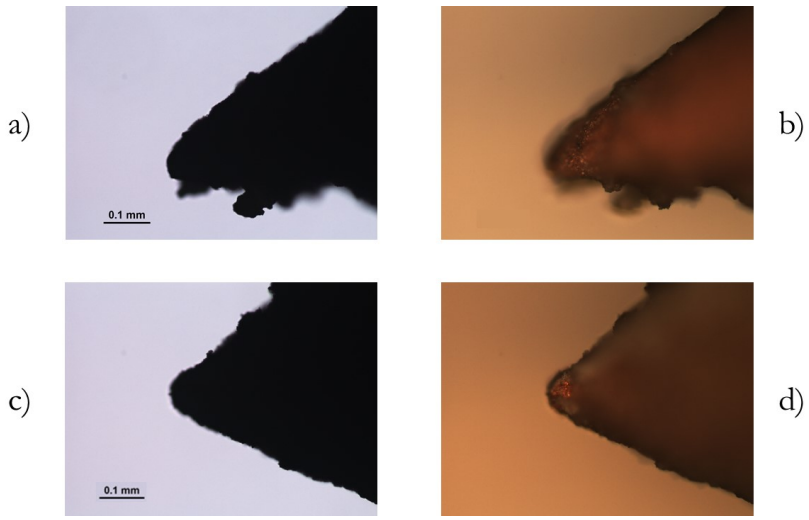


Figure 4.13: Images obtained in the optical microscope for the tips covered in electrolyte, using the method of the acetone solution. Images a) and b) correspond to the same tip, being a) its profile. Images c) and d) correspond to another tip, being c) its profile.

The tip we used in the next step of our work, this being the emission of copper onto the substrate, was the one in images c) and d), since this tip was the one with the most quantity of electrolyte, that we could see without the microscope.

### 4.2.2 Electrolyte Deposition with Evaporator

Even though the tip from images c) and d) of figure 4.13 allowed us to move forward with this work, an evaporator was also assembled, as has been referred in chapter 3.

Following the procedure from Soga and Kuwabara's article [36], we tried to deposit the electrolyte on a glass plate. As described on the referred article, we put some powder on the evaporator and heated it up to 590 °C. Since we did not have a shutter, it was not possible to control when the evaporated material would reach the glass. For that reason, the evaporation happened for a longer time than the described in [36]. Once the temperature reched 590 °C we only left the heating on for twenty more seconds, before turning the power supply off. The photograph of the glass substrate after this process can be seen in figure 4.14.

Figure 4.14: Glass plate after the evaporation of the electrolyte with a maximum temperature of 590 °C.

Since we were not going to make any measurements with the electrolyte deposited on the glass plate, we did not anneal, although the assembly built included a heating system to the sample holder, in order to allow the annealing.

It is possible to notice two different things from figure 4.14. The first one was that there was indeed the formation of a white film on the glass. The contrast between the part that was covered by the claws that hold the glass plate and the white film is noticeable. The second thing that is seen in that figure is the black flakes that seem to be disposed in a splash pattern.

At first, since the sample holder was made of aluminium and it was exposed to the electrolyte during the evaporation, we thought that the black flakes could be the result of the reaction of the aluminium with the electrolyte and that it would have contaminated the glass. For this reason, we decided to cover the surface of the sample holder with a nickel foil. We also replaced the claws with new ones, made of stainless steel.

While performing the heating to 590 °C, we noticed that there was a pressure peak around 400 °C. After confirming that all the powder had evaporated, we assumed that the pressure peak was due to the final evaporation of all powder. For that reason, after all the aluminium was covered, we decided to retry the evaporation, but this time only heat the sample to 420 °C, since there seemed to be no need to go to higher temperatures than that. Also, instead of a glass plate, we decided to try to deposit the electrolyte on two tips. Since that if we succeeded on depositing the electrolyte on the tips they might be used to try to emit copper, we decided that this time we would anneal. We did it for twelve hours, at 170 °C.

After the annealing, we took the tips out of the vacuum chamber. This time, there was no aluminium exposed to the electrolyte, so the reaction that had taken place in the previous test did not occur. There was a film deposited on the nickel foil that covered the aluminium and on the tips. However, there were still some black flakes on both places. Also this time we noticed that on the shadow of the evaporator there was a bigger deposit of electrolyte, with a different colour than the rest. Figure 4.15 shows this deposit. In this figure, it is visible that when we used the nickel foil to cover the aluminium we had to cover one of the three holes that should hold the tips. While cutting the foil, it was not possible to keep the three apertures, so we ended up with only two tip holders.

Since there was a corner of the nickel foil that was loose from the rest of the foil, we took it to the optical microscope, along with the tips and the glass plate from the first test. Figure 4.16 shows some of the images obtained from the microscope. In this figure are images from the glass plate (middle and interface between covered and exposed part), from the nickel foil (middle part, interface and covered part) and from the tip (top and middle). In all of the images from different parts of the samples it is possible to identify the black flakes mentioned before. However, it is visible that both the glass plate and the nickel foil had an acceptably regular film on them and the tips, even though the film was not regular, had some electrolyte deposited.

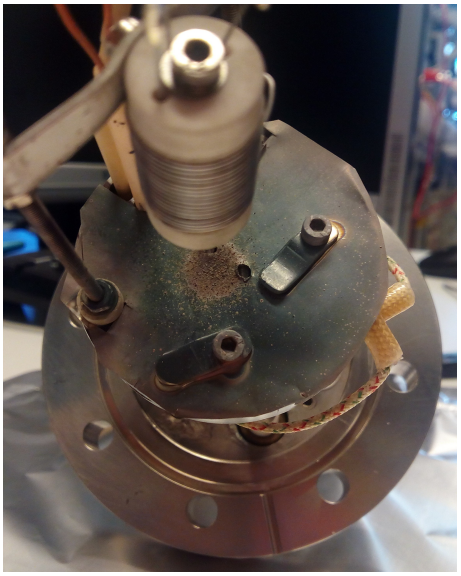

Figure 4.15: Electrolyte deposit formed during the evaporation made at 420 °C onto two tips.

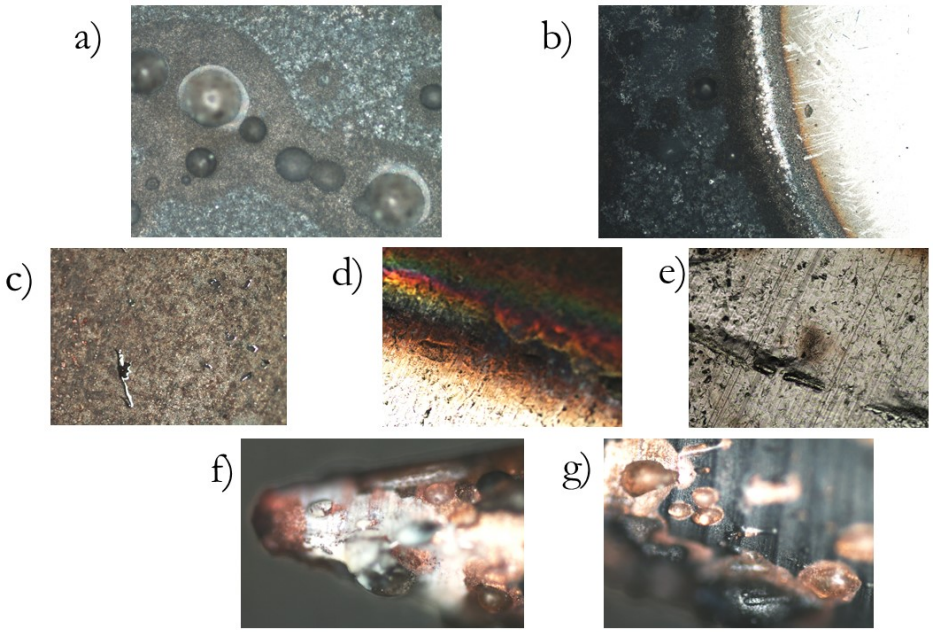


Figure 4.16: Images obtained under optical microscope. a) middle of the glass plate; b) interface between the exposed part (left) and the covered part (right) of the glass plate; c) middle of the nickel foil; d) interface between the covered part (lighter part) and the exposed part (darker part) of the nickel foil; e) covered part of the nickel foil; f) top of tip four after the evaporation deposition; g) middle of tip four after the evaporation deposition

Since there was no aluminium exposed when the nickel and the tips were covered by the electrolyte, we put aside the hypothesis of the black flakes being result of the reaction between the aluminium and the $Rb_4Cu_{16}I_7Cl_{13}$. Instead of that, we started questioning if the black flakes might be the result of the bubbling of the electrolyte, at high temperatures. When the electrolyte is bubbling, there might be the ejection of these flakes from the evaporator onto the glass plate, nickel or tip.

To test this hypothesis, we decided to repeat the previous test with different temperatures. We chose to try to deposit a thin film on glass plates, again, and heat them only to 300 °C and 200 °C. The reason to go for lower temperatures was to check if there would still be a film on the glass, even if we did not reach higher temperatures, since the last pressure peak of the evaporation was always present at 420 °C. Moreover, we decided to try to go for a slower heating rate to see if there was no ejection of big flakes. Since the temperature of evaporation would be lower, we also decided to leave the system at 300 °C and 200 °C for a longer time - one hour for the test at 300°C and one hour and a half for the test at 200 °C. The reason for this longer exposure times was the fact that the evaporation rate decreases exponentially with $1/T$, so it takes a longer time to deposit the same amount of material.

The results from the test at 300 °C revealed that there was also a film deposited on the glass plate and that this time this film could possibly be considered a thin film, since its thickness was visibly lower than the film deposited on the first glass plate. Figure 4.17 shows the glass plate after the evaporation at 300 °C.

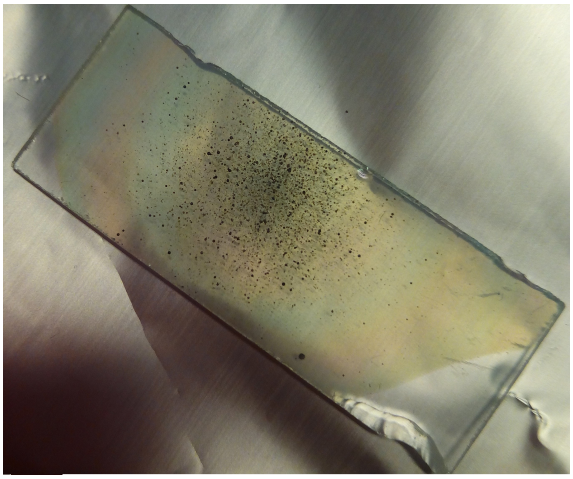

Figure 4.17: Glass plate after the evaporation of the electrolyte with a maximum temperature of 300 °C.

Even though the thickness was lower, which is good if we want to deposit the electrolyte on a tip whilst preserving its original geometry, there were still black flakes on the deposited film. The statement that a thinner film is better for the deposition on the tip is justified by the fact that if we deposit a thick film on a tip that is really sharp, the film is going to deform the tip and the tip's apex that is covered with the electrolyte will not be

as sharp as it could be. Since we know that the smaller the apex radius, the more intense is the emission, it would be desirable that the tip was as sharp as possible. A thick film would not help to reach that sharpness.

After taking the glass plate to the optical microscope, we could confirm that there was a fairly regular film on the glass plate and that there were, once again, some black flakes on the surface. However, this time these flakes were smaller and in a smaller quantity, as can be confirmed when comparing figure 4.14 and figure 4.17. The images taken from the optical microscope can be seen in figure 4.18. This figure shows an image from the middle of the glass plate, from the border of the glass plate and from the interface between an exposed area and a coverd one.

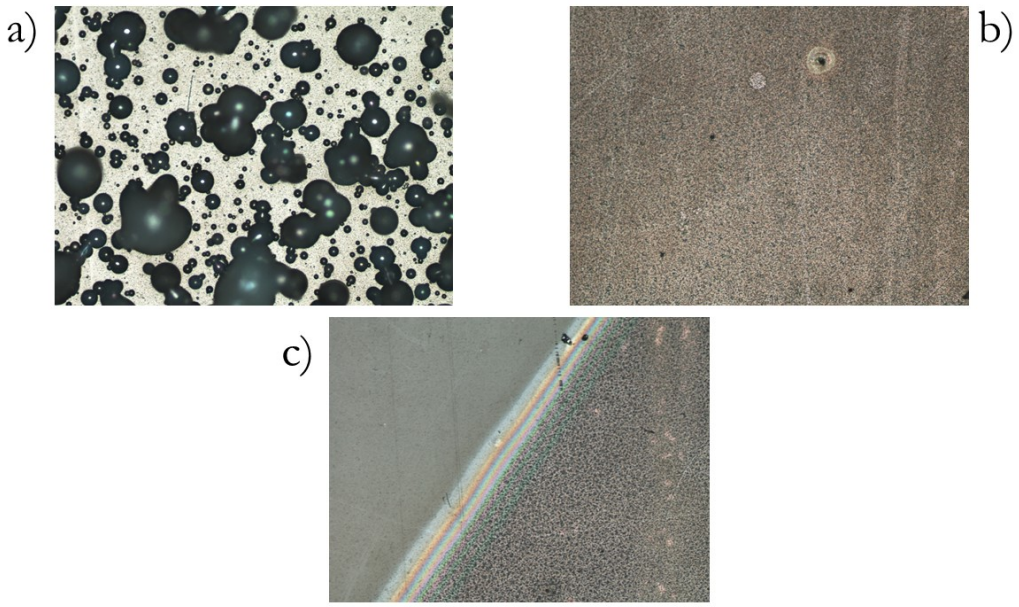


Figure 4.18: Images obtained from the optical microscope for the glass plate, after the evaporation of the electrolyte with a maximum temperature of 300°. a) middle of the glass plate; b) border of the glass plate; c) interface between the covered area and the exposed one.

We also decided to do the evaporation at only 200 °C, below the incongruent melting point of $Rb_4Cu_{16}I_7Cl_{13}$. We left the system at that temperature for an hour and a half, approximately. However, when we took the glass plate out of the vacuum chamber, there was not a film that we could see without using any aiding tools. When we put the glass under the optical microscope we confirmed that we had not deposited any film onto the glass. This result is to be expected, since 200 °C is the temperature at which this electrolyte is typically baked. If it evaporated at 200 °C it would not be possible to bake it at that temperature.

In order to try to remove the black flakes, we decided to clean the whole assembly by heating it up to 695 °C and, after that, try to make another evaporation.

To make sure we had some already deposited film to compare with the one we were making, we decided to repeat the evaporation at 300 °C. The procedure was the same used for the previous evaporation made at this temperature. After the evaporator hit 300 °C , we left it at that temperature for an hour.

When we took the glass plate out, we confirmed that we could not spot any visible black flakes. This was confirmed in the optical microscope. Figure 4.19 shows a photo of the glass after it was taken out of the vacuum chamber and two images obtained from the optical microscope: one from the film in the middle of the glass and another from the interface between the covered part of the glass and the exposed one. As was said before, these images show that no black flakes could be spotted on the film deposited onto the glass.

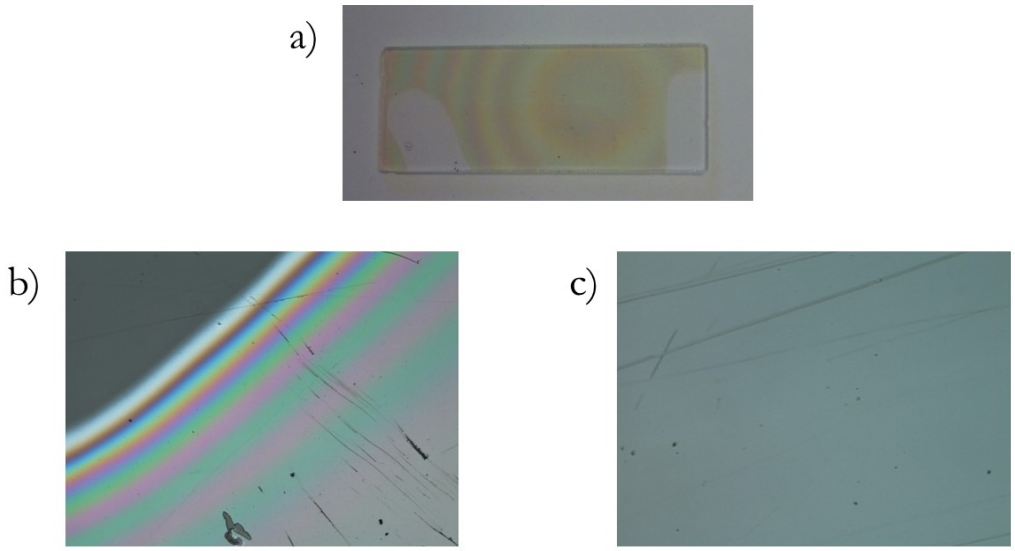


Figure 4.19: Images from the last glass plate onto which a film of $Rb_4Cu_{16}I_7Cl_{13}$ was deposited: a) glass plate with film deposited; b) interface between glass plate and deposited film under the optical microscope; c) middle of the film deposited onto the glass plate seen under the optical microscope .

After obtaining different films, even though we did not anneal them, we decided to check if the elements from our electrolyte were present and if their proportions were relatively close to what they were supposed to be. For this analysis, we used XPS again.

We analysed the films that resulted from the evaporations at 590 °C and 300 °C (both of them). Beside the glasses, we analysed part of the nickel that was exposed during the last 300 °C evaporation and a part of the nickel that was covered with the glass during this evaporation. The reason to analyse this last bit of nickel was the fact that when we opened the chamber after the cleaning at 695 °C, that is before the last evaporation at 300 °C, we noticed that, like the previous times, the top of the evaporator turned red but

also the nickel was showing some traces of this colour. Since we did not know where this red could have come from, we decided to analyse part of the exposed nickel so we could identify the elements present on it.

The XPS analysis allowed us to conclude that the glass with the film deposited at 590 °C was too contaminated with hydrocarbons for us to clearly identify the four elements that compose the solid electrolyte. The spectra mainly showed an oxygen peak and that of carbon.

The film deposited at the first 300 °C evaporation was lacking iodine. The spectra also showed an intense oxygen peak as well as an extra copper peak, which appears in the presence of copper oxide.

Both the nickel and the glass plate with the film from the last evaporation at 300 °C showed a lack in rubidium, but the rest of the spectra looked very similar to the one from pellet six - figure 4.2. This lack of rubidium on these two films made us wonder if the red colour on the evaporator could be due to the fact that this element was staying in it, since this red colour appeared during the first deposition we made and then started to deposit on the nickel, when we heated everything to a higher temperature, in order to clean the assembly. Figure 4.20 shows the red colouring on the evaporator.

Figure 4.20: Red colouring on the evaporator.

After analysing the XPS spectra from the red nickel, we concluded that the film deposited onto it had indeed some rubidium and an excess of chlorine. Iodine was not present and there was almost no copper on the film. From these results we started to assume that the red colour that appeared on the evaporator might be the result of rubidium reacting with the ceramics material, at high temperatures.

## 4.3 Copper Emission

The main objective of this work was to prove that we could have emission of copper ions from a copper tip covered in a copper-based solid electrolyte. For that, after the preparation and characterization of the electrolyte and the successful deposition of it onto a copper tip, it was necessary to apply a high voltage to the tip and see if we could measure any significant current on the substrate. The measuring of a current while

applying a voltage to the tip would tell us if any ions were arriving on the surface of the graphite or if any electrons were leaving it.

### 4.3.1 IV Curves

As described in the previous chapter, in section 3.4.2, we connected an electrometer to a data acquisition system, which was connected to a computer. This way, we could record the current as a function of time. Knowing at which time we varied the applied voltage, we were able to plot an IV curve. The resulting IV curve can be seen in figure 4.21. As it is shown in the figure, there was a current peak at 4.78 $kV$ and between 4.20 $kV$ and 4.80 $kV$ the current was high enough for us to assume that there was some ion emission from the tip or that there were some electrons leaving the graphite. We kept applying some voltage for 18 minutes. However, the time it took to go from 4.20 $kV$ to 4.80 $kV$ was about four minutes, that being the emission time for this test. The maximum value reached by the current was about 635 $pA$.

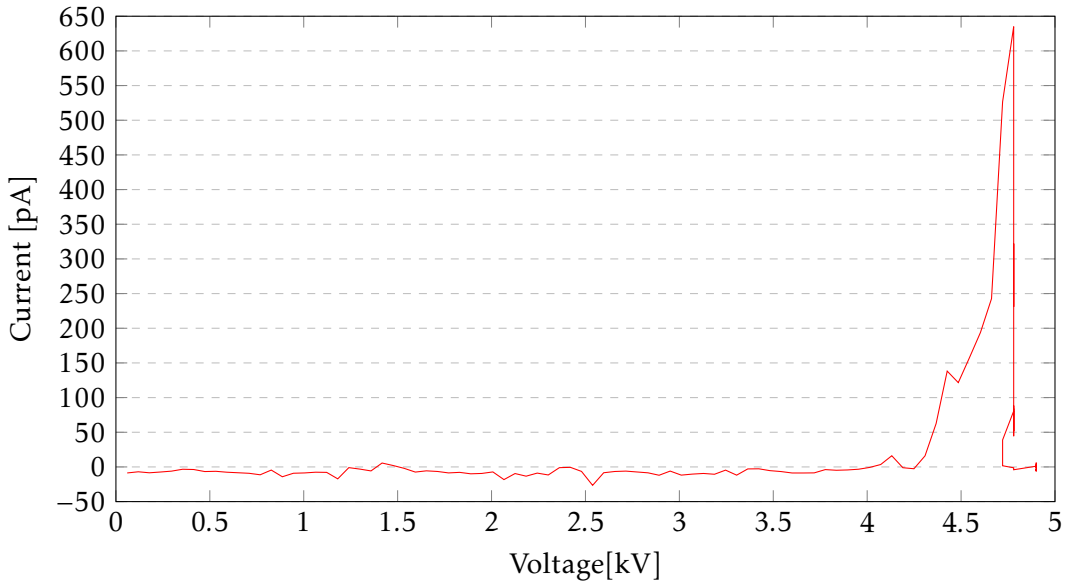


Figure 4.21: IV curve obtained for the deposition of copper in a graphite substrate.

We did two more voltage scannings, but even though in one of them the current reached a higher value at its peak, it only stayed at that value for a second. The rest of the time we were collecting data, the current value was always oscillating around zero.

### 4.3.2 Time-of-flight Secondary Ion Mass Spectroscopy

The applied voltage used on the tip was positive so it would repel the copper ions (and as result, also the rubidium ions). To confirm that we had indeed had the emission of these ions, we needed to analyse the graphite substrate. For that analysis, we used Time-of-Flight Secondary Ion Mass Spectroscopy, or ToF-SIMS.

This technique allows to identify the elements present on the surface of a sample. When a primary ion beam interacts with the surface of a material, it provides enough energy for the sample atoms to leave the surface as ions. The interaction between this primary beam and the sample results in the sputtering of secondary ions and ion clusters. After being emitted, these ions from the surface are accelerated to some specific energy towards the detector. The identification of the mass of each ion is based on the time it takes to reach the detector. Since the distance between the sample's surface and the detector is the same for all ions, those with smaller mass are the first ones being detected. The time-of-flight of each ion or cluster is registered and is posteriorly converted to mass. The amount of ions of each mass that reach the detector is summed up and this gives the intensity of each mass peak. By knowing the mass of each ion or ion cluster, one can identify the elements or molecules present at the surface.

After the application of the high voltage to the tip and after taking the graphite out of the assembly, we took it to the optical microscope. One of the obtained images can be seen in figure 4.22. It is possible to observe an area with a darker orange colour than its surroundings.

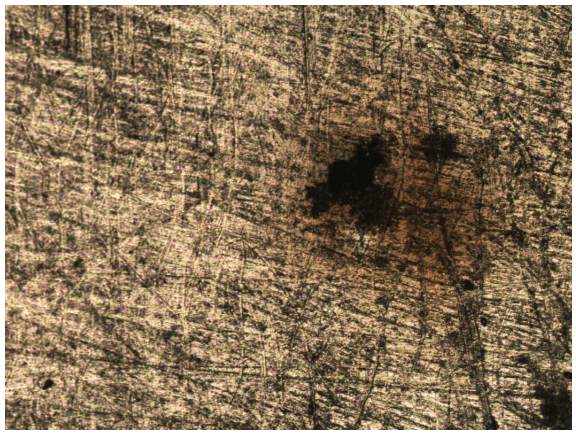

Figure 4.22: Image of the graphite substrate, obtained from the optical microscope. We can see an area with a darker orange colour than the surroundings.

The next step was to use ToF-SIMS to identify the ions present on the surface of the graphite. The equipment we worked with uses a gallium ion gun as the incident beam. We know that copper has two isotopes, with masses 62.9 $m/z$ and 64.9 $m/z$ and rubidium has isotopes with mass 84.9 $m/z$ and 86.9 $m/z$. Knowing this, we knew where we wanted to see the peaks in the mass spectra. In figures 4.23 and 4.24 two of the mass spectra obtained from ToF-SIMS can be seen.

In figure 4.23 it is possible to identify many peaks. Most of them are hydrocarbons and the ones that are not and have a significant intensity are identified. Even though the substrate was graphite, the carbon peak is small, comparing with the hydrocarbons. The reason for this was the fact that the sample was not well cleaned and so the contaminants of our hands and from the air contaminated the surface of the substrate. Also the fact

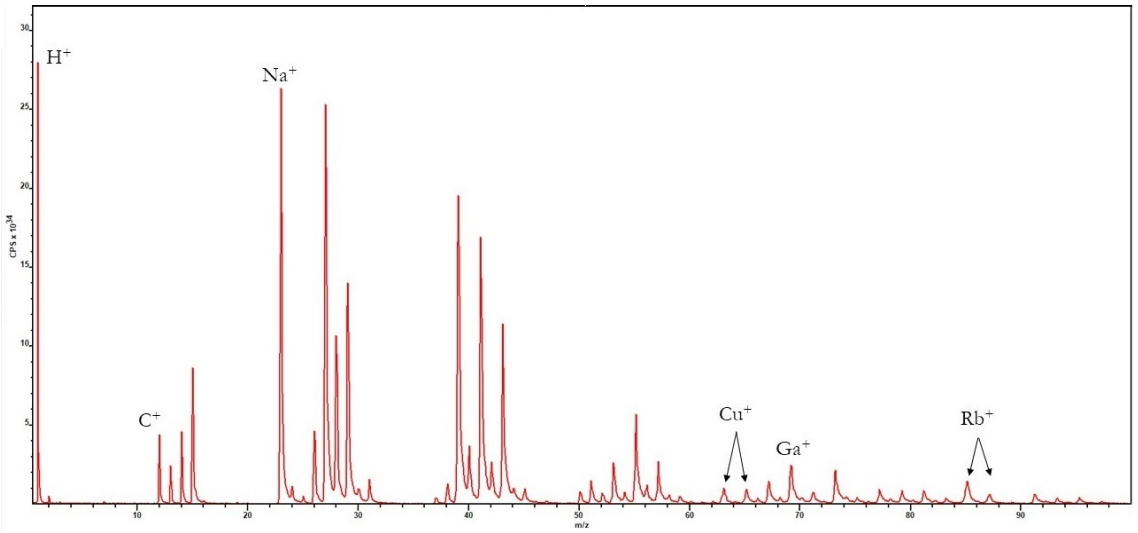


Figure 4.23: Mass spectra obtained from ToF-SIMS. There is no significant copper or rubidium peaks.

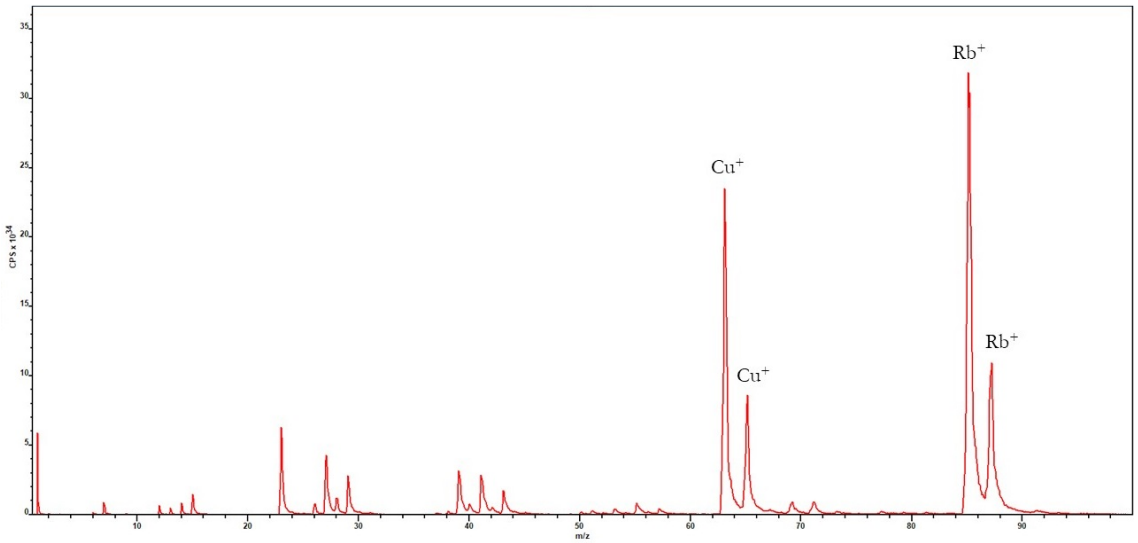


Figure 4.24: Mass spectra obtained from ToF-SIMS. The two peaks from the copper isotopes and the two peaks from the rubidium isotopes can be clearly seen.

that carbon has a low ionisation probability, much lower than that of hydrocarbons, contributes for the low intensity of the carbon peak. In this spectrum, the masses where we expected to see the peaks of copper and rubidium isotopes are also identified. However, even though there are peaks in those positions, their intensity is not relevant, comparing with the rest of the spectrum.

When we look at figure 4.24, though, the spectrum shows clearly the presence of copper and rubidium. This spectrum was obtained from a different area of the graphite's surface. After obtaining figure 4.23, we translated the sample so the primary ion beam would focus on a different zone.

The differences between the two spectra are clear. Even though in figure 4.24 there are still hydrocarbons, sodium and other contaminants that could be seen clearly in figure 4.23, their intensity is now much lower than the intensity of copper and rubidium peaks. From this spectrum, we can conclude that there was clearly copper and rubidium implanted in the graphite's surface. Thus, we can say that we succeeded in emitting copper ions from a copper tip covered in a copper-based solid electrolyte.

Another analysis that could have been made was to translate the sample on the sample holder and record the translation distances. This would allow to calculate how much of the substrate surface's area was covered by the copper, thus knowing the area over which the copper ions were deposited.

There is, however, one detail that can be pointed out. Like it was described in section 2.3, the mobile ion of this electrolyte was copper. If that is true, how can the intensity of rubidium peaks be higher than the intensity of copper peaks? If copper is mobile, it is expected that its intensity is much higher than the rest of the positive ions present in the electrolyte. The reason for the rubidium peaks being more intense than the copper ones is the fact that rubidium has a higher ionization probability, or a lower ionization potential. The fact that ToF-SIMS technique has different sensitivity factors for different species results in the fact that rubidium peaks are more intense than the copper ones. By taking the sensitivity factors from literature [43] and the intensities of the peaks, it is possible to correct this unconformity, making a first estimation of the right proportion between copper and rubidium ions present on the graphite. Table 4.4 shows this estimation. From this table we can say that 28.56 times more copper than rubidium ions were emitted from the electrolyte covering the copper tip.

Table 4.4: First estimation of the value for the real proportion between copper and rubidium ions on the graphite surface

| $\mathbf{(Cu/Rb)}_{RSF}$ | **Peak intensity ratio** | $\mathbf{(Cu/Rb)}_{Estimated}$ |
|---|---|---|
| 38.75 | 0.737 | 28.56 |

After analysing the ToF-SIMS spectra, in which is easily possible to identify the peaks of the two copper isotopes, it is clear that the objective of this thesis was reached.

Chapter 5

# Conclusions

The objective of this MSc thesis was to prove that it was possible to emit copper ions from a copper tip covered with a copper-based solid electrolyte.

For that, it was necessary to choose a solid electrolyte that had a considerable ionic conductivity and successfully synthesize it. The chosen electrolyte was the $Rb_4Cu_{16}I_7Cl_{13}$. To confirm that the obtained material was in the right phase, it was necessary to analyse the different pellets produced. After obtaining the correct phase of the material, it had to be deposited onto a copper tip.

The next step was to transfer the electrolyte onto the surface of a tip. Different deposition methods were tried: pressing the powdered material around a tip and annealing it, covering the tip with an acetone solution mixed with the electrolyte powder, and posteriorly bake it, and constructing an evaporator in order for the evaporated powder to be deposited onto the tips and then annealed.

After the electrolyte deposition onto the tips was successfully done, everything should be ready to put the tip and the substrate under vacuum and apply a voltage into this tip. For that, it was necessary to assemble a deposition set-up. This set-up consisted in a high voltage feeder connected to the tip, a Faraday cup, in which the substrate was placed, and a feed-through that allowed to control the position of the substrate from the outside of the vacuum chamber. It was necessary to make sure that the substrate was isolated from everything else, in order to obtain information about any ions arriving on its surface or any electrons leaving it.

This deposition set-up allowed to apply a voltage into the tip and to have some emission from it. The confirmation of what species were deposited onto the substrate was made by posteriorly analysing it.

Concerning the electrolyte preparation, we can say that we were able to successfully synthesize at least three pellets of $Rb_4Cu_{16}I_7Cl_{13}$. Even though two of those pellets had a

high quantity of oxygen in their constitution, the desired phase was obtained, which we could confirm from the XPS and Powder XRD results. The third successfully synthesized pellet had almost no oxygen in its constitution, suggesting that the small change we made in the synthesis procedure, using a higher argon flow and an oxygen scavenger, was enough to remove the oxygen from the pellets.

From the Powder XRD spectra of the pellet with higher amount of oxygen and the one from the pellet with lower amount of oxygen we can say that they looked similar. This means that Powder XRD is a good technique to analyse the obtained phase of a material but it should be used along with some other technique that allows to identify the elements present on that material. For us, that technique was XPS.

From the deposition techniques that were tested, neither of them worked perfectly. However, when using the acetone solution technique we obtained a tip that allowed us to get some electrolyte at the tip surface and move forward to the next step of our work. Even though the electrolyte's deposit on this tip was not regular and there were some areas in which the amount of deposited material was too high, we used this tip to test if it was possible to emit some copper from it.

After assembling the tip and the substrate onto the deposition set-up, we applied a positive voltage to the tip. While scanning this voltage, we noticed that at 4.20 $kV$ we were able to measure current in the order of the hundreds of $pA$. This current reached a maximum value of 635.08 $pA$, at 4.78$kV$. We kept applying voltage into the tip in the range that allowed the emission to occur for four minutes.

Aside from that first emission test, we did two more, with the same tip. One of them reached a higher current peak value, but we were only able to measure a significant current for some seconds, before it went back to oscillate around zero. The higher value registered for the current was 1.40 $nA$, at around 4.60 $kV$.

The graphite substrate was removed from the ion field emission set-up and was analysed with ToF-SIMS. From the resulting spectra, it was clear that we had an area on the substrate that had a copper film on it. Along with the copper ions on the surface, there were also rubidium ions. This is the second type of positive ions present on the $Rb_4Cu_{16}I_7Cl_{13}$ electrolyte, so it was expected that some of these ions had been emitted along with the copper. However, after making a first estimation of the proportion between copper ions and rubidium ions on the substrate, we concluded that approximately 28.56 times more copper ions were emitted than those of rubidium.

The results from the ToF-SIMS spectra are the proof we needed to be able to say that we successfully emitted copper ions from a tip covered with a copper-based solid electrolyte.

Concerning the long-term objectives of this project, we did not expect to immediately develop a new technique. Even though we were able to emit copper ions from the covered tip, which was the objective of this work, we cannot say that we were able to emit ions

that had migrated from the copper tip into the electrolyte. The long-term idea is to build a self-sustained ion source. For that, the ions from the copper tip should migrate to the electrolyte. In order to achieve that objective, the adhesion of the electrolyte onto the tip has to be improved and the emission time needs to be longer.

In order to make way for the future work that can be done on this subject, we started to work on an alternative technique to make the deposition of the electrolyte onto the tip - an evaporator. This assembly has two main parts: the evaporator itself and a sample holder, providing possibility of sample post-annealing. We were able to perform five evaporation tests with this technique. The first at 590 °C, the second at 420 °C, the third at 300 °C, the fourth at 200 °C and the last again at 300 °C. All of the evaporations were made onto glass plates, except the second one, which we tried to make directly onto two tips. The glass plates from the evaporations at 590°C and at 300°C revealed that it is possible to deposit a fairly regular film onto the glass and that if we desire to obtain a thin film, a lower temperature provides better results in terms of thin film morphology. We also noticed that both the glasses and the two tips had black flakes deposited onto them. However, the amount of flakes decreased from the evaporation at 590°C to the one at 300°C. The tips from the evaporation at 420°C showed a deposit of electrolyte on them, but the film was not as regular as the ones obtained on the glasses. The tips also had some black flakes on their surface.

The evaporation made at 200 °C did not deposit any film onto the glass plate. This result was expected, since at this temperature the electrolyte should still be stable and no evaporation should occur. Otherwise, this temperature would not be used to anneal this material.

The last evaporation made, again at 300 °C, revealed a fairly regular film, much thinner than the one obtained at 590°C. Also, the film obtained did not show any black flakes on it.

Regarding the general aspect of the last film we obtained, we could assume that a good temperature to make the deposition was 300 °C, concerning the aspect of the last glass plate - the thickness of the deposited film and the disappearance of the black flakes. However, the XPS analysis of that last film and of the part of nickel foil that was exposed to the material during the same evaporation showed that these films were lacking in rubidium, which appeared to be staying in the evaporator and could be the cause of the red colouring that appeared on it. We could confirm this idea from the spectra of the second nickel foil analysed, that had been exposed to a maximum temperature of 700 °C and also had a reddish colour. This spectra showed that the film on the nickel's surface had rubidium as well as an excess of chlorine, but there was no iodine on it and almost no copper.

The change in colouring of the ceramics material from which the evaporator was made could be the result of a reaction between it and the rubidium, at temperatures higher than 230 °C.

Even though we were able to reach the objective of this work, the emission of copper ions from a copper tip covered in a copper-based solid electrolyte, there is still a lot of room for improvement.

Chapter 6

# Future Work

The work described in this thesis was the starting point to the development of a new technology that should allow to achieve high lateral resolutions, when depositing copper onto substrates. With the purpose to reach the final goal of this project, there are aspects from this work that could be improved.

The first impasse reached during the development of the different tasks described in this thesis was the electrolyte synthesis. The limitations imposed by $Rb_4Cu_{16}I_7Cl_{13}$ and its sensibility resulted in the fact that it took longer than we were expecting for us to obtain the desired phase of the electrolyte. Hence, the first suggestion for those who might work on this project would be either to improve the synthesis of this ionic solid or to find another copper-based solid electrolyte that also has a considerable ionic conductivity and whose preparation is easier. The best solution would even be to choose a copper electrolyte that is sold already synthesized.

If the decision is to keep working with $Rb_4Cu_{16}I_7Cl_{13}$ and there is an interest in better know the characteristics of this electrolyte, it would be important to improve the quality of the contacts between the electrodes and the pellet of the material, during conductivity measurements. As has been described on this work, there is some literature that describes the processes used by some groups to obtain good contacts in the interface electrode-electrolyte as well as the materials they used. Copper is one of the favourite materials for the electrodes.

Even though the impasse of the electrolyte synthesis was the one that caused this work to be behind schedule, the main task of this work that did not work nearly as planned was the electrolyte deposition onto the tip.

The work done with the built evaporator showed us that it is possible to deposit thin films of the electrolyte onto glass plates and that it is also possible to deposit some of the

ionic conductor onto the tips. However, the source of the black flakes that we found on all glass plates except one and on the tips is still not clear. To investigate further if they are the result of the electrolyte's bubbling would be a good starting point to improve the evaporator and obtain regular films on the tips.

As has been referred before, in order to achieve the objective of getting a self-sustained ion source it is necessary that the adhesion of the electrolyte onto the tip is nearly perfect. For that, it is necessary that, among other things, the copper tip is not oxidised. The best way to assure this would be to include on the evaporator assembly a way of cleaning the tip already under vacuum. One way to do that would be by using a plasma. If thought through, it should be possible to include on the built evaporator the apparatus necessary to be able to produce appropriate discharge.

While following the procedure described in the article that inspired us to built this evaporator, we noticed that we could not control the exposure time of the glass plates and the tips to the evaporated electrolyte. This resulted from the fact that we did not built a shutter between our evaporator and the sample holder. Hence, the whole time we were heating the $Rb_4Cu_{16}I_7Cl_{13}$, while it was evaporating, the material was being deposited onto the samples, instead of them just being exposed to the evaporated material for a short period of time, when the temperature reached the value we wanted. This excess on the exposure time would be sorted out if there was a shutter to cover the samples during the heating.

Another aspect of the assembly that should be changed is the material of the evaporator. If our speculation that the red colouring that appeared in the crucible is to be true, it would be interesting to try to change this material into other type of ceramics. This way it would be possible to check if the crucible also turned red and if the films obtained with the new evaporator would also have a lack of rubidium.

Another disadvantage of the thermal evaporation that we used is the fact that the electrolyte gets decomposed when evaporating. That's the reason why it is necessary to anneal it after the deposition. The annealing allows for the components to reorganize themselves. There are other deposition techniques that allow to maintain the stoichiometry of the materials. One of them is the Pulsed Laser Deposition, or PLD. This technique is widely used to grow thin films onto substrates and its main advantage is that it does not decompose the materials when doing so. PLD technique is able to maintain the stoichiometry because it uses small laser pulses to evaporate the material that is supposed to form the thin film. The speed of these pulses is so high that the material does not have time to decompose before reaching the substrate. A good way to improve the deposition of thin films onto the tips would be to explore the possibility of using PLD to do so.

# Bibliography


[1] DREEBIT. *APPLICATIONS OF IONS*. http://www.dreebit-ibt.com/applications-of-ion-beams.html. Accessed September 12, 2017.

[2] F. H. Fahey. *What You Should Know About Radiation and Nuclear Medicine*. http://snmmi.files.cms-plus.com/Fahey_PAAB_Risk_May2012_final.pdf. Accessed September 12, 2017.

[3] A. B. Tolstogouzov, S. F. Belykh, V. S. Gurov, A. A. Lozovan, A. I. Taganov, O. M.N. D. Teodoro, A. A. Trubitsyn, and S. P. Chenakin. "Ion Beam Sources Based on Room Temperature Ionic Liquids for Aerospace Applications, Nanotechnology, and Microprobe Analysis (Review)." In: *Pleiades Publishing* 58.1 (2015), pp. 1–14. DOI: 10.1134/S002044121501011X.

[4] AZoNano. *Lithography, Photolithography, Electron Beam Lithography and X-Ray Lithography – Nano Fabrication Techniques*. https://www.azonano.com/article.aspx?ArticleID=659. Accessed September 17, 2017.

[5] B. Wu and A. Kumar. "Extreme ultraviolet lithography and three dimensional integrated circuit - A review." In: *Applied Physics Reviews* 1.1 (2014). ISSN: 19319401. DOI: 10.1063/1.4863412.

[6] FEBIP. *What is FEBIP?* http://www.febip.org/index.php?id=69. Accessed February 1, 2017.

[7] V. P. Verma, J. Huang, and S. R. Bakshi. *Presentation on Electron Sources*.

[8] C. Escher, S. Thomann, C. Andreoli, and H.-w. Fink. "Vacuum ion emission from solid electrolytes : An alternative source." In: *Applied Physics Letters* 89 (2006), pp. 6–7. DOI: 10.1063/1.2264092.

[9] F. Fernandes. "Ion-beam Sources Based on Superionic Solid Electrolytes." Master dissertation. UNL, 2015, p. 66.

[10] J. J. Hren and S. Ranganathan. *Field-Ion Microscopy*. Springer Science + Business Media, 1968, p. 250. ISBN: 978-1-4899-6241-6. DOI: 10.1007/978-1-4899-6513-4.

[11] T. T. Tsong. "Field ion emission." In: *Atom-probe field ion microscopy*. Cambridge: Cambridge University Press, pp. 10–102. DOI: 10.1017/CBO9780511599842.003. URL: http://ebooks.cambridge.org/ref/id/CBO9780511599842A011.

[12] C. Escher, T. Latychevskaia, H.-w. Fink, and D. W. Pohl. "Direct Evidence for Conduction Pathways in a Solid Electrolyte." In: *Physical Review Letters* 97 (2006), pp. 1–4. DOI: 10.1103/PhysRevLett.97.136601.

[13] R. Agrawal and R. K Gupta. "Review Superionic solids : composite electrolyte phase – an overview." In: *JOURNAL OF MATERIALS SCIENCE 34* 34 (1999), pp. 1131–1162.

[14] B. B. Owens. "Solid state electrolytes : overview of materials and applications during the last third of the Twentieth Century." In: *Journal of Power Sources* 90 (2000), pp. 2–8.

[15] D. T. Martins. "Compact Ion-source Based on Superionic Rubidium Silver Iodide (RbAg4I5) Solid Electrolyte." Master dissertation. UNL, 2013, p. 78.

[16] T. E. Warner. *Synthesis, Properties and Mineralogy of Important Inorganic Materials*. John Wiley & Sons, Ltd, 2011. ISBN: 9780470746127.

[17] IONODE. *Conductivity Theory*. http://ionode.com/theory/conductivity-theory. Accessed February 6, 2017.

[18] C. Kittel. *Introduction to Solid State Physics*. 8th. John Wiley & Sons, Inc, 1988, p. 681. ISBN: 047141526X.

[19] P. P. Kumar and S. Yashonath. "Ionic conduction in the solid state." In: *Journal of Chemical Sciences* 118.1 (2006), pp. 135–154. ISSN: 02534134. DOI: 10.1007/BF02708775.

[20] P. Kumar. "Theory of a higher-order phase transition: The superconducting transition in Ba0.6K0.4BiO3." In: *Physical Review B* 68.6 (2003), pp. 68–75. ISSN: 0163-1829. DOI: 10.1103/PhysRevB.68.064505. URL: https://link.aps.org/doi/10.1103/PhysRevB.68.064505.

[21] A. I. Zia and S. C. Mukhopadhyay. *Electrochemical Sensing: Carcinogens in Beverages*. Vol. 20. 2016. ISBN: 978-3-319-32654-2. DOI: 10.1007/978-3-319-32655-9. URL: http://link.springer.com/10.1007/978-3-319-32655-9.

[22] G. Instruments. *Basics of EIS: Electrochemical Impedance Spectroscopy*. https://www.gamry.com/application-notes/EIS/basics-of-electrochemical-impedance-spectroscopy/. Accessed September 8, 2017.

[23] L. K. M. Arunkumar Jayakumar, Tejas Trivedi, Deepak Sharma, Marilou Rebosura. "Real Time Applications of Electrochemical Impedance Spectroscopy -A Technical Assessment." In: October (2016). URL: https://www.researchgate.net/publication/309352822.

[24] G. Instruments. *Introduction to Electrochemical Impedance Spectroscopy*. 2015. URL: https://www.gamry.com/assets/Uploads/Basics-of-Electrochemical-Impedance-Spectroscopy.pdf.

[25] S.-M. Park and J.-S. Yoo. "Electrochemical Impedance Spectroscopy for Better Electrochemical Measurements." In: *Analytical Chemistry* 75 (2003), 455 A–461 A. ISSN: 0003-2700. DOI: 10.1021/ac0313973.

[26] J. Bauerle. "Study of solid electrolyte polarization by a complex admittance method." In: *Physycal Chemichal Solids* 30 (1969), pp. 2657–2670. ISSN: 00381098. DOI: 10.1016/0038-1098(69)90484-0.

[27] E. Barsoukov and J. R. Macdonald. *Impedance Spectroscopy*. 2005, pp. 1–595. ISBN: 9780471716242. DOI: 10.1002/0471716243. arXiv: 0709.1163. URL: http://doi.wiley.com/10.1002/0471716243.

[28] K. L. Barbalace. *EnvironmentalChemistry.com*. https://environmentalchemistry.com/yogi/periodic/Cu.html. Accessed September 17, 2017.

[29] S. Geller, J. Akridge, and S. Wilber. "Crystal Structure and conductivity of the solid electrolyte $\alpha$-RbCu3Cl3I2." In: *Physical Review B* 19.10 (1979), pp. 5396–5402.

[30] R. Kanno, K. Ohno, and Y. Kawamoto. "Neutron Diffraction Study of High Ionic conductor Rb4Cu16I7+xCl13-x at 50-300 K: Correlation with Ionic Conductivity.pdf." In: *Solid State Chemistry* 102 (1993), pp. 79–92.

[31] T. Warner, P. Edwards, W. Timms, and D. Fray. "A study of the mass transport properties of the solid state copper(I) ion conductor Rb4Cu16I7Cl13 and its application in the determination of the thermodynamic stability of Nd2CuO4." In: *Journal of Solid State Chemistry* 98.2 (1992), pp. 415–422. ISSN: 1095726X 00224596. DOI: 10.1016/S0022-4596(05)80252-X.

[32] K. S. K. Kuwabara, K. Hanafusa. "Solid electrolyte cells with a copper ion conductor Rb4Cu16I7Cl13 . Mixed-phase cathodes containing metal oxides." In: *Applied Electrochemistry* 18 (1988), pp. 705–709.

[33] R. N. Prasad and N. M. Abhyankar. "Thin Film Solid State Cells Using Rb4Cu16I7Cl13 Electrolyte and their Limitations." In: *Thin Solid Films* 164.1 (1988), pp. 345–351.

[34] O. Y. T. Takahashi, R. Kanno, Y. Takeda. "Solid State Ionics- The CuCI-CuI-RbCl System." In: *Solid State Ionics* 3/4 (1981), pp. 283–287.

[35] Hositrad. *Set Screw Contacts - Ber. Copper*. http://webshop.hositrad.com/default.asp?pageid=85&docid=118&artdetail=7429-02-A. Accessed August 16, 2017.

[36] K Soga and K Kuwabara. "Preparation and electrical conductivity of thin films of Rb4Cul6 I7Cl13." In: *Applied Electrochemistry* 12 (1982), pp. 185–191.

[37] M. Biesinger. *Auger Peaks and the Auger Parameter*. http://www.xpsfitting.com/2012/08/auger-peaks-and-auger-parameter.html. Accessed September 27, 2017.

[38] R. P. Vasquez. "CuI by XPS." In: *Surface Science Spectra* 5.4 (1998), pp. 262–266. ISSN: 1055-5269. DOI: 10.1116/1.1247882. URL: http://avs.scitation.org/doi/10.1116/1.1247882.

[39] R. P. Vasquez. "CuCl by XPS." In: *Surface Science Spectra* 2.2 (1993), pp. 138–143. ISSN: 1055-5269. DOI: 10.1116/1.1247732. URL: http://avs.scitation.org/doi/10.1116/1.1247732.

[40] R. P. Vasquez. "CuCl2 by XPS." In: *Surface Science Spectra* 2.2 (1993), pp. 160–164. ISSN: 1055-5269. DOI: 10.1116/1.1247736. URL: http://avs.scitation.org/doi/10.1116/1.1247736.

[41] R. Nave. *Bragg's Law*. http://hyperphysics.phy-astr.gsu.edu/hbase/quantum/bragg.html. Accessed August 19, 2017.

[42] J. Grebenkemper. *Powder X-ray Diffraction*. https://chem.libretexts.org/Core/Analytical_Chemistry/Instrumental_Analysis/Diffraction_Scattering_Techniques/Powder_X-ray_Diffraction. Accessed August 19, 2017.

[43] R. G. Wilson. "SIMS quantification in Si, GaAs, and diamond - an update." In: *International Journal of Mass Spectrometry and Ion Processes* 143.C (1995), pp. 43–49. ISSN: 01681176. DOI: 10.1016/0168-1176(94)04136-U.

Appendix

# Ion Field Emission Setup

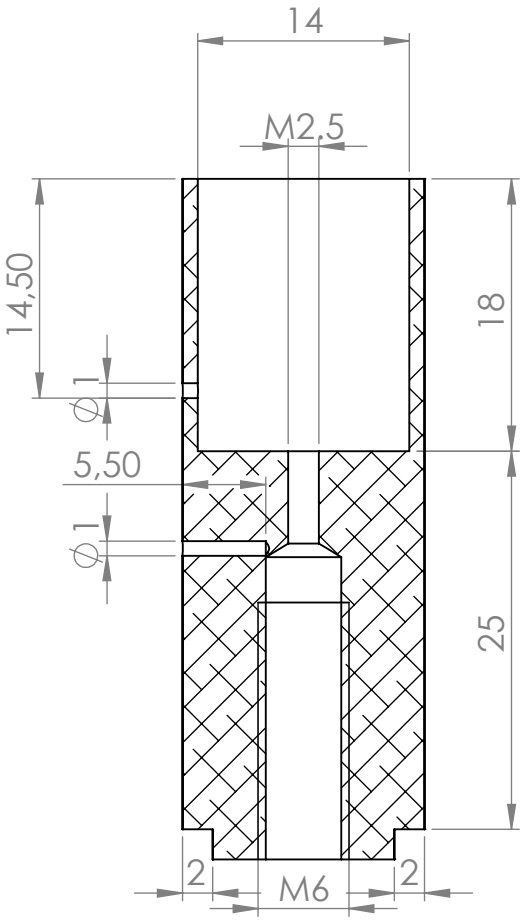


SECTION B-B

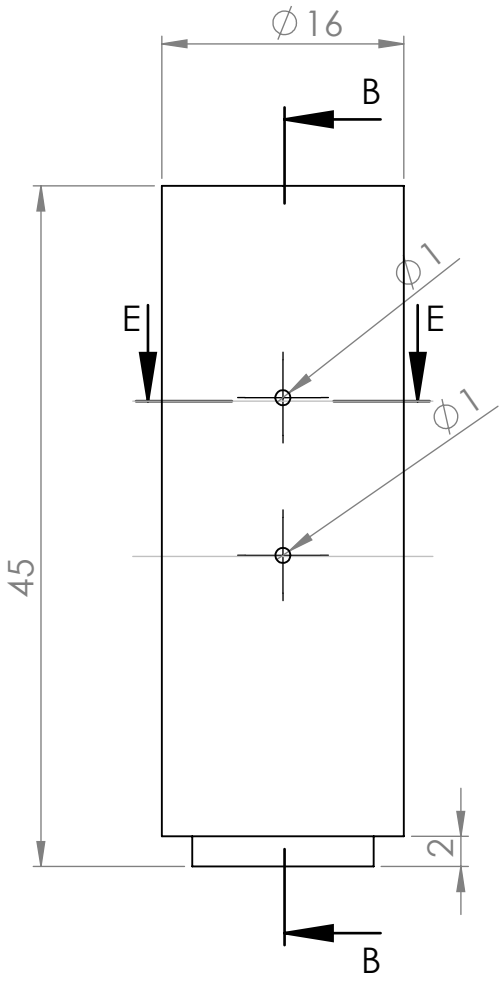


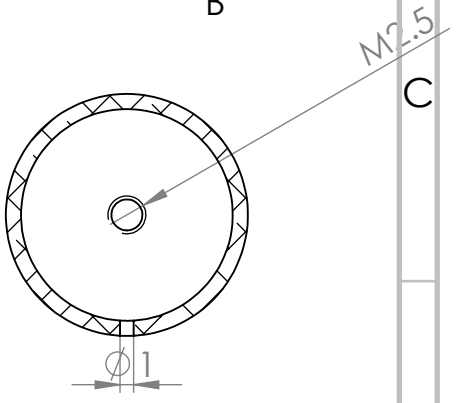


SECTION E-E

| | | |
|---|---|---|
| MATERIAL: Aluminium 1060-Alloy | Faraday Cup | A4 |
| | SCALE:2:1 | SHEET 1 OF 1 |

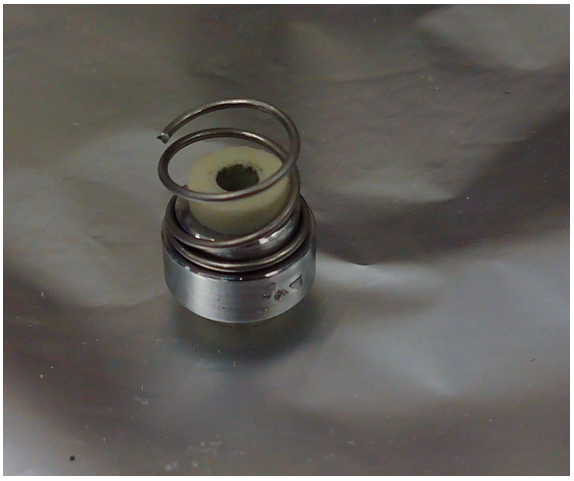

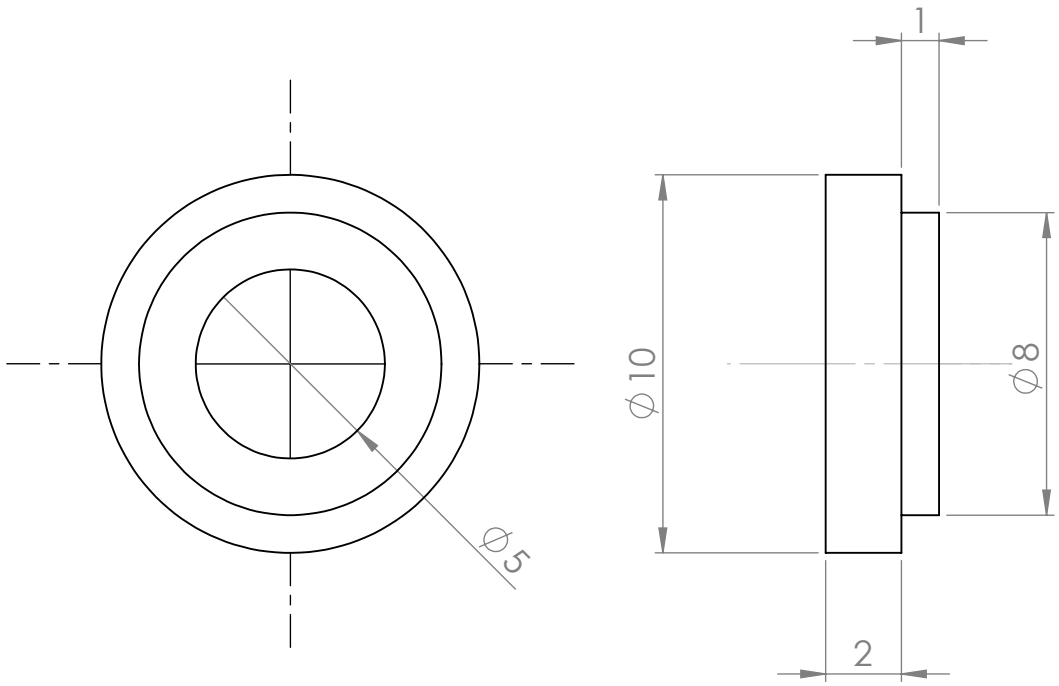


| | | |
|---|---|---|
| MATERIAL: Aluminium 1060-Alloy | Substrate Support | A4 |
| | SCALE:5:1 | SHEET 1 OF 1 |

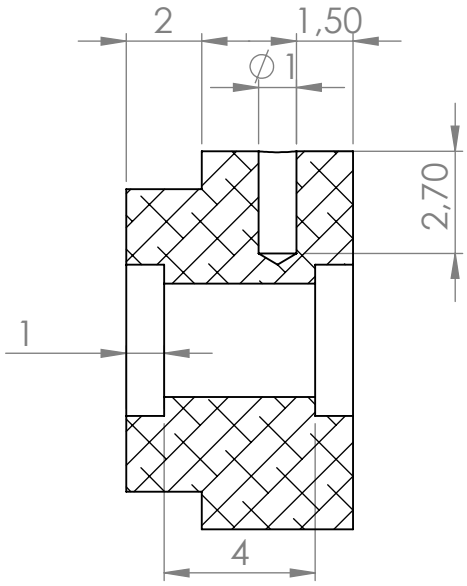


SECTION A-A

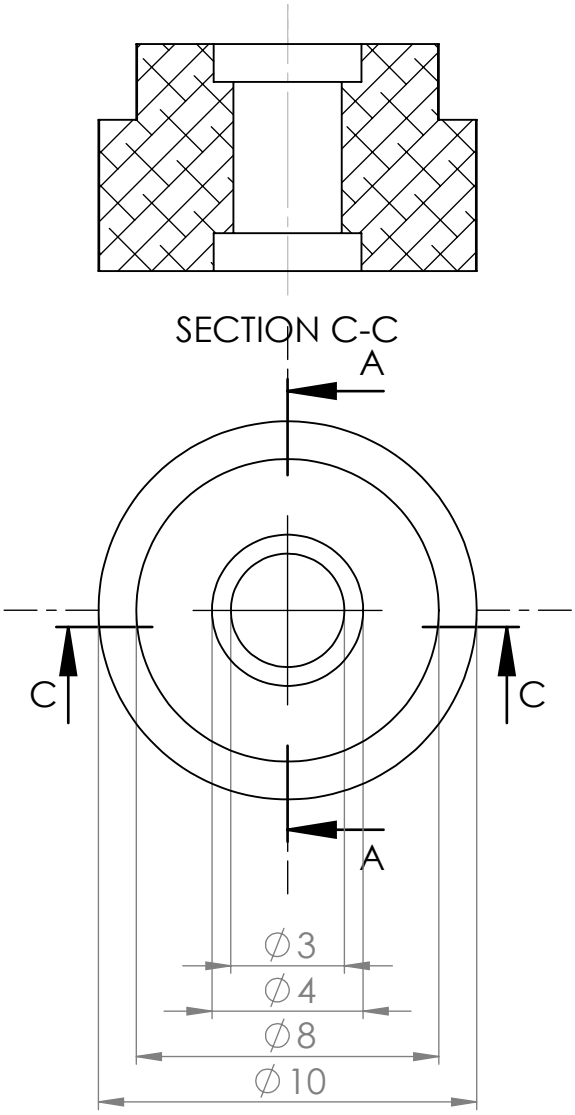


SECTION C-C

| | | |
|---|---|---|
| MATERIAL: Aluminium 1060-Alloy | Base Support | A4 |
| | SCALE:5:1 | SHEET 1 OF 1 |

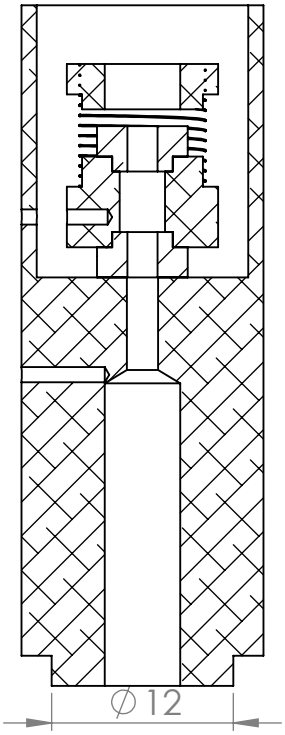


SECTION B-B

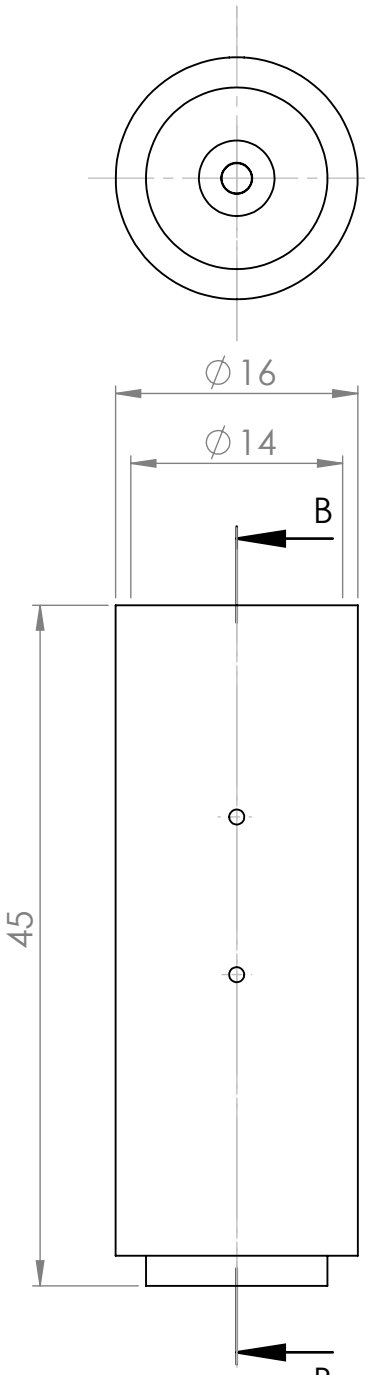


# Faraday Cup Assembly

A4

SCALE:2:1

SHEET 1 OF 1

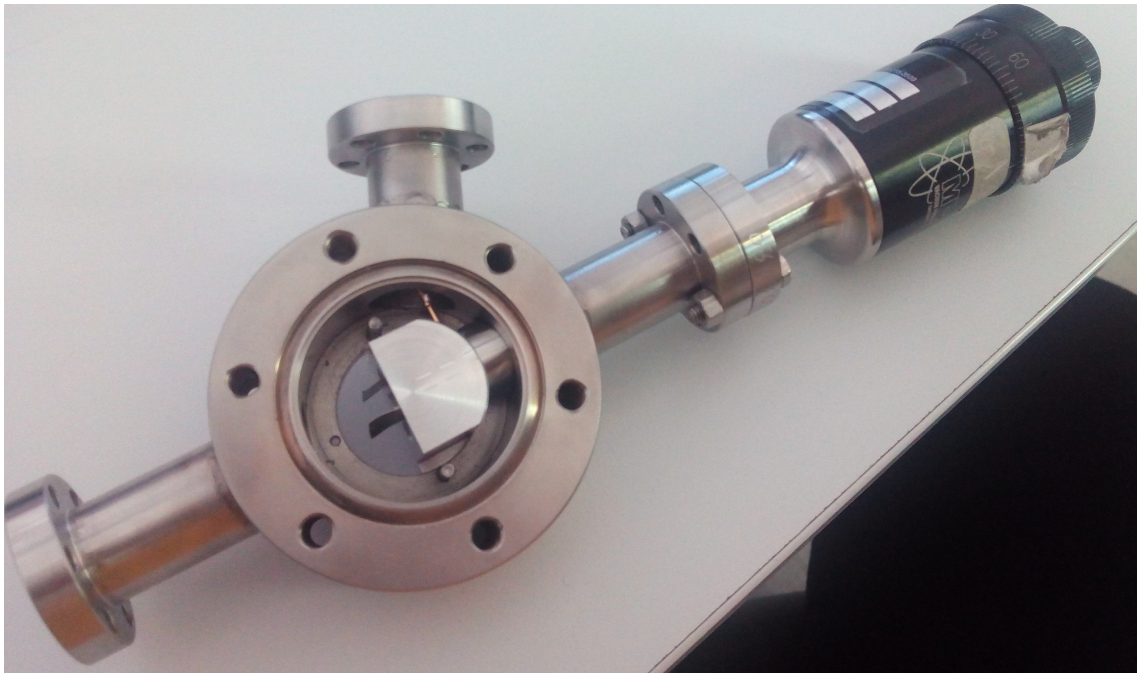

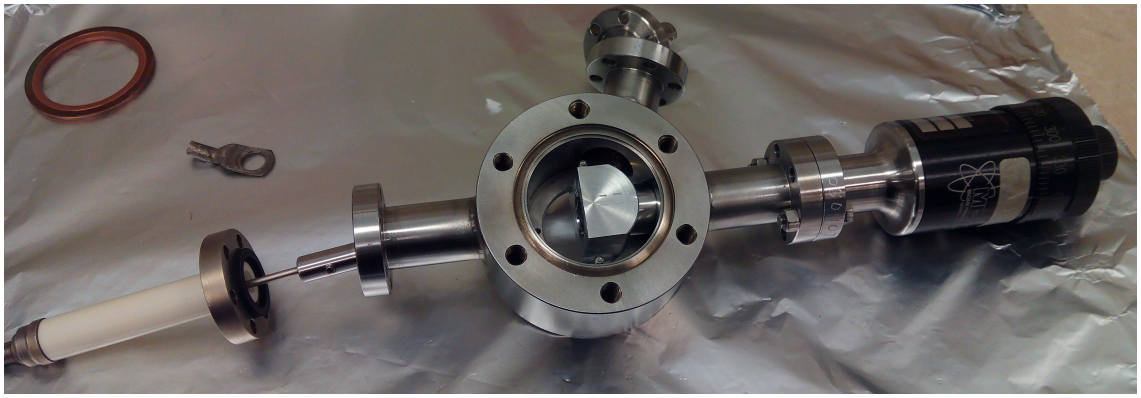

APPENDIX B

# Evaporation Assembly

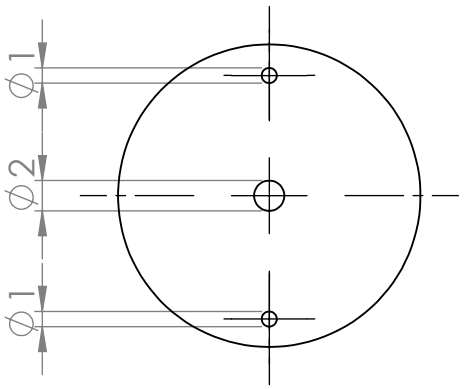


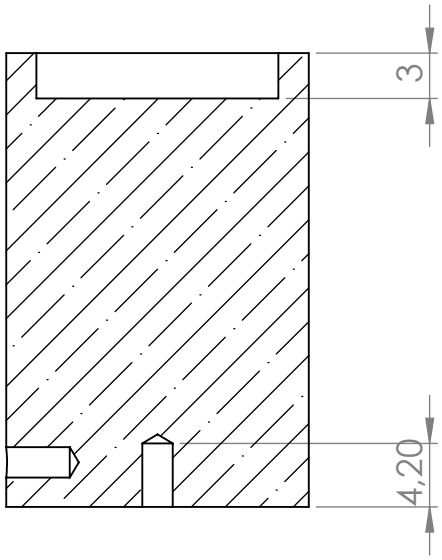


SECTION A-A

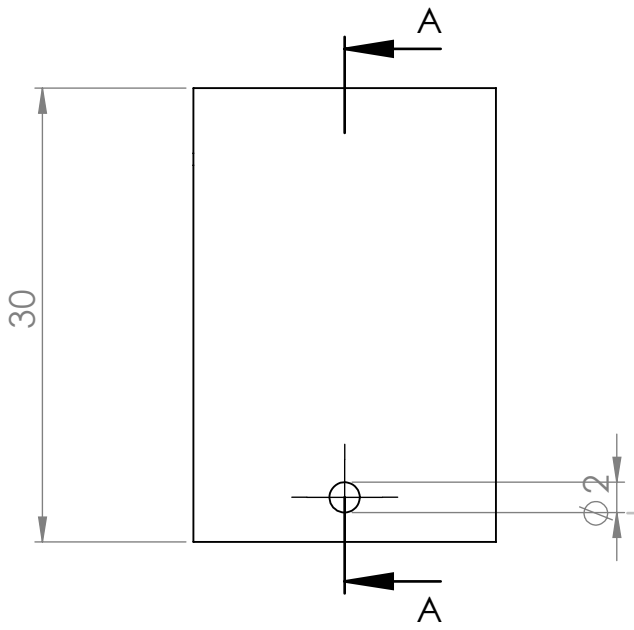


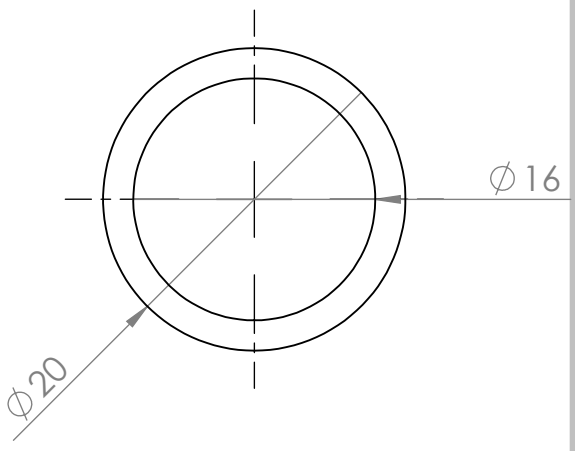


| | | |
|---|---|---|
| MATERIAL: Ceramics | Crucible | A4 |
| | SCALE:2:1 | SHEET 1 OF 1 |

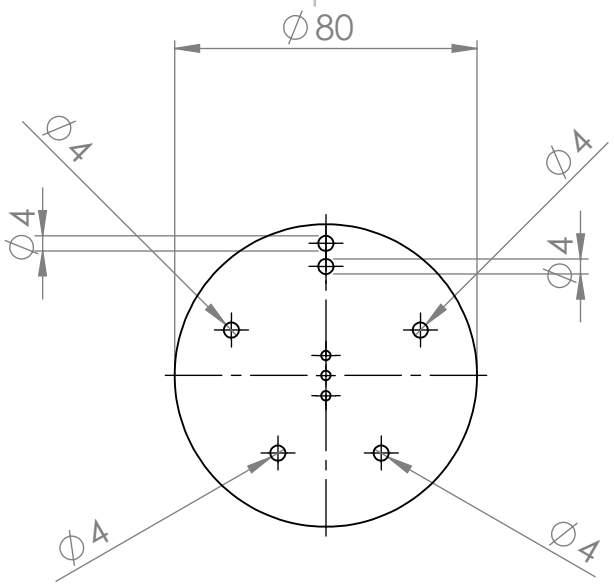


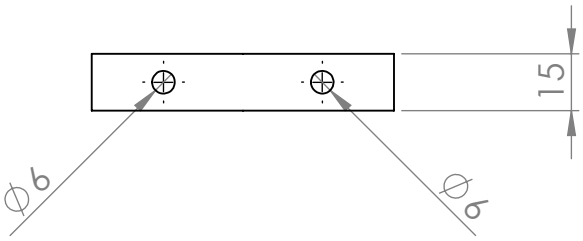


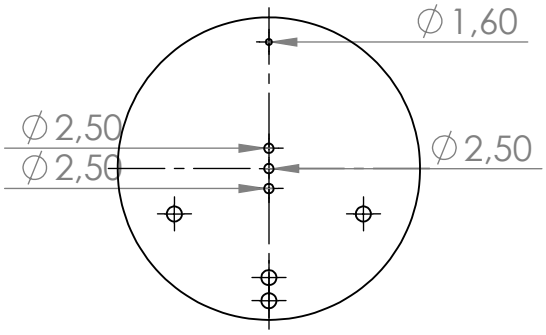


| | | |
|---|---|---|
| MATERIAL: Aluminium 1060-Alloy | Sample Holder | A4 |
| | SCALE:1:2 | SHEET 1 OF 1 |

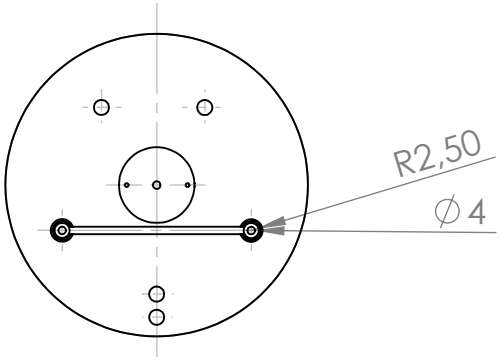


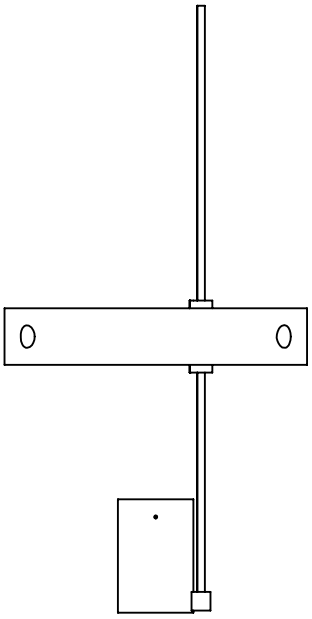

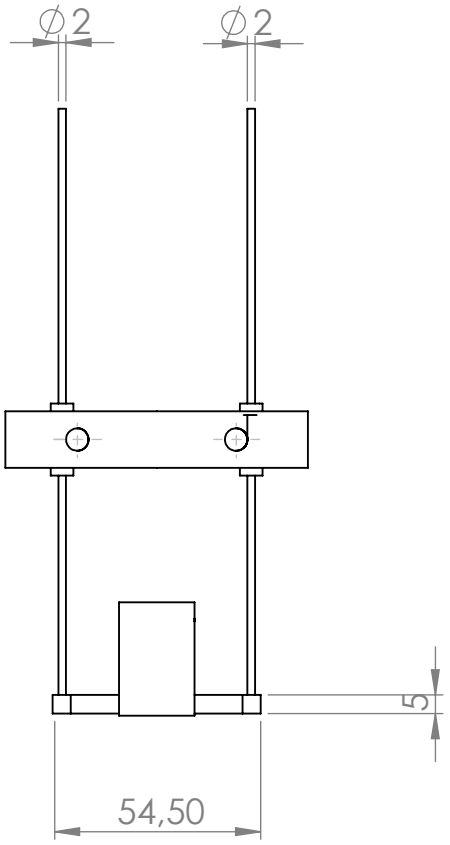


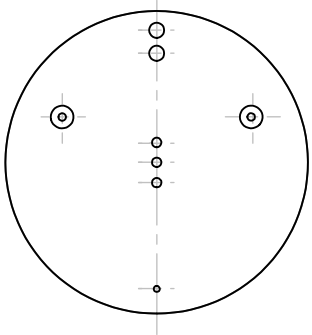

# Evaporator Assembly

A4

SCALE:1:2

SHEET 1 OF 1

ANNEX I

# COMPOUNDS SPECIFICATION SHEETS

SIGMA-ALDRICH®

sigma-aldrich.com

3050 Spruce Street, Saint Louis, MO 63103, USA
Website: www.sigmaaldrich.com
Email USA: techserv@sial.com
Outside USA: eurtechserv@sial.com

# Product Specification

Product Name:
Rubidium chloride – 99.8% trace metals basis

| | |
|---|---|
| **Product Number:** | **215260** |
| CAS Number: | 7791-11-9 |
| MDL: | MFCD00011187 |
| Formula: | ClRb |
| Formula Weight: | 120.92 g/mol |


| TEST | Specification |
|---|---|
| Appearance (Color) | White |
| Appearance (Form) | Powder or Crystals or Chunk(s) |
| Titration by AgNO3 | 28.8 - 29.8 % |
| % Cl | |
| ICP Major Analysis | Conforms |
| Confirms Rb Component | |
| Purity | Conforms |
| 99.8% Based on Trace Metals Analysis of ICP and AA Combined | |
| Trace Metal Analysis | ≤ 2500.0 ppm |
| Atomic Absorption | ≤ 2500.0 ppm |

Specification: PRD.1.ZQ5.10000039817

**3050 Spruce Street, Saint Louis, MO 63103, USA**
**Website: www.sigmaaldrich.com**
**Email USA: techserv@sial.com**
**Outside USA: eurtechserv@sial.com**

# Product Specification

Product Name:
Copper(I) chloride – anhydrous, beads, ≥99.99% trace metals basis

| | |
|---|---|
| **Product Number:** | **651745** |
| CAS Number: | 7758-89-6 |
| MDL: | MFCD00010971 |
| Formula: | ClCu |
| Formula Weight: | 99.00 g/mol |

CuCl

| TEST | Specification |
|---|---|
| Appearance (Color) | Conforms to Requirements |
| Clear to White | |
| Appearance (Form) | Beads |
| ICP Major Analysis | Confirmed |
| Confirms Copper Component | |
| Trace Metal Analysis | ≤ 100.0 ppm |
| Purity | Meets Requirements |
| 99.99+% Based On Trace Metals Analysis | |

Specification: PRD.0.ZQ5.10000028314

SIGMA-ALDRICH®
sigma-aldrich.com

3050 Spruce Street, Saint Louis, MO 63103, USA
Website: www.sigmaaldrich.com
Email USA: techserv@sial.com
Outside USA: eurtechserv@sial.com

# Product Specification

Product Name:
Copper(I) iodide – 99.999% trace metals basis

| | |
|---|---|
| **Product Number:** | **215554** |
| CAS Number: | 7681-65-4 |
| MDL: | MFCD00010978 |
| Formula: | CuI |
| Formula Weight: | 190.45 g/mol |


| TEST | Specification |
|---|---|
| Appearance (Color) | Conforms to Requirements |
| Grey-Tan | |
| Appearance (Form) | Powder or Chunks |
| Complexiometric EDTA | 31.0 - 34.0 % |
| % Cu | |
| ICP Major Analysis | Confirmed |
| Confirms Copper Component | |
| Purity | Meets Requirements |
| 99.999% Based On Trace Metals Analysis | |
| Trace Metal Analysis | ≤ 15.0 ppm |

Specification: PRD.0.ZQ5.10000066095